เซนเซอร์เคมีไฟฟ้าสำหรับการตรวจวัดฮิวแมนแพปพิลโลมาไวรัสดีเอ็นเอ ซี-รีแอคทีฟโปรตีน

และสีผสมอาหาร

นายศักดิ์ดา จำปาสา



วิทยานิพนธ์นี้เป็นส่วนหนึ่งของการศึกษาตามหลักสูตรปริญญาวิทยาศาสตรดุษฎีบัณฑิต
สาขาวิชาปิโตรเคมี
คณะวิทยาศาสตร์ จุฬาลงกรณ์มหาวิทยาลัย
ปีการศึกษา 2560

# ELECTROCHEMICAL SENSORS FOR HUMAN PAPILLOMAVIRUS DNA, C-REACTIVE PROTEIN AND FOOD COLORANTS DETECTIONS

Mr. Sakda Jampasa



A Dissertation Submitted in Partial Fulfillment of the Requirements
for the Degree of Doctor of Philosophy Program in Petrochemistry
Faculty of Science
Chulalongkorn University
Academic Year 2017

| | |
|---|---|
| Thesis Title | ELECTROCHEMICAL SENSORS FOR HUMAN PAPILLOMAVIRUS DNA, C-REACTIVE PROTEIN AND FOOD COLORANTS DETECTIONS |
| By | Mr. Sakda Jampasa |
| Field of Study | Petrochemistry |
| Thesis Advisor | Professor Dr.Orawon Chailapakul, Ph.D. |
| Thesis Co-Advisor | Professor Dr.Tirayut Vilaivan, Ph.D.<br>Associate Professor Dr.Weena Siangproh, Ph.D. |

Accepted by the Faculty of Science, Chulalongkorn University in Partial Fulfillment of the Requirements for the Doctoral Degree

.....Dean of the Faculty of Science
(Associate Professor Dr.Polkit Sangvanich, Ph.D.)

THESIS COMMITTEE

.....Chairman
(Associate Professor Dr.Napida Hinchiranan, Ph.D.)

.....Thesis Advisor
(Professor Dr.Orawon Chailapakul, Ph.D.)

.....Thesis Co-Advisor
(Professor Dr.Tirayut Vilaivan, Ph.D.)

.....Thesis Co-Advisor
(Associate Professor Dr.Weena Siangproh, Ph.D.)

.....Examiner
(Associate Professor Dr.Nuanphun Chantarasiri, Ph.D.)

.....Examiner
(Dr.Chatr Panithipongwut Kowalski, Ph.D.)

.....External Examiner
(Dr.Rawiwan Laocharoensuk, Ph.D.)

ศักดิ์ดา จำปาสา : เซนเซอร์เคมีไฟฟ้าสำหรับการตรวจวัดฮิวแมนแพปพิลโลมาไวรัสดีเอ็นเอ ซี-รีแอคทีฟโปรตีน และสีผสมอาหาร (ELECTROCHEMICAL SENSORS FOR HUMAN PAPILLOMAVIRUS DNA, C-REACTIVE PROTEIN AND FOOD COLORANTS DETECTIONS) อ.ที่ปรึกษาวิทยานิพนธ์หลัก: ศ. ดร. อรวรรณ ชัยลภากุล, อ.ที่ปรึกษาวิทยานิพนธ์ร่วม: ศ. ดร. ธีรยุทธ วีไลวัลย์, รศ. ดร. วีณา เสียงเพราะ, 141 หน้า.

วิทยานิพนธ์ฉบับนี้มุ่งเน้นพัฒนาเซนเซอร์ทางเคมีไฟฟ้าเพื่อการตรวจวัดสารบ่งชี้ทางชีวภาพด้านการแพทย์และสีผสมอาหาร งานวิจัยสามารถแบ่งออกเป็นสองส่วน ในส่วนที่หนึ่ง ได้แก่ การพัฒนาเซนเซอร์ทางเคมีไฟฟ้าเพื่อใช้ในการตรวจวัดสารบ่งชี้ทางชีวภาพด้านการแพทย์ที่สำคัญ ซึ่งสามารถแบ่งออกเป็นสองงานวิจัยย่อยตามสารบ่งชี้ที่ต้องการตรวจวัด งานวิจัยย่อยแรกคือการพัฒนาเซนเซอร์ทางเคมีไฟฟ้าเพื่อใช้ในการตรวจวัดดีเอ็นเอของไวรัสเอชพีวีความเสี่ยงสูง ชนิด 16 และ 18 พร้อมกัน ซึ่งเป็นตัวบ่งชี้ความเสี่ยงของการเกิดมะเร็งปากมดลูก งานวิจัยนี้ใช้โพรบพิโรลิดินิลเพปไทด์นิวคลีอิกแอซิดที่มีความจำเพาะเจาะจงสูงต่อการจับกับดีเอ็นเอของไวรัสทั้งสองชนิด โพรบที่สองถูกติดฉลากด้วยแอนทราควิโนนซึ่งเป็นตัวให้สัญญาณทางเคมีไฟฟ้าเมื่อมีการจับกับดีเอ็นเอเป้าหมาย เซนเซอร์ที่พัฒนาขึ้นให้ความเป็นเส้นตรงอยู่ในช่วง 0.1 – 100 นาโนโมลาร์ ค่าขีดจำกัดต่ำสุดของการตรวจวัดเท่ากับ 40 และ 60 พิโคโมลาร์ สำหรับไวรัสเอชพีวีชนิด 16 และ 18 ตามลำดับ เซนเซอร์ที่พัฒนาขึ้นมีความว่องไวและจำเพาะเจาะจงสูง พร้อมทั้งประสบผลสำเร็จในการตรวจวัดดีเอ็นเอของไวรัสทั้งสองชนิดจากตัวอย่างเซลไลน์หลังจากผ่านการเพิ่มปริมาณด้วยเทคนิคพีซีอาร์ สำหรับงานวิจัยย่อยที่สอง เป็นการสร้างอิมมูโนเซนเซอร์ทางเคมีไฟฟ้ารูปแบบแซนวิชเพื่อใช้ในการตรวจวัดซี-รีแอคทีฟโปรตีนซึ่งเป็นตัวบ่งชี้ความเสี่ยงของการเกิดโรคหัวใจ สัญญาณทางเคมีไฟฟ้าที่ตรวจวัดได้มีค่าสูงขึ้นตามความเข้มข้นของโปรตีนที่มีอยู่ในระบบ ซึ่งมีค่าความเป็นเส้นตรงอยู่ในช่วง 0.01 – 150 ไมโครกรัมต่อมิลลิลิตร และมีค่าขีดจำกัดต่ำสุดของการตรวจวัดอยู่ที่ 1.50 นาโนกรัมต่อมิลลิลิตร เซนเซอร์ที่พัฒนาขึ้นประสบผลสำเร็จในการตรวจวัดซี-รีแอคทีฟโปรตีนในตัวอย่างจริงพร้อมให้ผลเป็นที่น่าพอใจเมื่อเปรียบเทียบกับตัวอย่างที่ได้รับการรับรอง ในส่วนที่สอง เป็นการพัฒนาเซนเซอร์ทางเคมีไฟฟ้าเพื่อใช้ในการตรวจวัดสีผสมอาหารสังเคราะห์ ได้แก่ ซันเซตเย็ลโลว์และตาร์ตราซีน ขั้วไฟฟ้าที่ใช้คือขั้วไฟฟ้าแบบพิมพ์สกรีนราคาถูกซึ่งถูกดัดแปรด้วยกราฟีนออกไซด์เพื่อเพิ่มค่าขีดจำกัดของการตรวจวัด แผ่นฟิล์มกราฟีนถูกเคลือบลงบนผิวหน้าขั้วด้วยวิธีการรีดิวซ์ทางเคมีไฟฟ้า ซึ่งเป็นวิธีที่ง่าย ไม่ต้องใช้สารเคมีและไม่ก่อสารพิษ จากผลการทดลองพบว่า ขั้วไฟฟ้าที่ถูกดัดแปรผิวหน้าด้วยกราฟีนให้สัญญาณการตอบสนองที่สูงกว่าเมื่อเทียบกับขั้วที่ไม่ผ่านการดัดแปร ค่าความเป็นเส้นตรงของการตรวจวัดอยู่ในช่วง 0.01 – 20 ไมโครโมลาร์ และ 0.02 – 20 ไมโครโมลาร์ ค่าขีดจำกัดต่ำสุดของการตรวจวัดเท่ากับ 0.05 และ 4.5 นาโนโมลาร์ สำหรับซันเซตเย็ลโลว์และตาร์ตราซีน ตามลำดับ เซนเซอร์ทางเคมีไฟฟ้าทั้งหมดที่พัฒนาขึ้นมีความว่องไวและมีความจำเพาะเจาะจงต่อการตรวจวัดสูง ราคาถูกและสามารถพกพาได้ ดังนั้นเซนเซอร์ที่พัฒนาขึ้นจึงสามารถนำไปใช้เป็นอีกหนึ่งเซนเซอร์ทางเลือกที่จะนำไปตรวจวิเคราะห์สารทางด้านเภสัชกรรม สิ่งแวดล้อม และอื่น ๆ ได้

สาขาวิชา ปิโตรเคมี
ปีการศึกษา 2560

ลายมือชื่อนิสิต .....
ลายมือชื่อ อ.ที่ปรึกษาหลัก .....
ลายมือชื่อ อ.ที่ปรึกษาร่วม .....
ลายมือชื่อ อ.ที่ปรึกษาร่วม .....

## 5672874023 : MAJOR PETROCHEMISTRY

KEYWORDS: ELECTROCHEMICAL DETECTION / HUMAN PAPILLOMAVIRUS / C-REACTIVE PROTEIN / ANTHRAQUINONE / FOOD COLORANTS

SAKDA JAMPASA: ELECTROCHEMICAL SENSORS FOR HUMAN PAPILLOMAVIRUS DNA, C-REACTIVE PROTEIN AND FOOD COLORANTS DETECTIONS. ADVISOR: PROF. DR.ORAWON CHAILAPAKUL, Ph.D., CO-ADVISOR: PROF. DR.TIRAYUT VILAIVAN, Ph.D., ASSOC. PROF. DR.WEENA SIANGPROH, Ph.D., 141 pp.

In this dissertation, electrochemical sensors for determination of medical biomolecular markers and food colorants were developed. The research can be divided into two parts. In the first part, electrochemical sensors for determination of clinically important biomarkers were studied. There was two subprojects based on the target markers. The first subproject was the development of electrochemical sensor for the simultaneous detection of high-risk human papillomaviruses (HPV) DNA type 16 and 18 as biomarkers for cervical cancer. In this work, a highly specific pyrrolidinyl peptide nucleic acid was employed as DNA capture probe for both target DNAs. A second PNA probe labeled with a redox-active anthraquinone (AQ) tag was used to generate the electrochemical signal upon binding to the DNA target. The developed sensor showed a linear range between 0.1 and 100 nM, and the limits of detection (LODs) of 40 and 60 pM (S/N = 3) for HPV types 16 and 18 were found, respectively. This developed sensor was highly sensitive and selective, and was successfully applied to detect DNAs obtained cell lines after amplification by polymerase chain reaction (PCR). For the second subproject, a sandwich-type electrochemical immunosensor was designed to detect C-reactive protein (CRP) - a biomarker for cardiovascular diseases. The observed electrochemical signal increased proportionally to CRP level presented in the system with a linear range from 0.01 to 150 µg/mL and LOD of be 1.50 ng/mL. This developed sensor was successfully applied to determine CRP in practical samples, giving results that are in agreement with certified samples. For the second part of the research, an electrochemical sensor for the determination of synthetic colorants, sunset yellow (SY) and tartrazine (TZ) was developed. The employed electrode was modified using graphene oxide to enhance detection. Furthermore, a screen-printed electrode type was a low-cost screen-printed carbon electrode (SPCE) modified with graphene oxide to enhance the performance of the detection. The graphene film was coated onto the electrode surface via a simple electrochemical reduction process that does not require toxic chemicals and generates no toxic wastes. From the obtained results, the modified electrode exhibited higher electrochemical signal response compared to the unmodified electrode. Linearity of detection was in the range of 0.01 – 20 µM and 0.02 – 20 µM, and LODs were 0.50 and 4.5 nM for SY and TZ, respectively. All developed electrochemical sensors were highly sensitive and selective, inexpensive and portable which are suitable for use as alternative sensors for pharmaceutical, environmental and other analyses.



Field of Study: Petrochemistry
Academic Year: 2017

Student's Signature .....
Advisor's Signature .....
Co-Advisor's Signature .....
Co-Advisor's Signature .....

# ACKNOWLEDGEMENTS

First of all, I would like to extend my sincere gratitude to my advisor, Professor Dr.Orawon Chailapakul, and my co-advisors Professor Dr.Tirayut Vilaivan and Associate Professor Dr.Weena Siangproh for their guidance, support, motivation, enthusiasm, encouragement, and immense knowledge. This work would not have been possible without them. Under their guidance, I successfully overcame many difficulties and learned a lot. They inspired me to strive to become a quality scientist who could accomplish even the toughest research challenge. It has been an honor to be Ph.D. student under their supervision.

My deepest gratitude goes to Dr.Rawiwan Laocharoensuk, who has generously offered her time, expertise, wisdom, and continuous encouragement in guiding and mentoring me through the whole research process. I am also thankful for her encouragement to use correct English in my writings and for her comments and suggestions on countless revisions of my manuscripts. Without her advice, this dissertation would not have developed to this stage.

I am also truly grateful for my Ph.D. thesis committees: Associate Professor Dr.Napida Hinchiranan, Associate Professor Dr.Nuanphun Chantarasiri and Dr.Chatr Panithipongwut Kowalski, for their time, insightful comments and questions.

I acknowledge the funding sources that supported my Ph.D. work. I was funded by Human Resource Development in Science Project (Science Achievement Scholarship of Thailand, SAST). Also, I would like to thank the members of Electrochemistry and Optical Spectroscopy Center of Excellence (EOSCE) and Organic Synthesis Research Unit (OSRU) for their help, kindness and warm friendship. I would like to extend my sincere appreciation to my close friend, Mr.Rattavut Teerakapibal, who gave constructive advices and suggestions to improve my writing skills.

Lastly, my education and my life would not have been successful without them; I would like to pay highest regards to my beloved family for their unconditional love, trust, timely encouragement, and endless patience; especially my mother who always works hard for me. Since I was born, I have never seen my mother stop working. Hence, from now on, all my success I awarded to her.

**CONTENTS**

Page

Page

Page

Page

Page

# LIST OF TABLES

# LIST OF FIGURES

# LIST OF ABBREVIATIONS

| | |
|---|---|
| A | Electrode surface area |
| AQ | Anthraquinone |
| ASD | A position downstream |
| ASU | A position upstream |
| AuNPs | Gold nanoparticles |
| BDDE | Boron-doped diamond electrode |
| BSA | Bovine serum albumin |
| CE | Counter electrode |
| CRP | C-reactive protein |
| CV | Cyclic voltammetry |
| $C_o(0,t)$ | Concentration of oxidized form |
| $C_R(0,t)$ | Concentration of reduced form |
| ℃ | Degree celsius |
| D | Diffusion coefficient |
| DNA | Deoxyribonucleic acid |
| DPV | Differential-pulse voltammetry |
| E° | Standard potential for the redox reaction |
| E-DNA | Electrochemical DNA biosensor |
| EIS | Electrochemical impedance spectroscopy |
| ELISA | Enzyme-linked immunosorbent assay |
| $E_p$ | Peak potential |
| $E_{p,a}$ | Anodic peak potential |
| $E_{p,c}$ | Cathodic peak potential |
| ERGO | Electrochemically-reduced graphene oxide |
| eV | Electron volt |
| $\Delta E_p$ | Peak separation potential |
| F | Faraday's constant (96,487 coulombs) |
| G | Graphene |

| | |
|---|---|
| GC-MS | Gas chromatography-mass spectrometry |
| GO | Graphene oxide |
| HPLC | High performance liquid chromatography |
| HPV | Human papillomavirus |
| ISE | Ion-selective electrode |
| $\Delta i$ | Current difference |
| $I_p$ | Peak current |
| $I_{p,a}$ | Anodic peak current |
| $I_{p,c}$ | Cathodic peak current |
| $k_{et}$ | Electron-transfer rate constant |
| kΩ | kilo-ohm |
| LC/MS | Liquid chromatography-mass spectrometry |
| LOD | Limit of detection |
| LOQ | Limit of quantification |
| LSV | Linear sweep voltammetry |
| M | Molar |
| mg/mL | milligram per milliliter |
| mM | Millimolar |
| mm | Millimeter |
| mV $s^{-1}$ | Milli volt per second |
| n | Number of electrons transferred in the reaction |
| nM | Nanomolar |
| O | Oxidized form of redox coupled |
| PB | Phosphate buffer |
| PBS | Phosphate buffer saline |
| PCR | Polymerase chain reaction |
| pM | Picomolar |
| PNA | Peptide nucleic acid |
| PVC | Polyvinyl chloride |
| C | Coulombs |

| | |
|---|---|
| R | Reduced form of redox coupled |
| RE | Reference electrode |
| $R_{et}$ | Electron-transfer resistance |
| RSD | The relative standard deviation |
| SEM | Scanning electron microscopy |
| SPCE | Screen-printed carbon electrode |
| SPGE | Screen-printed graphene electrode |
| SWV | Square-wave voltammetry |
| SY | Sunset yellow |
| T | Kelvin temperature |
| t | Time |
| TLC | Thin layer chromatography |
| TZ | Tartrazine |
| v | Scan rate |
| V | Volt |
| WE | Working electrode |
| µA | Microampere |
| µg/mL | Microgram per milliliter |
| µL | Microliter |
| µM | Micromolar |

# CHAPTER I

# INTRODUCTION

## 1.1 Introduction

The rapid growth of technologies makes changes in human lifestyles, causing a considerable problem in health [1]. Various non-communicable diseases have been discovered and are affecting millions of people each year worldwide. According to clinical diagnosis, most symptoms appear in the late stages of the diseases. For many diseases, early diagnosis is essential for the success of the treatment and improving patient survival rate [2]. In general, measuring the level of one or more biomarkers associated with the disease is a better indicator of the presence and/or severity of the disease than physical examination.

During the past few decades, numerous analytical approaches for example liquid chromatography-mass spectrometry (LC/MS), gas chromatography-mass spectrometry (GC-MS), high performance liquid chromatography (HPLC), thin layer chromatography (TLC), and spectroscopy have been developed for various applications in the life sciences [3-6]. These techniques provide highly accurate, selective, and sensitive determination. Nevertheless, these aforementioned techniques still have some limitations in terms of requirement of derivatization step, time consumption and/or high running costs and sophisticated instrumental setup. These reasons devalue them from an ideal routine analysis and are unsuitable for countries with limited resources and personnel. Therefore, tools or method developments which provide all these requirements are still in needed for new revolution in our life science.

Electrochemical technique has been proven to be an effective solution and alternative method because of its inherent miniaturization, less time consumption, simple instrumentation setup and low cost. These advantages make electrochemical technique suitable to develop and use as a potential tool for scientific developments especially where the health safety is concern.

In this work, simple, sensitive and selective electrochemical sensors for determination of important medical biomarkers for diseases diagnosis and synthetic colorants for food quality control were developed. The first important medical biomarker examined using the developed electrochemical sensor was for high-risk human papillomaviruses DNA type 16 and 18 (HPV). These viruses have been shown to be the major cause of cervical cancer which is one of the leading types of fatal cancer in women around the world [7]. It mostly occurs in women within the age range of 30–50 years old, and the number of cervical cancer patients has increased continuously to a current population of around 500,000 people with a mortality of 200,000 per year. Among these cases, 80% of all the patients are from developing countries who have limited public healthcare resources [8]. Various techniques have been developed and implemented over the last few decades for the diagnosis of HPV infections. Currently, the most widely used techniques for screening and diagnosing HPV infection are Digene Hybrid Capture assay (HC2), Pap smear test and polymerase chain reaction (PCR) with generic primers [9, 10]. However, the first two aforementioned techniques exhibit low sensitivity and specificity, require experts to analyze the data, are time consuming, and require complicated and expensive instrumentation which are unsuitable for countries with limited resources and personnel [11]. Because we realize in cervical cancer crisis that caused by high-risk HPV, it is our inspiration to develop a screening method for the examination of HPV DNA in the primary stage of cervical cancer, which can save the life or reduce the

mortality rate of these patients. The motivation and details of developed electrochemical sensor are described in Chapter III, part I.

For the second research, the electrochemical sensor for determination of C-reactive protein, cardiovascular disease maker, was developed. C-reactive protein (CRP) is an acute-phase protein produced in the liver and is considered as a valuable biomarker for inflammation or cardiovascular diseases in clinical diagnosis. Currently, the level of CRP present has been used to identify specific diseases via medical diagnostics such as diabetes and cancers [12]. According to the American Heart Association and the United States Centers for Disease Control and Prevention (AHA/CDC), the cardiovascular disease risk levels are assessed by CRP concentrations in human blood serum: CRP concentration less than 1 μg/mL represents a low risk state, concentration between 1 and 3 μg/mL is considered as moderate risk and any concentration above 3 μg/mL represents high risk [13-15]. In clinical laboratories, CRP is typically examined by immunonephelometric or immunoturbidimetric assays [16]. These approaches are expensive, time-consuming, require expertise and advanced instrumentation. Moreover, its poor sensitivity also limits its robustness to detect low levels of CRP. Therefore, a rapid, highly sensitive, selective and operationally convenient approach is still in great demand for determination of trace CRP levels with rapid turn-around time. To overcome this challenge, we therefore developed a simple, highly sensitive and selective electrochemical biosensor for determining CRP. Analytical performance, such as sensitivity, specificity and reproducibility of the proposed sensors were collectively examined. The details of the fabrication, detection and application of electrochemical CRP biosensor were described in Chapter III, part II.

In the last part of this dissertation, a simple and highly sensitive electrochemical sensor based on an electrochemically reduced graphene oxide-modified screen-printed carbon electrode (ERGO-SPCE) for simultaneous

determination of synthetic colorants, sunset yellow (SY) and tartrazine (TZ) was developed. SY and TZ, classified as azo dyes, are common synthetic colorants that are extensively employed in the food industries due to their low production cost, charming color uniformity and excellent water solubility as well as their high stability to light, oxygen and pH [17-19]. However, they can cause detrimental effects to health when they are excessively consumed. According to the Notification of the Ministry of Public Health (No. 21) B.E. 2522 (1979), these food colorants can only be incorporated in certain food products, and they must be within a specified dosage with a justifiable purpose. Various techniques have been developed and applied over the last few decades for the examination of SY and TZ. Currently, the most widely used techniques for the determination of these colorants are spectrophotometry, high performance liquid chromatography (HPLC), column chromatography and capillary electrophoresis [20-23]. Nevertheless, the first two aforementioned techniques have some disadvantages. In particular, these two techniques exhibit low sensitivity and specificity, require expertise, are time-consuming, and require instrumentation that is complicated as well as expensive. According to the aforementioned limitations, in the last part of this research we therefore introduced a simple and highly sensitive electrochemical sensor to use as a novel method for the determination of SY and TZ in beverages. A green and facile routine electrochemical reduction method was employed to produce an ERGO film onto the electrode surface in one step. Analytical parameters, such as the sensitivity, selectivity and reproducibility, were also investigated. This developed electrochemical sensor was also applied to quantify the amounts of SY and TZ in practical samples to validate the performance of the developed sensor. The details for the construction and application of this developed sensor were demonstrated in Chapter IV.

## 1.2 Objectives of the research

This research consists of three main development goals:

1. To develop electrochemical DNA biosensor for the detection of high-risk HPV DNA type 16 and 18 to be used as a novel screening tool for early stage diagnosis of cervical cancer.

2. To develop a portable, low-cost and sensitive electrochemical immunosensor for determination of C-reactive protein as a cardiovascular disease biomarker.

3. To develop a simple and highly sensitive electrochemical sensor using an electrochemically reduced graphene oxide-modified screen-printed carbon electrode (ERGO-SPCE) for the simultaneous determination of two widely-used synthetic colorants: sunset yellow (SY) and tartrazine (TZ).

## 1.3 Scope of the research

To achieve the research objectives, the scope of the research was set as follows:

1. Electrochemical DNA biosensor for the detection of high-risk HPV DNA type 16 and 18 was developed. In this work, we report the design and fabrication of two new "signal-on" E-DNA sensors employing the principle of PNA-DNA sandwich hybridization assay. This detection mode offers a strong signal, which increases proportionally and evidently depending on the target DNA concentration present. The sensor is comprised of an unlabeled acpcPNA capture probe (P1) and an AQ-modified acpcPNA signaling probes (AQ-P2). AQ-P2 is specifically designed to hybridize with the target DNA at upstream (ASU) or downstream (ASD) positions on the sequence recognized by the P1 probe to ensure efficient electronic communication between the labeled molecule and the electrode surface. The influences of the sensor design and relevant parameters were systematically

investigated and discussed. Analytical parameters, such as the sensitivity, specificity and reproducibility were collectively evaluated. Finally, this developed sensor was applied to detect a PCR-amplified sample derived from HPV type 16 (SiHa) and 18 (HeLa) positive human cancer cell lines to evaluate the applicability of this sensor in cervical cancer screening.

2. A novel electrochemical immunosensor based on anthraquinone-labeled signaling antibody using screen-printed graphene electrode (SPGE) for a simple and highly sensitive determination of C-reactive protein (CRP) was proposed. A sandwich-type format was also employed for CRP detection since it offers high sensitivity, specificity, and kinetics. Signaling antibody was covalently modified with anthraquinone as a redox label in an aqueous solution to make them electrochemically detectable. Determination of CRP was conducted by measuring the electrochemical signal response of the AQ attached onto the signaling antibody using differential pulse voltammetry (DPV). Under optimal condition, the sensitivity, specificity and reproducibility of the proposed sensors were collectively examined. Relevant characterizations were also conducted. This developed immunosensor was eventually applied to determine CRP in human serum sample to evaluate the applicability of this sensor in determining CRP level.



3. A simple and highly sensitive electrochemical sensor based on an ERGO-SPCE for the determination of SY and TZ was reported. A green and facile routine electrochemical reduction method was employed to produce an ERGO film onto the electrode surface in one step. This disposable SPCE employed was inexpensively and easily prepared. Analytical parameters such as the sensitivity, selectivity and reproducibility were investigated. This developed electrochemical sensor was also applied to quantify the amounts of SY and TZ in real samples to validate the performance of the developed sensor.

There are five chapters in this dissertation. Chapter I is the introduction. Chapter II is the theory arranged into topics as follows: electrochemical technique, electrochemical biosensor and peptide nucleic acid. Chapter III, part I, reports on the development of electrochemical method for HPV DNA determination using the developed DNA sensor. Chapter III, part II, presents the development of electrochemical CRP immunosensor based on AQ-labeled signaling antibody. Chapter IV reports on the development of electrochemical sensing platform using electrochemically-reduced graphene oxide-modified screen-printed carbon electrode (ERGO-SPCE) for determination of synthetic colorants. Lastly, chapter V is the conclusions and future perspectives.

# CHAPTER II

# THEORY

## 2.1 Electrochemical technique

Electrochemistry is a type of analytical chemistry concerned with the interrelation between electricity and chemical reaction. Over the past few decades, scientists have reported on the use of electrochemistry to measure the electrical properties obtained from chemical reaction for various applications. From those studies, there are many data obtained such as thermodynamic data of a reaction, the generation of an unstable intermediate such as a radical ion, as well as a rate of decay or spectroscopic properties of substances. The most important is the establishment of numerous electrochemical methods to quantitatively determine the analyte of interest. The monitoring signals are based on the electrical signal produced or changed, such as current, potential, and charge after chemical reactions occurred. The method has been proven to be extremely selective and sensitive. However, their applications require an understanding of the fundamental principles of electrode reactions and the electrical properties of the electrode-solution interfaces. Electroanalytical measurements can be generally categorized into two principal types, so called potentiometric and voltammetric techniques [24, 25].

Potentiometric or zero current technique is a type of electroanalytical technique in which the data of the sample concentration is achieved from the measurement of the potential occurred across a membrane. Various types of membrane resources have been introduced and established to offer a high selectivity and sensitivity of detection. An extensively used potentiometric sensor is an ion-selective electrode (ISE). This membrane electrode converts the activity of a specific ion dissolved in a solution into an electrical potential. Under condition of

zero current, the generated potential is measured in which the potential is plotted with logarithmically varied according to the concentration of the electroactive species according to the Nernst equation [24].

The next category of electroanalytical technique is voltammetric or controlled-potential technique. The principle of this measurement is depended on the change of charge-transfer processes at the electrode-solution interface during applying the potential. This technique is normally applied to observe cathodic and anodic characteristics of any substances where the redox reaction occurs at the electrode surface (Equation 2.1) [24, 25].

$$O + ne^- \longrightarrow R \qquad \text{(Equation 2.1)}$$

where O and R are the oxidized and reduced forms of redox coupled, respectively. n is the number of electron. The reaction occurs in a potential region that makes the electron transfer thermodynamically or kinetically favorable.

This technique requires an external potential source to drive the transfer of electrons in the electric circuit. The generated current or electrode reaction rate is controlled by the different processes such as mass or electron transfer at the electrode surface. Moreover, other surface phenomena including adsorption, desorption, or crystallization can affect the electrode reaction as shown in Figure 2.1. In general, the main objective of using controlled-potential technique is to obtain a current response of the redox reaction which is related to the concentration of the target analyte. High sensitivity, selectivity, wide linear range, and low-cost instrumentation set up are also the advantages of this technique. These make it is suitable for applications in various analytical purposes. Due to the aforementioned

advantages, the electrochemical measurement based on controlled-potential principle is therefore employed in all experiments performed in this dissertation.

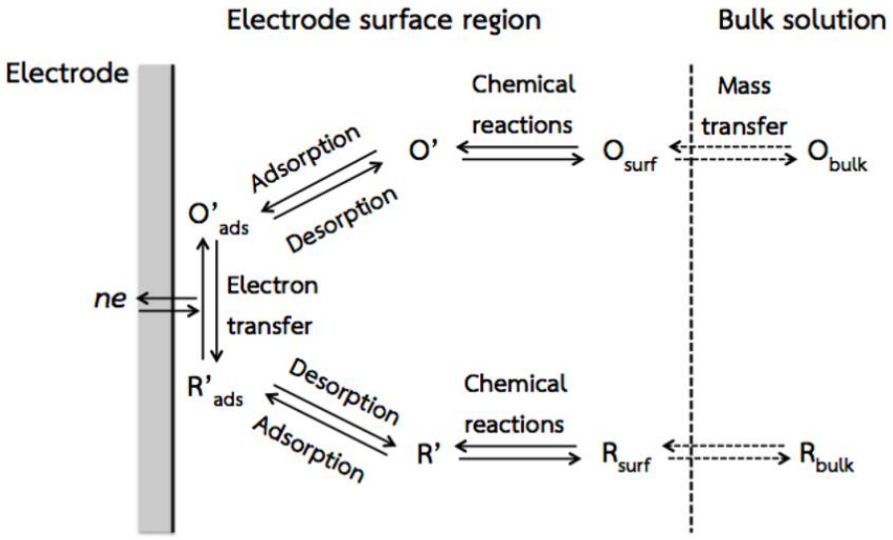


**Figure 2.1** Pathway of electrode reaction [26].

### 2.1.1 Voltammetry

Voltammetry is a class of electroanalytical methods in which the generated current is determined as a function of applied potential or voltage. The resulting current-potential plot is called a voltammogram. This method can be applied to investigate the electrochemical properties of any electroactive species that can be oxidized or reduced depending on the direction of the applied potential. When the potential is applied to more negative direction, it becomes more strongly reducing, the reduction reaction consequently occurs. In contrast, it becomes more strongly oxidizing when the potential of electrode is applied to more positive way. Voltammetry can be categorized into several types depended on the potential waveform, for example linear sweep voltammetry (LSV), , cyclic voltammetry (CV), staircase voltammetry, normal pulse voltammetry, differential pulse voltammetry

(DPV), square wave voltammetry (SWV),. Each type of voltammetry can be differently applied based on the nature of the target analyte and sensitivity requirement [24, 25].

#### 2.1.1.1 Cyclic voltammetry (CV)

Cyclic voltammetry (CV) is a simple but elegant electrochemical approach for observing redox reactions of an analyte at the electrode-solution interfaces [27]. The electrochemical cell uses a working electrode (WE), counter electrode (CE) and reference electrode (RE), which in combination are sometimes referred to as a three-electrode system. The potential of the working electrode is applied against a reference electrode (RE) which maintains a constant potential and the subsequent applied potential generates an excitation signal. Various materials can be employed for the construction of the working electrodes, for example glassy carbon, platinum, and gold [28-30]. The counter electrode or the auxiliary electrode can be any material which conducts electricity easily and will not react with the bulk solution. An electrolyte is normally used to dissolve sample to guarantee sufficient conductivity and reduce the migration current. In CV technique, the developed current in an electrochemical cell is measured under conditions where the voltage is in excess of that predicted by the Nernst equation. Electrodes are fixed in unstirred solutions during the cyclic voltammetry which results in characteristic diffusion controlled peaks. In CV technique, a triangular potential waveform with single or multiple cycles is applied to the WE. The potential waveform is illustrated in Figure 2.2(A). For example, in this case, it is supposed that there is only the oxidized form (O) in the initial solution. To obtain the cyclic voltammogram, the potential is scanned to more negative direction for the first half-cycle, starting from a potential where no reduction arises. When the applied potential reaches the formal potential ($E^0$) of the redox process, a cathodic current starts to increase and eventually

appears as a peak form. During the potential scan to the negative direction, R molecules are produced and accumulated near the surface. After the applied potential crosses at least 90/n mV beyond the cathodic peak, the potential sweep is reversed to the positive direction. R molecules are re-oxidized to O, and the anodic peak consequently observed. An ideal cyclic voltammogram of a reversible redox couple during a single potential cycle is shown in Figure 2.2(B).

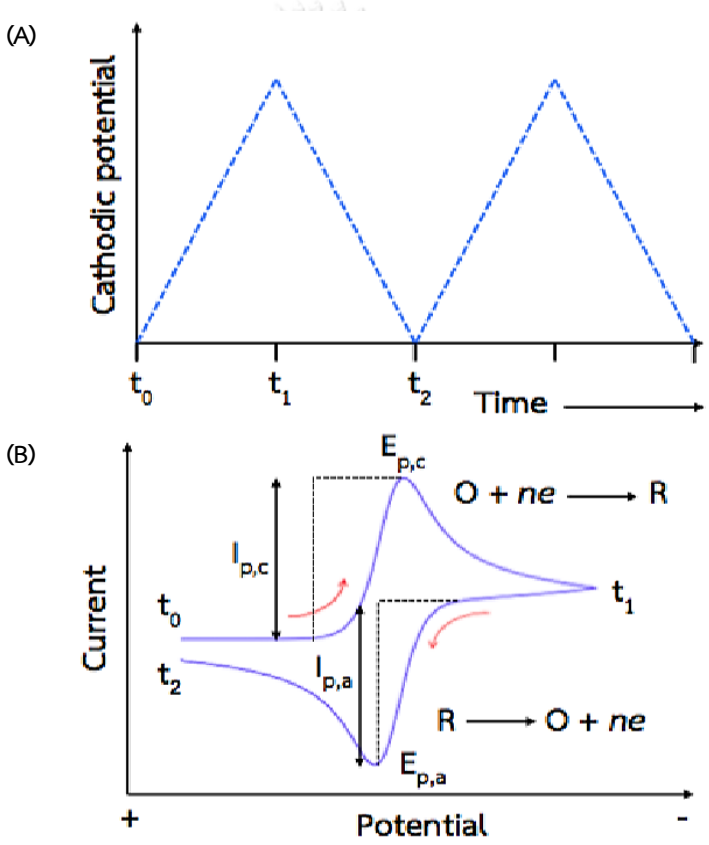


**Figure 2.2** Illustration of a triangular potential waveform of CV (A), typical cyclic voltammogram for a reversible process (B) [27].

According to Figure 2.2(B), the measurements can be characterized by a peak potential. $E_p$ is the peak potential that the current reaches its maximum value and $i_p$ is the peak current. The $i_{p,a}$ and $E_{p,a}$ are the anodic peak current and the anodic peak

potential for oxidation reaction, respectively. Similarly, the $i_{p,c}$ and $E_{p,c}$ represent the cathodic peak current and the cathodic peak potential for reduction reaction. However, this technique is frequently used for only qualitative determination of a redox species due to its low sensitivity.

**2.1.1.2 Square wave voltammetry (SWV)**

Square Wave Voltammetry (SWV) is one of the most powerful techniques in cyclic voltammetry for determining at trace levels of organic and inorganic compounds [31, 32]. The higher sensitivities can be obtained using SWV in comparison to those obtained by normal pulse voltammetry and differential pulse voltammetry. The applied potential wave form for this technique is presented in Figure 2.3(A). The potential wave form consists of a square wave of constant amplitude superimposed on a staircase wave form. The current is measured twice during each square wave cycle, one at the end of the forward pulse ($i_f$), and again at the end of the reverse pulse ($i_r$). The technique distinguishes against charging current by interrupting the current measurement to the end of the pulse. The difference current ($i_f$ - $i_r$) between the two measurements is schemed versus the potential staircase. SWV produces peaks for faradaic processes, where the peak height obtained is proportional to the concentration of the analyte in solution (Figure 2.3(B)).



Compared to other voltammetric techniques, the square wave voltammetry (SWV) offers several advantages include high speed, increased analytical sensitivity [29].

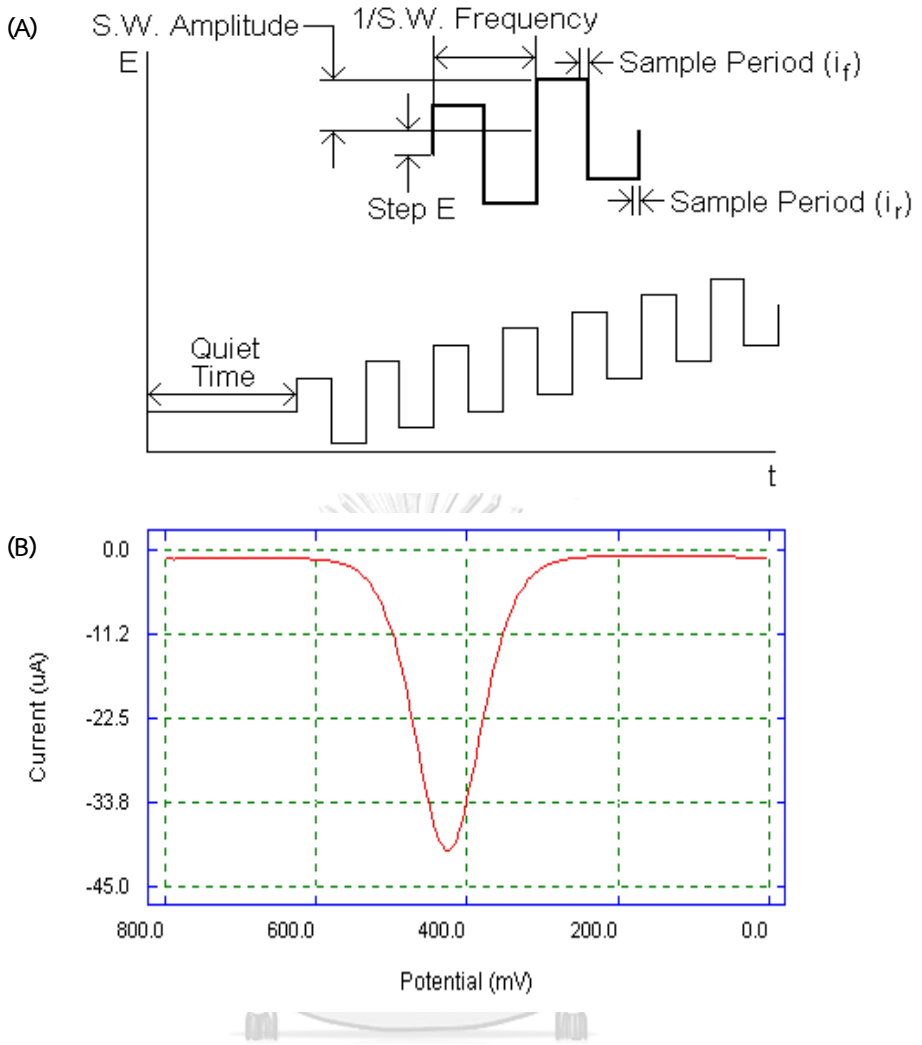


**Figure 2.3** Potential wave form for square wave voltammetry (A), a typical square wave voltammogram (B) [33].



### 2.1.1.3 Differential Pulse Voltammetry (DPV)

Differential-pulse voltammetry (DPV) is an extremely useful method for detecting trace levels of organic and inorganic species. The waveform of DPV is presented in Figure 2.4. The fixed-magnitude pulses which superimposed on a linear potential ramp, are applied to the working electrode. In this technique, current is measured at two points of each pulse. The first sample period is before the application of the pulse ($t_1$), and at the end of the pulse for the second sample period ($t_2$), respectively. The first current (i1) is instrumentally subtracted from the

second current (i2). The current difference (ΔI = i1 - i2) of each pulse is measured and plotted against the base potential, resulting in differential pulse voltammogram. The obtained peak height is proportional to the concentration of the corresponding analytes.

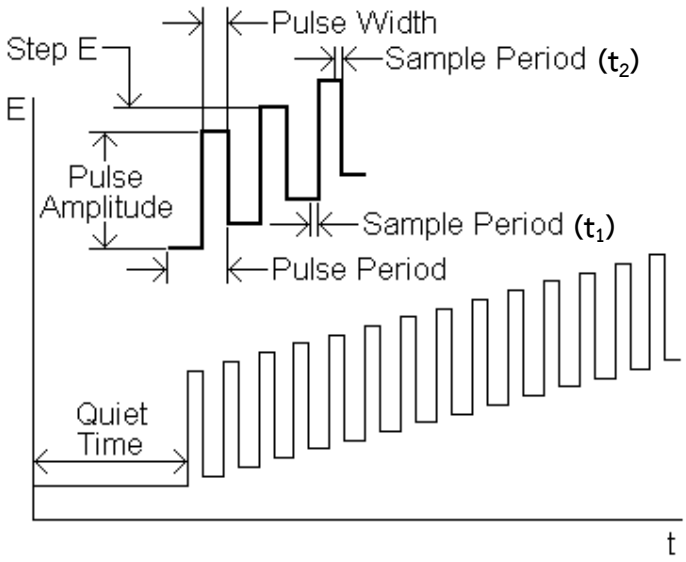


**Figure 2.4** Potential-time waveform in DPV [34].

The characteristics of differential pulse voltammetry are as follow:

(1) Reversible reactions exhibit symmetrical peaks whereas irreversible reactions display asymmetrical peaks.

(2) In reversible reactions, the peak potential is equal to $E_{1/2}^{r}$-ΔE. This peak current is proportional to the corresponding concentration of an analyte.

In the aforementioned cyclic voltammetric techniques, the use of technique is based upon the characteristic and kinetic of a redox species. Hence, to obtain the highest sensitivity and selectivity of detection, optimization of suitable technique is always necessary.

## 2.2 Electrochemical biosensor

Electrochemical biosensor is a sensor for the detection of an analyte that involve the detection of a biological analyte by an electrochemical technique [35]. The principle of this class of sensor is based on an interaction between a biological material and target analyte. This interaction generates a redox reaction, resulting in movement of electrons which is detected by transducer. This interaction signal is then converted to electrical signals, which are amplified and measured. Thus, electrochemical biosensor involves changing chemical/biological interactions into electrical signals. Enzymes, antibodies, nucleic acids and lectins are the most common biological materials used as a probe [36-38].

The ideal biosensor should be characterized by important characteristics as follows:

Specificity: A biosensor should respond to the target analyte specifically.

Durability: It should withstand repeated usage, perhaps after a suitable regeneration method.

Independent nature: It should not be easily affected by the surrounding environments such as temperature and pH.

Stability in results: the obtained results can be repeated.

Portability: it should be minimized and easy to use in everywhere.



### 2.2.1 Components of an electrochemical biosensor

An electrochemical biosensor mainly consists of three parts. The first part, a biological receptor such as enzymes, antibodies etc., of which the main function is to bind selectively with the target analyte and may subsequently induce a chemical reaction. The second part of a biosensor is a transducer. The function of the transducer is to convert the biological interaction into a measurable signal. This

detected signal is eventually processed and displayed on a displaying unit which is the third part of a biosensor component (often a computerized one). This signal is transformed in a user-friendly way. In order to fabricate electrochemical biosensor, the biological receptor is immobilized on the transducer surface (in electrochemical technique, the transducer refers to electrode surface) which acts as a point of contact between the transducer and analyte. When the bio-receptor component on the surface interacts with the target analyte, a physicochemical change of the transducer surface is produced. This change is detected by the transducer and converted into electric signals. The signals were then amplified, interpreted and finally displayed in a form that can be related to the amount of analyte presented in the sample [39]. Component of an electrochemical biosensor is summarized in Figure 2.5.

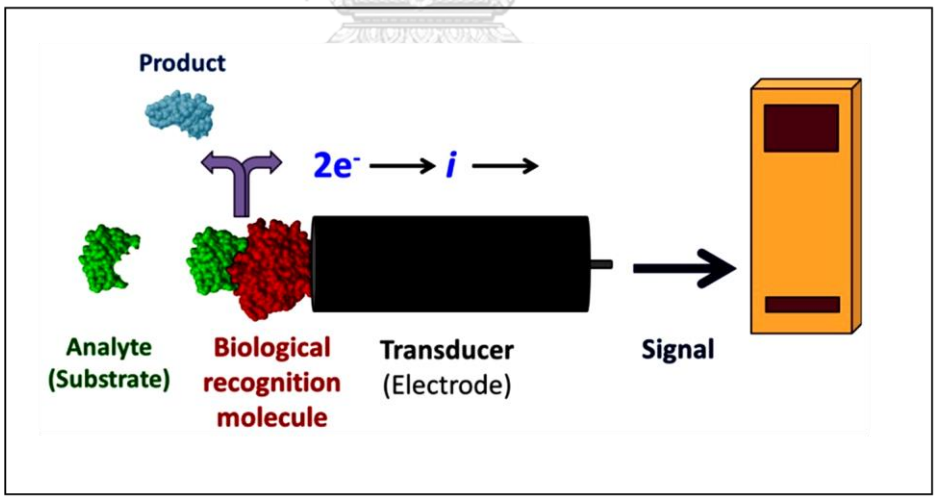


**Figure 2.5** Component of an electrochemical biosensor [39].

### 2.2.2 Applications of an electrochemical biosensor

Electrochemical biosensors have been extensively applied for various fields of our life science [35]. The application of a biosensor can be summarized as follows:

Clinical application: it has been employed in diagnosis of various diseases.

Industrial application: numerous manufacturing methods can be monitored by biosensors to provide the assistance regarding to increase the quality and quantity of obtained product.

Environmental application: a biosensor helps in evaluating the quality of water, heavy metal, organic molecules or microbial contamination of natural resources helping in developing steps to obtain a better environment.

Military application: a biosensor helps to identify explosives, drugs etc.

Drug development: it assists to detect and analyze certain side effects caused by medicine which has demonstrated a very usefulness for drug designing.

The benefits of electrochemical biosensors include accuracy in results, short-time detection capability, ease of preparation and use, and the possibility for multiplex and continuous monitoring. So it becomes a compatible with many detection motifs.



## 2.3 Peptide nucleic acid (PNA)

Peptide nucleic acid (PNA) is an important synthetic analogue of DNA. PNA was introduced by Nielsen's group more than twenty years ago [40-42]. PNA consists of a peptide-like backbone replacing the sugar-phosphate in natural DNA or RNA (Figure 2.6). PNA is widely used in nucleic acid sensing applications due to its excellent characteristics, such as a strong and sequence-specific binding to DNA and RNA and resistance to nucleases and proteases. PNA binds to its complementary DNA or RNA following the Watson & Crick base pairing rules similar to DNA-DNA and DNA-RNA duplexes [42]. Because of these excellent properties, PNA has become one of

the most widely used probes apart from oligodeoxynucleotice for biosensing of nucleic acids. The use of PNA probe in electrochemical DNA biosensors has been shown to give higher sensitivity and specificity, fast hybridization kinetics that is independent of ionic strength and allow the use of shorter probe length than DNA or RNA [43].

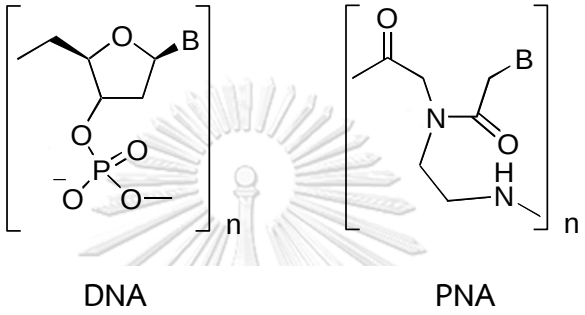


**Figure 2.6** Comparison of PNA and DNA structures.

### 2.3.1 Structural development of peptide nucleic acid

After the discovery of PNA, many research groups have attempted to develop new PNA systems that can provide the improvement of properties such as binding affinity or specificity. Recently, a new pyrrolidinyl PNA system was developed by Vilaivan's group. The newly developed PNA system (known as acpcPNA) possesses an $\alpha,\beta$-peptide backbone deriving from D-proline/2-aminocyclopentanecarboxylic acid [44, 45]. The repeating units of DNA, Nielsen's PNA and acpcPNA are illustrated in Figure 2.7. The acpcPNA shows a stronger binding affinity and higher specificity toward complementary DNA target than Nielsen's PNA. This PNA system has been used as a probe to detect the target DNA in combination with suitable detection techniques such as MALDI-TOF mass spectrometry, surface plasmon resonance (SPR), and electrochemical detection [46-49].

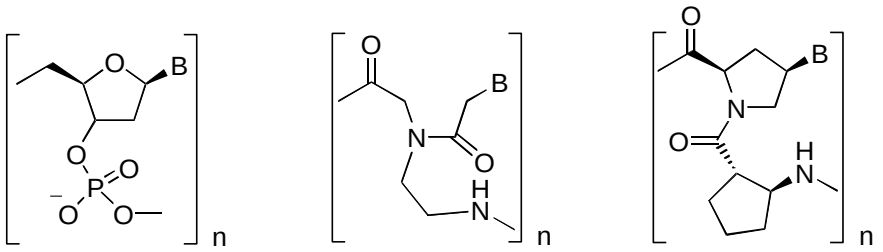


**DNA** **Nielsen's PNA** **Vilaivan's *SS*-acpc PNA**

**B = A, T, C, G**

**Figure 2.7** Contrast of the repeating units between DNA, Nielsen's PNA and acpcPNA [40, 44].

As aforementioned advantages of this PNA system, it is therefore suitable to be developed and employed as a sensing probe and coupled with a portable electrochemical sensing technique.

## 2.4 Immunoassay

Immunoassay methods have been widely used in numerous important areas such as diagnosis of diseases, therapeutic drug monitoring, clinical pharmacokinetic and bioequivalence studies in drug discovery and pharmaceutical industries [16]. This method integrates the binding reaction of a target molecule (antigen) with an antibody. The antibodies have a common structure but they have differently special components that assist them recognize and bind to specific antigens. The specificity of antibodies which enable them to interact to various antigens is displayed in Figure 2.8.

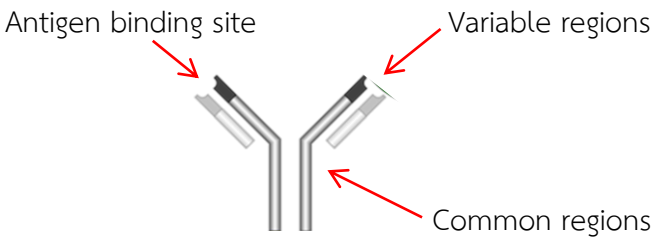


**Figure 2.8** Schematic representation of antibody structure.

Immunoassays can be considered as one of bioanalytical methods that offer sensitive and selective determination of an interested analyte. This bioanalytical method involves specific interaction between antigen and antibody. Depending on the type of assays, labels are always attached either on the antigen or the antigen to generate measurable signal. These label molecules can either be radioactive isotopes, redox-species, chemiluminescent tags or enzymes that cause changes in color, produce light or generate electrical signal [16]. In the process, when the immunoanalytical reagents are mixed and incubated, the analyte is bound to the antibody establishing an immune complex. This complex is physically or chemically separated from the excess reagent. Analysis is obtained by evaluating the label activity in either of the bound or free fraction. To determine the analyte in a sample, a standard curve is then constructed. This curve represents the evaluated signal as a function of the concentration of the analyte. The basic components of an immunoassay are illustrated in Figure 2.9.

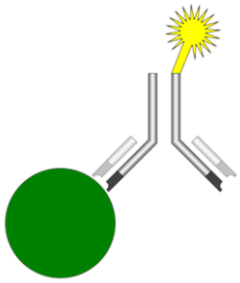

**Figure 2.9** Illustration of the basic components of an immunoassay, which includes an analyte (green), an antibody (black), and a detectable label (yellow).

### 2.4.1 Enzyme-linked immunosorbent assay (ELISA)

ELISA is one of the most popular immunoassay which operates on principles very similar to other immunoassay techniques. ELISA principle relies on specific antibodies to bind with target antigen, and a detection system used to specify the presence and quantity of antigen binding [16]. ELISA is a plate-based assay technique designed for measuring and quantifying target antigens such as peptides, proteins, antibodies and hormones. In an ELISA, an antigen must be anchored to a solid surface and then complexed with an antibody that is linked to an enzyme. Detection is accomplished by assessing the conjugated enzyme activity via incubation with a substrate to produce a measureable product. The most essential element of the detection method is a highly specific antibody-antigen interaction.

### 2.4.2 Common types of ELISA

ELISAs can be accomplished with a number of modifications to the basic process: direct, indirect, sandwich or competitive. The key step involves immobilization of the antigen to the assay plate which can be directly or indirectly performed. The antigen is then detected either directly (enzyme-labeled primary antibody) or indirectly (enzyme-labeled secondary antibody). The signaling antibodies are usually labeled with alkaline phosphatase (AP) or horseradish peroxidase (HRP).

Various substrates are available for performing the ELISA with an HRP or AP conjugate. The selection of substrate depends upon the required assay sensitivity and the instrumentation available for signal-detection (spectrophotometer, fluorometer or luminometer). Among the standard assay formats, it is important to differentiate between the particular approaches that exist specifically for the detection step since the detection step (as either direct or indirect detection) largely determines the sensitivity of an ELISA. The most common types of ELISA are as follow:

Direct ELISA:

For direct detection, coated antigen on the multi-well plate is measured by adding an enzyme-conjugated antibody to form the antigen-antibody complex and followed by washing step to remove excess enzyme-conjugated antibody. The signal of the antigen is detected by adding the enzyme's substrate. A direct ELISA test is considered to be the simplest type of ELISA.

Indirect ELISA:

For indirect detection, the antigen is detected in two stages or layers. First, an unlabeled primary antibody, which is specific for the antigen, is applied to bind with an antigen. Next, an enzyme-conjugated secondary antibody is bound to the first antibody. The secondary antibody is often polyclonal. The indirect assay is the most popular format for ELISA.



Sandwich ELISA:

Sandwich ELISAs typically require the use of matched antibody pairs, where each antibody is specific for a different epitope of the antigen molecule. A first antibody is coated to the wells and the sample solution is then added to the well, followed by adding of a secondary antibody (known as detection antibody) in order to determine the concentration of the sample. This type of ELISA provides high specificity, selectivity and sensitivity as well as flexibility of methods used.

Competitive ELISA

Competitive ELISA is a competitive binding process between original antigen and added antigen. This method is different in some respects compared to direct, indirect and sandwich ELISA assays. The competitive ELISA is normally applied to determine the concentration of an analyte in a sample by detecting interference in an expected signal output. The advantage of this method is its sensitivity to compositional differences in complex antigen mixtures, even when the specific detecting antibody is present in relatively small amounts. The four common types of ELISA are displayed in Figure 2.10.

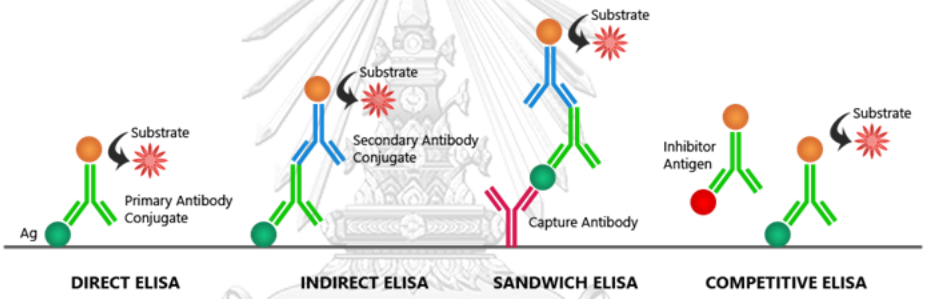


**Figure 2.10** Illustration of four most common ELISA types [16].



## 2.5 Food additives

Food additives can be any substances that are added to food to maintain or improve the quality of a food in some way for example to enhance the safety, freshness, taste, texture, or appearance of food. Some food additives have been in use for centuries for preservation such as salt, sugar and sulfur dioxide. Many different food additives have been developed to date to meet the requirements of food production. Additives are required to certify processed food remains safe and in good condition throughout its journey from factories to warehouses and shops, and finally to consumers.

Food additives can be obtained from plants, animals, or minerals and they can also be obtained from synthesis. They are purposely added to food to perform certain technological purposes. There are several food additives utilized, all of them are designed to do a specific function in making food safer or more appealing. However, these food additives can only be incorporated in certain food products, and they must fall within a specified dosage as well as have a justified purpose. A food additive overdose is considered as food adulteration, as these foods possess toxicity or lack any technical-functional purpose. Therefore, the use of food additives in the food industry requires ethical consideration [20-23].

### 2.5.1 Food colorant

Food colorants, either synthetic or in a natural form, are classified as a color additive which can be any dye, pigment or substance which when added to a food, drug or cosmetic, or to the human body, is capable of imparting color.

Sunset yellow (SY, E110) and tartrazine (TZ, E102), classified as azo dyes, are common synthetic colorants that are extensively employed in the food industry due to their low production cost, charming color uniformity and excellent water solubility as well as their high stability to light, oxygen and pH [17-19]. The structures of them are illustrated in Figure 2.11. However, they can cause detrimental effects to health when they are excessively consumed. Because they are harmful to human health, the use of colorants as food additives is strictly controlled by laws and regulations. The maximum acceptable content by the international and national legislation is 100 μg/mL when they are employed individually or in combination. The European University Association and some European countries such as Finland and Norway have already excluded these colorants and consider them to be carcinogenic agents According to Thai Food Act B.E. 2547, notification 281, colorants are not permitted to be incorporated into many food categories such as pickled/osmosed fruit, fresh-cut

fruit, processed meat, smoked meat and dried meat. Yet, some manufacturers illegally incorporate these substances into their products. The presence of colorants in food samples indicates that some food producers lack responsibility and ethics, and it also indicates that these colorants are still widely used in foods beyond the use permitted by rules and regulations. Therefore, a detection method that determines these synthetic colorants shortly, simply, sensitively and selectively is still in demand and important for food safety and human health.

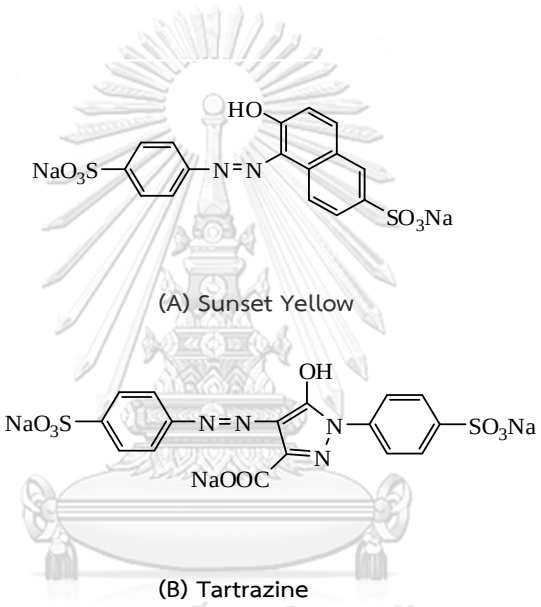




**Figure 2.11** Displaying the structures of synthetic colorants, sunset yellow (A) and tartrazine (B).

# CHAPTER III

# DEVELOPMENT OF ELECTROCHEMICAL SENSORS FOR CLINICALLY IMPORTANT BIOMARKERS DETECTIONS

In this chapter, the applications of the developed electrochemical biosensor can be separated into two parts. Part I presents the development of "signal on" electrochemical DNA biosensor (E-DNA) for the simultaneous determination of cervical cancer marker, high-risk human papillomaviruses (HPV) type 16 and 18 DNA, employing pyrrolidinyl peptide nucleic acid probes. Part II develops a novel electrochemical immunosensor based on anthraquinone-labeled signaling antibody using a screen-printed graphene electrode (SPGE) for a simple and highly sensitive determination of C-reactive protein (CRP).

# Part I:

## Influence of the DNA sensor design on the performance of the multiplex detection of HPV type 16 and 18 DNA

Sakda Jampasa [a], Weena Siangproh [b], Rawiwan Laocharoensuk [c], Pattamawadee Yanatatsaneejit [d], Tirayut Vilaivan [e], Orawon Chailapakul [f, g,*]

[a] Program in Petrochemistry, Faculty of Science, Chulalongkorn University, Pathumwan, Bangkok 10330, Thailand

[b] Department of Chemistry, Faculty of Science, Srinakharinwirot University, Bangkok 10110, Thailand

[c] National Nanotechnology Center (NANOTEC), National Science and Technology Development Agency (NSTDA), Pathumthani 12120, Thailand

[d] Human Genetics Research Group, Department of Botany, Faculty of Science, Chulalongkorn University, Bangkok 10330, Thailand

[e] Organic Synthesis Research Unit, Department of Chemistry, Faculty of Science, Chulalongkorn University, Pathumwan, Bangkok 10330, Thailand

[f] Electrochemistry and Optical Spectroscopy Center of Excellence, Department of Chemistry, Faculty of Science, Chulalongkorn University, Pathumwan, Bangkok 10330, Thailand

[g] National Center of Excellence for Petroleum, Petrochemicals, and Advanced Materials, Chulalongkorn University, Pathumwan, Bangkok 10330, Thailand

[*]Author for correspondence

Manuscript submitted to: Sensors and Actuators B: Chemical

**ABSTRACT**

In this work, we designed and fabricated two new "signal-on" electrochemical DNA sensors based on a sandwich-hybridization employing pyrrolidinyl peptide nucleic acid probes with electrochemical sensing. The sensors comprised a capture PNA probe (P1) immobilized on a screen-printed carbon electrode (SPCE) and an anthraquinone-labeled signaling probe (AQ-P2) designed to be partially complementary to the target DNA either at upstream (ASU) or downstream (ASD) positions on the DNA sequence hybridized to the P1 probe. In the presence of the DNA target, the ASD sensor showed a higher signal response and a higher electron-transfer rate constant ($k_{et}$) when compared to the ASU sensor. The ASD sensor was therefore applied to simultaneously detect two high-risk human papillomavirus (HPV) DNA sequences. The target DNA was detected in the range of 0.1 to 100 nM, and the limits of detection (LODs) of 40 and 60 pM (S/N = 3) were obtained for HPV types 16 and 18, respectively. This developed sensor exhibited very high sensitivity and selectivity in determining the target DNA and was successfully applied to detect a PCR-amplified sample derived from HPV type 16 (SiHa) and 18 (HeLa) positive human cancer cell lines. The results suggested that the sensor performance is dependent on the relative positions of the capture and signaling probes. These findings are relevant for designing effective sensors, and the developed sensor can be readily applied to detect a wide range of DNA targets.

### 3.1 Introduction

Due to growing demands in DNA and RNA medical diagnostics, numerous DNA sensors using electrochemical, fluorescent and chemiluminescent methods have been continuously developed during the past few decades [50-53]. Although several of the detection approaches feature remarkably high sensitivity and generalizability, a DNA sensing methodology that is highly sensitive, selective, rapid and operationally convenient and requires relatively low quantities of sample volume has yet to be realized. Electrochemical DNA sensors (E-DNA) have attracted great interest because of their simplicity, portability, short analysis time, relatively low cost, high sensitivity, and small sample volume requirement - all of these are desirable for point-of-care diagnosis [54, 55]. The first E-DNA sensor introduced in 2003 was the electrochemical equivalent of an optical “molecular beacon” detection system [54]. General E-DNA sensing strategies based on the detection of hybridization-induced changes or shifts in the electrochemical signal of electrode-bound DNA probes carrying a redox-active tag such as ferrocene or methylene blue have been developed [56-58]. E-DNA sensors can be categorized into two modes of detection based on the observed signal: “signal-on” and “signal-off” [59, 60].



For a “signal-off” sensor, the mechanism is dependent on the change in the distance of the redox tag from the electrode caused by DNA-induced conformational change of the probe [61, 62]. These “signal-off” sensors inherently suffer from limited signaling capacity, in which only a maximum of 100% signal suppression can be attained under any experimental conditions [63-65]. In addition, at a low DNA concentration, the small change will be difficult to detect in the presence of large background signal from the probe. Furthermore, the signal may be subjected to various interferences, leading to false-positive results.

For the “signal-on” E-DNA sensors, a much-improved signal was obtained in the presence of complementary DNA without the aforementioned limitations.

Several “signal-on” E-DNA architectures have been developed including DNA pseudoknot, hybridization-based double-stranded DNA, a triblock structure, an inverted stem-loop, a triplex DNA structure, and a traditional E-DNA sensor probed at new frequencies [66-71].

According to previous reports, several factors can affect the performance of a DNA sensor. These include the sensor architecture, signaling mechanism and capture probe [72, 73]. The probe itself is arguably one of the most important factors that will determine the ultimate performance of the sensor. Due to several favorable characteristics of peptide nucleic acid (PNA), the use of PNA instead of DNA as probes has found widespread acceptance for the development of DNA biosensors [43]. PNA is an artificial DNA analogue in which the ribose phosphate ester backbone is replaced by a pseudo-peptide backbone. Following the discovery of the first PNA system, aegPNA, a conformationally restricted pyrrolidinyl PNA system with an $\alpha/\beta$-peptide backbone derived from D-proline/2-aminocyclopentanecarboxylic acid (acpcPNA) was then introduced by Vilaivan and co-workers [40-42, 45, 74, 75]. This acpcPNA system exhibits a stronger binding affinity and a higher specificity toward a complementary target DNA than DNA or aegPNA, and has been widely applied as a DNA sensing probe [48]. We had previously developed a “signal-off” E-DNA sensor for the examination of HPV type 16 DNA, employing an anthraquinone (AQ)-labeled acpcPNA as the probe immobilized on a screen-printed carbon electrode. A decreased electrochemical signal was caused by the increased rigidity of the PNA-DNA duplex compared to the unhybridized PNA probe, which affected the accessibility and electron transfer between the redox-active AQ label and the electrode surface. This DNA sensing platform was successfully applied to detect HPV type 16 DNA from PCR-amplified samples [73].

In this work, we report the design and fabrication of two new "signal-on" E-DNA sensors that utilize two PNA probes to electrochemically detect DNA in a

sandwich hybridization assay. The sensor is comprised of an unlabeled acpcPNA capture probe (P1) and an AQ-modified acpcPNA signaling probe (AQ-P2). AQ-P2 is specifically designed to hybridize with the target DNA at upstream (ASU) or downstream (ASD) positions on the sequence recognized by the P1 probe to ensure efficient electronic communication between the labeled molecule and the electrode surface. The influences of the sensor design and analytical parameters, such as the sensitivity, specificity and reproducibility were evaluated. Finally, this developed sensor was applied to detect a PCR-amplified sample derived from HPV type 16 (SiHa) and 18 (HeLa) positive human cancer cell lines to evaluate the applicability of this sensor in cervical cancer screening.

## 3.2 Experimental

### 3.2.1 Chemicals and reagents

For the fabrication of the SPCE, graphene ink and silver/silver chloride pads were purchased from The Gwent Group, United Kingdom. The screen-printed block was made by Chaiyaboon Co. Ltd. (Bangkok, Thailand). Polyvinyl chloride (PVC) used as the substrate for fabricating the electrode was obtained from a local market. Glutaraldehyde (Glu) (50% in water, Biochemica grade) was purchased from Fluka. Cysteamine (Cys) was obtained from Sigma-Aldrich. Potassium tetrachloroaurate(III) was purchased from Wako, Japan. The redox reporter, 4-(anthraquinone-2-oxy) butyric acid, was synthesized as previously reported [49]. Chemicals for preparation of the phosphate buffer saline (PBS) pH 7.4 which consisted of 140 mM NaCl, 2 mM $KH_2PO_4$, 10 mM $Na_2HPO_4$, and 2 mM KCl were purchased from Merck and were of analytical grade. Millipore Milli-Q purified water was used throughout the experiments.

The cervical cancer cell lines with type 16 (SiHa) and type 18 (HeLa) HPV infections were obtained from the Human Genetics Research Group, Department of Botany, Faculty of Science, Chulalongkorn University. Synthetic oligodeoxynucleotides of HPV type 16 and 18 sequences derived from a partial sequence of the L1 gene of HPV type 16 and 18 were chosen as the model target. The corresponding regions of the same gene in other types of HPV DNA were employed to design the non-complementary DNA to study the specificity of detection. These oligodeoxynucleotides as well as the forward and reverse primers used for the PCR were purchased from Pacific Science (Bangkok, Thailand). The sequences of the DNA oligonucleotides, primers and probes are tabulated in Table 3.1.

**Table 3.1** The sequences of the oligonucleotides, primers and employed probes

| Oligonucleotide | Sequence (5′-3′) |
|---|---|
| **HPV type 16** | |
| P1(16)-ASD | Lys-CATACACCTCCAGC-$NH_2$ (written in the N⟶C direction) |
| P1(16)-ASU | Lys-CATACACCTCCAGC-$NH_2$ (written in the N⟶C direction) |
| P2(16)-ASD | AQ-O-O-TTGCTTGTCA-Lys$NH_2$ (written in the N⟶C direction) |
| P2(16)-ASU | AQ-O-O-AAGAAGATCC-Lys$NH_2$ (written in the N⟶C direction) |
| HPV DNA(16)-ASD | 5′-GCTGGAGGTGTATG TTTT TGACAAGCAA-3′ |
| HPV DNA(16)-ASU | 5′-GGATCTTCTT TAGG GCTGGAGGTGTATG-3′ |
| Reverse primer type (16) | 5′-GCCTTAAATCCTGCTTGTAG-3′ |
| Forward primer type (16) | 5′-CACTATTTTGGAGGACTGGA-3′ |
| **HPV type 18** | |
| P1(18)-ASD | Lys-GGATGCTGCACCGG-$NH_2$ (written in the N⟶C direction) |
| P2(18)-ASD | AQ-O-O-ATTACCTGTC-Lys$NH_2$ (written in the N⟶C direction) |
| HPV DNA(18)-ASD | 5′-CCGGTGCAGCATCC TTTT GACAGGTAAT-3′ |
| Reverse primer type (18) | 5′-CCAAGGGGATATTGATCTAAG-3′ |
| Forward primer type (18) | 5′-GGATTGGAACTTTGGTGTTC-3′ |
| **Non complementary DNA** | |
| HPV DNA type 31 | 5′-CCAAAAGCCCAAGGAAGATCCATTTAAA-3′ |
| HPV DNA type 33 | 5′-CACATCCACCCGCACATCGTCTGCAAAA-3′ |

### 3.2.2 Apparatus and measurements

All electrochemical measurements and electrochemical impedance spectroscopy (EIS) were performed on a PGSTAT 30 potentiostat (Metrohm Siam Company Ltd.) and controlled with the General Purpose Electrochemical System (GPES) software. The surface morphologies of the Au-modified electrodes were verified using scanning electron microscopy (SEM) and 3D optical microscopy. In addition, energy dispersive X-ray (EDX) analysis was also employed to verify the presence of AuNPs on the electrode surface. The molecular weights of the PNA probes were determined on a Microflex MALDI-TOF mass spectrometer (Bruker Daltonik, Germany).

Electrochemical detection of the target DNA was accomplished using differential pulse voltammetry (DPV) under the optimized conditions: 50 mV amplitude and 15 mV step potential. Cyclic voltammetry (CV) with different scan rates in the range from 200 to 280 mV $s^{-1}$ was applied to investigate the kinetic rates of electron transfer of both sensors. Calibration curves were constructed by sequential addition of the target DNA from 0.1 nM to 1000 nM.



### 3.2.3 Design of sensors

The designs of the two sensors are shown in Figure 3.1. Fabrication of the sensors involved the immobilization of an unlabeled P1 capture probe onto a cysteamine/gold-modified electrode via an N-terminal lysine residue using glutaraldehyde as a cross-linking agent. The redox-active AQ label was covalently attached to the N-terminus of the signaling probe P2 through an amide bond. The AQ-P2 signaling probe (green line) was designed to be partially complementary to the upstream (ASU) (Figure 3.1(A)) or downstream (ASD) (Figure 3.1(B)) positions on the sequence hybridized by P1 probe (blue line), where a site upstream and

downstream both refer to relative positions at 5′ and 3′ in DNA (red line), respectively. A 4-base unhybridized gap was included in both systems as a spacer.

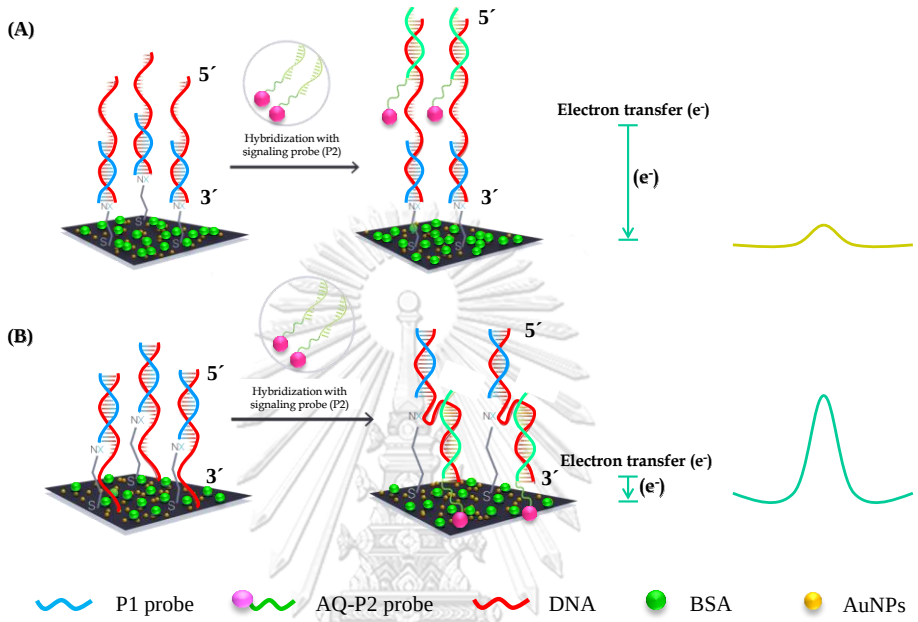


**Figure 3.1** Sensor architectures of ASU (A) and ASD (B) format.



### 3.2.4 Synthesis and labeling of the PNA probe

The conformationally constrained acpcPNA probes P1(16): Lys-CATACACCTCCAGC-$NH_2$ and P1(18): Lys-GGATGCTGCACCGG-$NH_2$ were employed as the capture probes. For the signaling probe (AQ-P2), the sequences AQ-O-O-TTGCTTGTCA-Lys$NH_2$, AQ-O-O-ATTACCTGTC-Lys$NH_2$ and AQ-O-O-AAGAAGATCC-Lys$NH_2$ were designed for P2(16)-ASD, P2(18)-ASD and P2(16)-ASU sensors, respectively (all sequences were written in the N to C direction, AQ = anthraquinone, O = aminoethoxyethoxyacetic acid). For the study of influence of sensor deign, only type 16 sequences were chosen as a model. Lysinamide was incorporated at the C-termini of the P2 probes as a PNA solubility enhancer and at the N-termini of the P1 probes

as a handle for immobilization of the P1 probe. All PNA probes were synthesized and labeled according to the previously developed procedure [45]. The PNA probes were synthesized on a Tentagel resin equipped with a Rink amide linker by standard Fmoc solid-phase peptide synthesis, as previously described [45]. After completion of the PNA syntheses, two units of {2-[2-(Fmoc-amino)ethoxy]ethoxy}acetic acid (O-linker) were incorporated at the N-terminus of the P2 probe to enhance the surface accessibility of the redox label. The Fmoc group of the O-linker of the P2 probe was removed by a brief treatment of 2% 1,8-diazabicycloundec-7-ene (DBU) + 20% piperidine in dimethylformamide (DMF) while still on the solid support (0.5 μmol). The free amino group was then treated with 4-(anthraquinone-2-oxy) butyric acid (4 equiv.), 1-[bis(dimethylamino)methylene]-1H-1,2,3-triazolo[4,5-b]pyridinium-3-oxide hexafluoro-phosphate (HATU) (4 equiv.), and *N*,*N*-diisopropylethylamine (DIEA) (16 equiv.) in DMF overnight at room temperature (25 °C). The progress of the reaction was monitored by MALDI-TOF MS analysis. The modified PNA on the solid support was then treated with 1:1 (v/v) aqueous ammonia:dioxane in a sealed tube at 60 °C overnight to remove the nucleobase protecting groups. The AQ-labeled P2 probe (AQ-P2) was then cleaved from the solid support with trifluoroacetic acid (TFA) and purified by reverse-phase HPLC (C18 column, 0.1% (v/v) TFA in $H_2O$-MeOH gradient). The identity of all PNA probes was verified by MALDI-TOF MS analysis, and the purity was confirmed to be >90% by reverse-phase HPLC.



### 3.2.5 Sample preparation

The PNA capture probes and DNA stock solutions were prepared in MQ water and kept in the refrigerator until use. The concentrations of the stock solutions were determined spectrophotometrically from the calculated molar extinction coefficients at 260 nm ($\boldsymbol{\varepsilon}_{260}$). The working PNA and DNA solutions were prepared by dilution of the stock solutions in PBS. The protocol for the amplification of SiHa (HPV type 16

positive) and HeLa (HPV type 18 positive) is illustrated as following. For the amplification of SiHa (HPV type 16 positive) and HeLa (HPV type 18 positive), HPVL1-F (5'-CACTATTTTGGAGGACTGGA-3'), HPVL1-R (5'-GCCTTAAATCCTGCTTGTAG-3'), HPVL1-F (5'-GGATTGGAACTTTGGTGTTC-3') and HPVL1-R (5'-CCAAGGGGATATTGATCTAAG-3') were employed as primers. The amplified fragment from the HPV L1 gene region consisted of 240 bp for type 16 and 195 bp for type 18. The reaction contained 0.4 μM of each primer, 0.2 mM deoxynucleotide triphosphate mixture, 1x buffer (KCl, Tris) + 1.5 mM $MgCl_2$, 0.5 U of Taq polymerase and 100 ng/μL of the cell line DNA sample. The amplification was conducted at 95 °C for 10 min, followed by 35 cycles at 95 °C for 10 s, 52 °C (SiHa) or 50 °C (HeLa) for 30 s, 72 °C for 30 s, and finally 72 °C for 7 min. The obtained PCR products were evaluated by size resolution in comparison with the known molecular weight markers using 2% (w/v) agarose gel-TBE electrophoresis and UV-transillumination visualization. Prior to the electrochemical detection of the cell line samples, the DNA duplexes were first denatured by heating at 100 °C for 10 min, followed by immediate cooling in an ice bath.



### 3.2.6 Fabrication of a dual-working SPCE

The disposable SPCE was prepared using an in-house screen-printing method as previously described [76]. The pattern of the electrode was designed using Adobe Illustrator (Figure 3.2). First, silver/silver chloride ink was printed onto a polyvinyl chloride (PVC) substrate as a base layer to be used as both a pseudo-reference electrode (RE) and the conductive pads. The commercial graphene ink was then printed onto the same PVC substrate as the second layer to form both the working (WE) (3 mm i.d.) and counter electrode (CE). Lastly, the insulator (nail polish) was then screened. The finished electrode was heated at 55 °C for 1 h to remove the residual solvents.

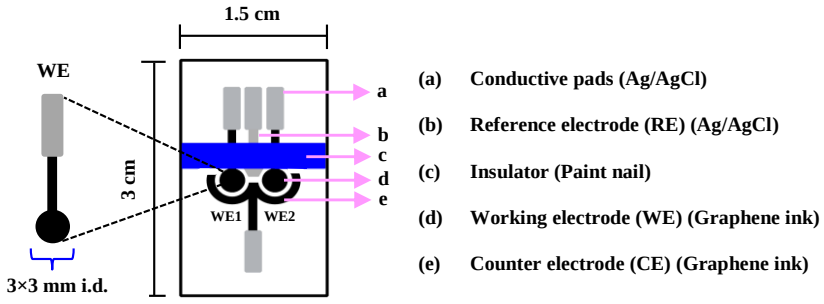


**Figure 3.2** The design of a dual-working SPCE.

### 3.2.7 Preparation of the DNA sensor and electrochemical measurement

Prior to the modification, the electrode surface was first cleaned with MQ water. The preparation of the sensor was previously described [77]. Briefly, 20 µL of a 5 mM potassium tetrachloroaurate(III) solution containing 0.5 M $H_2SO_4$ was dropped onto the electrode, and subsequent electrodeposition of gold nanoparticles (AuNPs) onto the electrode surface was induced by applying a constant potential of -0.5 V for 100 s. The Au-modified electrode (Au/SPCE) was then rinsed with MQ water and dried at ambient temperature. The Au/SPCE was subsequently treated with 2.5 µL of 10 mM Cys in PBS and left overnight at room temperature in a sealed box under a humid environment (minimum 90%) to prevent the evaporation of the solution. The prepared electrodes consisting of a self-assembled monolayer (SAM) of Cys (Cys/Au/SPCE) were rinsed twice separately with PBS and MQ water. Activation of the surface was then accomplished by incubating the Cys/Au/SPCE in Glu (15% w/v in PBS) for 4 h, followed by rinsing twice with PBS.

After formation of the Glu/Cys/Au/SPCE, the next step was the immobilization of the P1 capture probe by cross-linking of its lysine with the amino groups of Cys on the electrode surface. A 2.5 µL solution of the P1 probe (5 µM) was dropped onto the modified electrode and left in a humid box at RT overnight. Then, the electrodes were thoroughly washed twice with PBS to remove the excess and non-specifically adsorbed P1 probe on the electrode surface. The blocking step was next performed by dropping 2.5 µL of a 0.2% (w/v) bovine serum albumin (BSA) solution onto the P1-modified electrodes, followed by leaving for 1 h at RT. The electrode was then washed twice with PBS. These electrodes were denoted as P1/BSA/Glu/Cys/Au/SPCE. For the hybridization step, a designated concentration of the target DNA or denatured PCR product (2.5 µL) was dropped onto the working electrode region and left for 20 min, followed by extensive washing with PBS. The second hybridization with the AQ-P2 signaling probe was subsequently performed. The AQ-P2 solution (30 µM, 2.5 µL) was dropped onto the electrode surface and left for 30 min. The electrode was then rinsed with PBS to remove the excess AQ-P2 probe. PBS buffer (20 µL) was dropped onto the electrode surface again prior to the electrochemical measurement. In all cases, DPV was carried out at room temperature (25 ± 1 °C) with a 50 mV amplitude and 15 mV step potential. The preparations of the sensor are summarized in Figure 3.3.

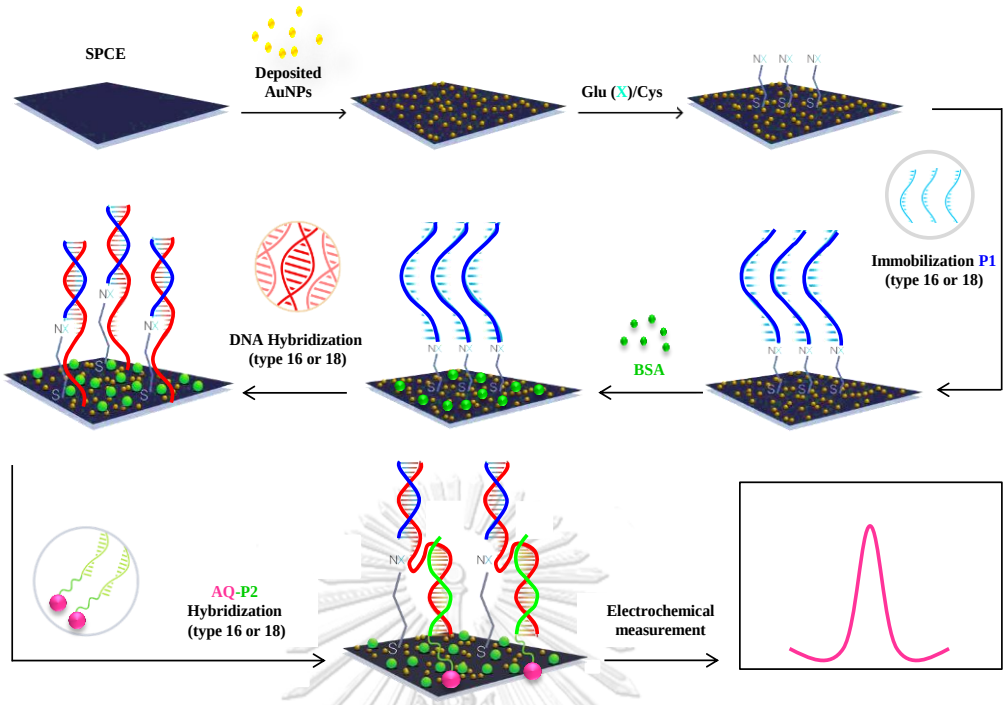


**Figure 3.3** Schematic illustration of preparation of the DNA sensor and electrochemical measurement.

For evaluation of the specificity, the electrochemical measurement was performed as above using the non-complementary oligodeoxynucleotides corresponding to partial sequences of the L1 genes of HPV type 31 and 33 DNA (Table 3.1).



## 3.3 Results and Discussion

### 3.3.1 Characterization of the modified electrode

#### 3.3.1.1 SEM and 3D optical microscopic techniques

To characterize the surface morphologies of the unmodified and modified electrodes, SEM and 3D optical microscopic techniques were employed. AuNPs were first electro-deposited onto the electrode surface to enhance the conductivity of the sensor and to immobilize the capture probe. When AuNPs were electro-deposited

onto the electrode surface, a homogenous distribution and size were observed (Figure 3.4(B)), while the unmodified electrode had no AuNPs present (Figure 3.4(A)). This result proved that AuNPs were successfully deposited onto the electrode surface [78]. The uniform distribution of granular AuNPs could substantially increase the effective surface area of the electrode, which will largely increase the probe loading amount [79].

An optical microscopic technique was also utilized to observe the distribution of AuNPs on the entire electrode surface. As presented in Figure 3.4(D), the Au/SPCE exhibited a homogeneous yellow color from the AuNPs over the entire electrode surface (observed by the naked eye), indicating that the entire electrode surface was uniformly covered by AuNPs compared to the SPCE (Figure 3.4(C)). In addition, the changed surface roughness was examined after the electrodeposition of AuNPs and was calculated to be 3.00 ± 0.08 μm and 2.59 ± 0.11 μm (n = 5) using 3D optical microscopy for the SPCE and Au/SPCE, respectively. This result was also supported by colored-gradient height maps. The red, green and blue colors represent the various depths or surface roughnesses of the electrode surface from the highest to lowest level. As demonstrated in Figure 3.4(D) (inset), most of the surface area was blue after the electrodeposition of AuNPs, which implied that the electrode surface was relatively smooth compared to unmodified electrode (Figure 3.4(C) (inset)). The addition of AuNPs on the electrode surface provides more PNA capture probe anchoring sites. This can lead to an increase of the target DNA hybridization onto the electrode surface, which will ultimately amplify the signal.

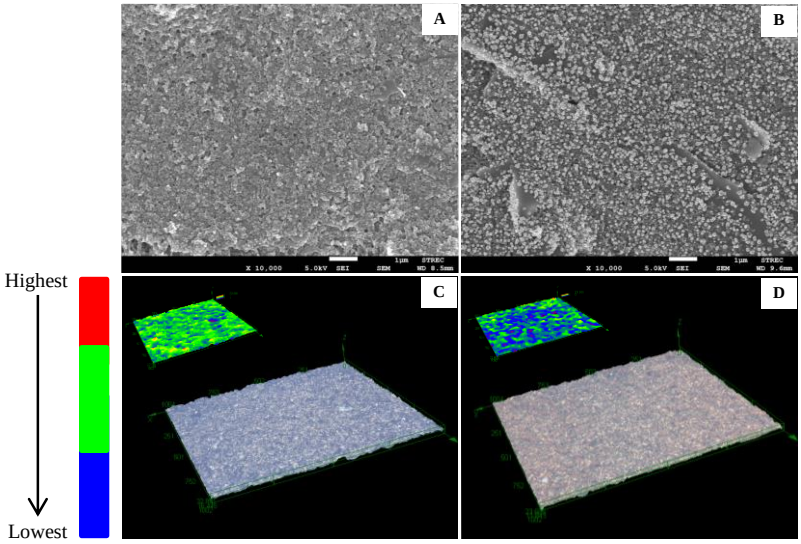


**Figure 3.4** SEM and optical images of the unmodified (A and C) and Au-modified SPCE (B and D).

### 3.3.1.2 Calculation of the electroactive surface areas of the modified electrode

The effective surface area (A) of the unmodified and AuNP-modified SPCEs were calculated employing CV in a 10.0 mM $Fe(CN)_6^{4-/3-}$ solution containing 0.1 M KCl at various scan rates, according to the Randles-Sevcik equation:



$$i_p = 2.69 \times 10^5 \, A \, D^{1/2} \, n^{3/2} \, v^{1/2} \, C \qquad \text{(Equation 3.1)}$$

where D is the diffusion coefficient of $Fe(CN)_6^{4-/3-}$, C is the concentration of $Fe(CN)_6^{4-/3-}$, and n is the number of involved electrons. As shown in Figure 3.5, the peak currents ($i_p$) of both the AuNP-modified (Figures. 3.5(C) and (D)) and unmodified electrodes (Figures. 3.5(A) and (B)) were proportional to the square root of the scan rate. With constant parameters of D ($7.6 \times 10^{-6}$ $cm^2$ $s^{-1}$), C (10 mM) and n (1 electron), approximate values of the electroactive surface areas were successfully achieved. The electroactive surface areas were determined to be 0.084 ± 0.0031 $cm^2$ and 0.024

± 0.0054 $cm^2$ for the AuNP-modified and unmodified electrodes, respectively, where the electroactive surface area of the electrode increased by 3.5-fold upon incorporating AuNPs. The increased electroactive surface area can also represent the enhanced conductivity of the electrode. These results suggest that AuNPs truly improved the sensitivity of the sensor as expected [52].

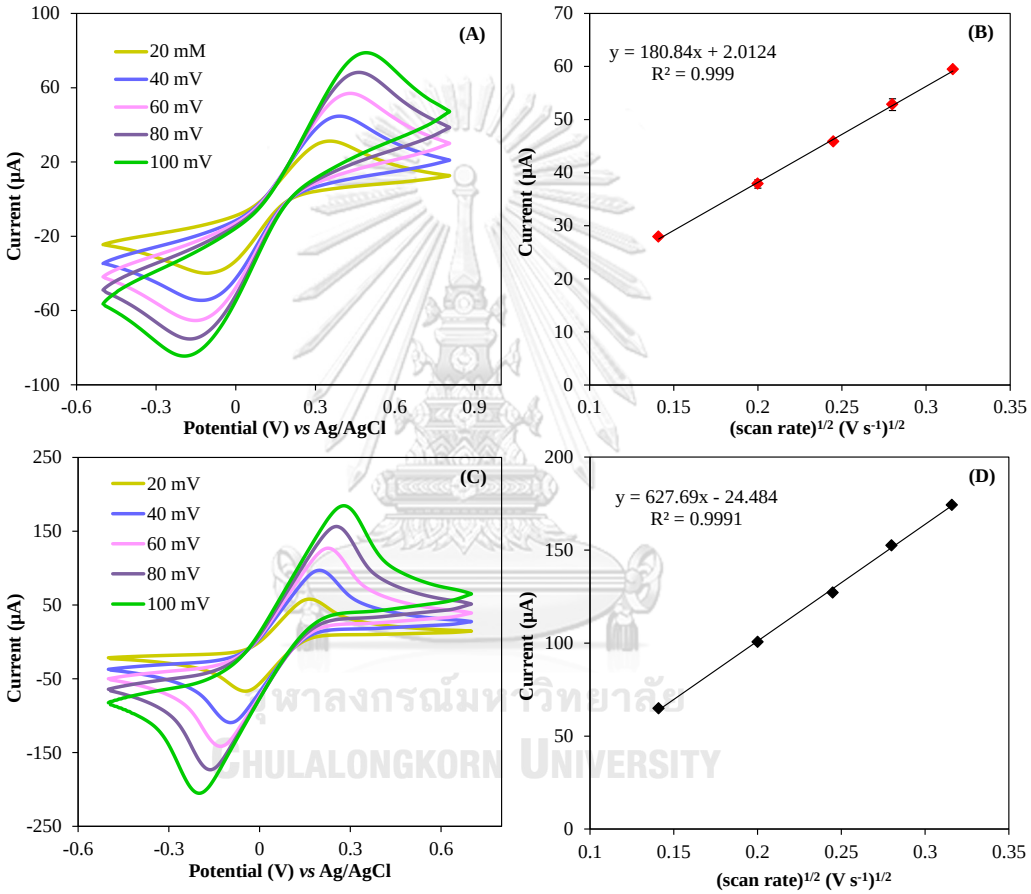


**Figure 3.5** CVs of the unmodified (A and B) and Au-modified SPCE (C and D) in 10.0 mM $Fe(CN)_6^{4-/3-}$ at different scan rates from 20 to 100 mV $s^{-1}$.

### 3.3.1.3 EDX spectrum analysis of AuNPs

Energy dispersive X-ray (EDX) analysis was also employed to detect the presence of AuNPs on the electrode surface. The spectrum shows a characteristic peak at 2.10 keV for the AuNPs (Figure 3.6(B)). The peak from the EDX analysis indicated that AuNPs (less than 100 nm in size) and gold nanoparticle agglomerates (≥ 250 nm) (Figure 3.6(A)) were present on the electrode surface [80].

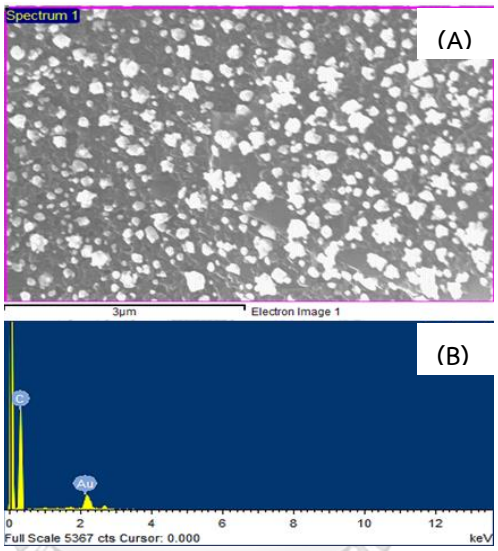


**Figure 3.6** Particles size of AuNPs (A) and EDX spectrum analysis (B).



### 3.3.1.4 Characterization of the modified electrode step by step using EIS

EIS was employed to verify the successful fabrication of the sensor step by step. In this characterization, the fabricated sensor using HPV type 16 was only utilized. This method studied the impedance changes of surface-transfer electrodes. The EIS profiles with different modified electrodes are illustrated in Figure 3.7. In the Nyquist plots, the semicircle diameters in the high-frequency region reflect the electron-transfer resistance ($R_{et}$), which controls the electron-transfer kinetics of the redox probe employed $Fe(CN)_6^{4-/3-}$ at the electrode interface. The Au/SPCE exhibited a nearly straight line at high frequencies (curve b (inset)), whereas the bare SPCE was

nonlinear with an extremely high $R_{et}$ of 7568 Ω (%RSD = 1.33) (curve a). This conspicuously demonstrated the excellent electron-transfer kinetics of the modified electrode. When Cys and Glu were self-assembled on the AuNP-modified SPCE, a 115 Ω (%RSD = 3.12) increase in $R_{et}$ (curve c (inset)) was observed. This increase in the resistance is explained by the fact that Cys and Glu possess nonconductive properties. These self-assemblies also possessed surface blocking properties, which made the surface accessibility difficult for the $Fe(CN)_6^{4-/3-}$ redox couple. Additionally, after the immobilization of the P1 capture probe and the blocking step, the $R_{et}$ further increased to 413 Ω (curve d (inset)) (%RSD = 5.01). This indicates that the immobilization of the P1 probe was successful. When the P1 capture probe was hybridized with the target DNA, $R_{et}$ greatly increased to 1132 Ω (%RSD = 6.23) (curve e (inset)). This is likely attributed to the PNA-DNA duplexes formed on the electrode surface, which resulted in a considerable increase in the negative charge of the DNA layer. Therefore, the electrostatic barrier to the negatively charged $Fe(CN)_6^{4-/3-}$ redox couple increased, causing an increase in the charge-transfer resistance [52]. This result suggests that DNA hybridization on the electrode surface was favorable. Moreover, the $R_{et}$ increased by 174.09 % after the hybridization step was conducted. This also indicates that the EIS method can be used to identify HPV DNA.

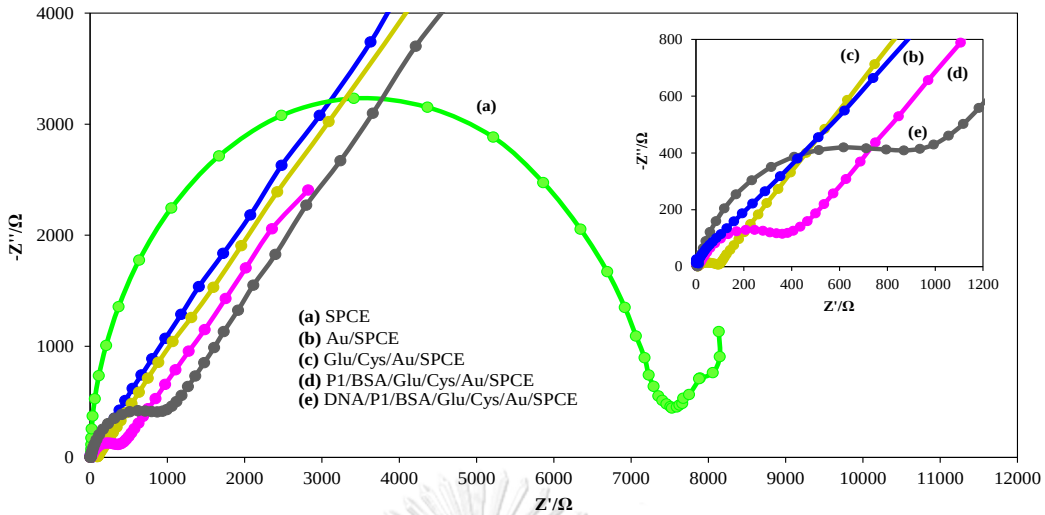


**Figure 3.7** Nyquist impedance comparison between unmodified (a) and the modified electrode for type 16 (inset b-e) in DNA detection in 10 mM $Fe(CN)_6^{4-/3-}$.

### 3.3.2 Influence of the sensor design and characteristics

The sensor architecture and signaling mechanism of these two proposed sensors are shown in Figure 3.1. A DNA target sequence associated with HPV type 16 DNA was chosen as a model. The P1 probe employed in the fabrication of both sensor designs possessed the same 14-base sequence, while the P2 probe for each design consisted of different 10-base sequences depending on its recognition site. The AQ redox-active label was located at the N-terminus of the P2 probe to ensure efficient electron transfer to the electrode surface. The successful syntheses of the capture P1 and labeled P2 probes were confirmed by MALDI-TOF mass spectrometry (Figure 3.8). The identities of the PNA capture probes were verified by MALDI-TOF MS after the syntheses. The *m/z* values of the P1 capture probes were found to be 4757.7 [P1(16): calcd *m/z* for $M{\cdot}H^+$ = 4759.1] and 4944.0 [P1(18): calcd *m/z* for $M{\cdot}H^+$ = 4945.4] for HPV types 16 and 18 (Figures 3.8(A) and (C)), respectively. These *m/z* values confirmed that the syntheses of the P1 capture probes were successful. In the syntheses of the P2 probes, they were modified with redox-active AQ to make them

electrochemically detectable. The unlabeled P2 probes showed mass peaks at *m/z* = 3494.4 (calcd *m/z* for $M{\cdot}H^+$ = 3495.3) and 3463.5 (calcd *m/z* for $M{\cdot}H^+$ = 3464.0) for types 16 and 18 (ASD), and 3538.6 (calcd *m/z* for $M{\cdot}H^+$ = 3540.1) for type 16 (ASU), respectively. After labeling with AQ, the *m/z* value increased to 4074.9 for type 16 (ASD) [P2(16)-ASD: calcd *m/z* for $M{\cdot}H^+$ = 4077.7] and 4046.9 for type 18 (ASD) [P2(18)-ASD: calcd *m/z* for $M{\cdot}H^+$ = 4047.9], and 4115.9 for type 16 (ASU) [P2(16)-ASU: calcd *m/z* for $M{\cdot}H^+$ = 4116.9] sensors (Figures 3.8(B), (D), (E) and (F)). The mass increment of 580 Da coincides with the mass of the AQ label and two O-linker units, thus indicating the successful labeling of the P2 probes. The electrochemical behavior of the AQ-labeled P2 probes was investigated using DPV, where the redox peak of AQ appeared at approximately -0.75 V. This peak was then used to monitor the target DNA and the sensor behavior.

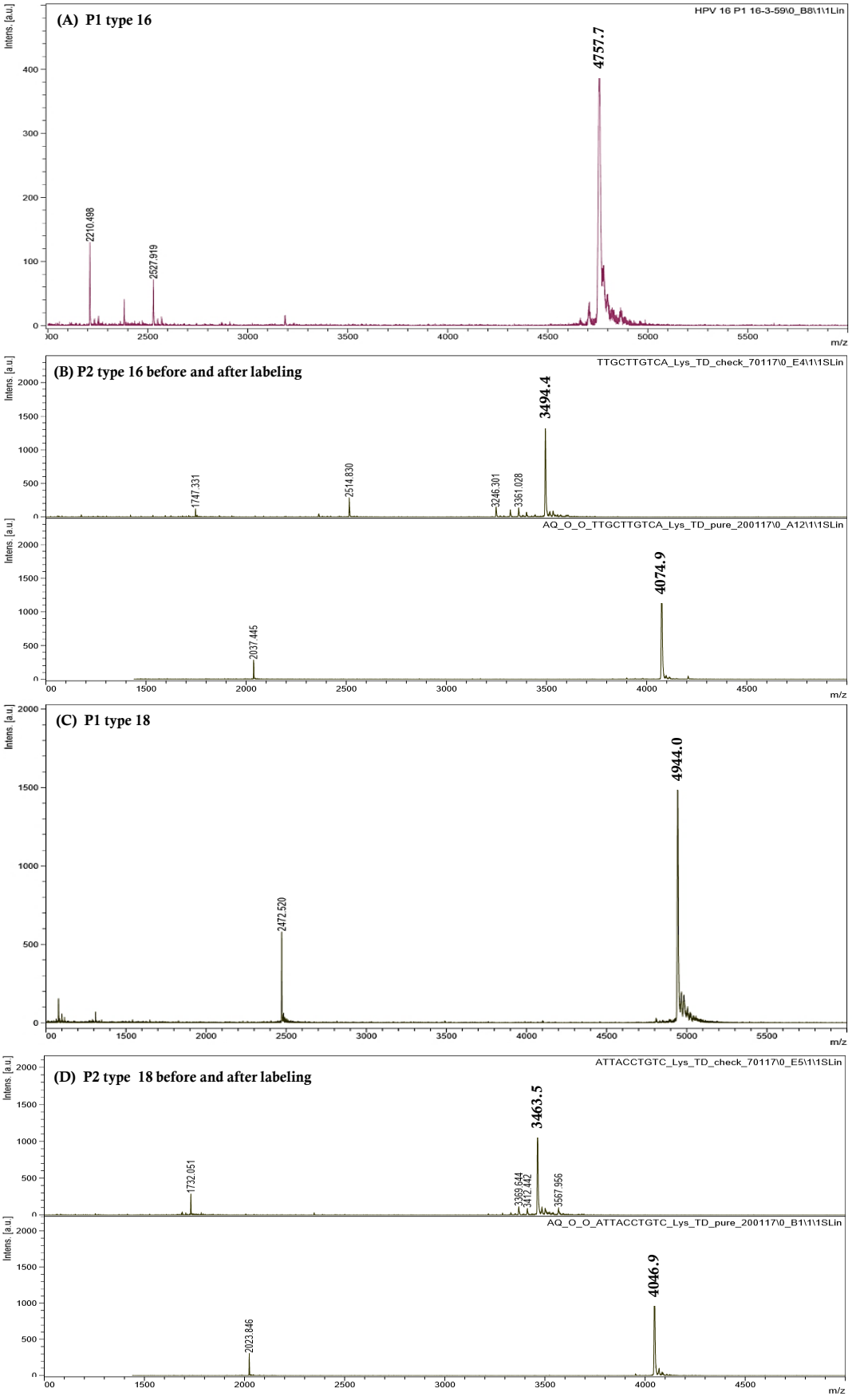
(A) P1 type 16
HPV 16 P1 16-3-59\0_B8\1\1Lin
4757.7
2210.498
2527.919
Intens. [a.u.]
m/z
(B) P2 type 16 before and after labeling
TTGCTTGTCA_Lys_TD_check_70117\0_E4\1\1SLin
3494.4
1747.331
2514.830
3246.301
3361.028
AQ_O_O_TTGCTTGTCA_Lys_TD_pure_200117\0_A12\1\1SLin
4074.9
2037.445
(C) P1 type 18
4944.0
2472.520
(D) P2 type 18 before and after labeling
ATTACCTGTC_Lys_TD_check_70117\0_E5\1\1SLin
3463.5
1732.051
3369.644
3412.442
3567.956
AQ_O_O_ATTACCTGTC_Lys_TD_pure_200117\0_B1\1\1SLin
4046.9
2023.846

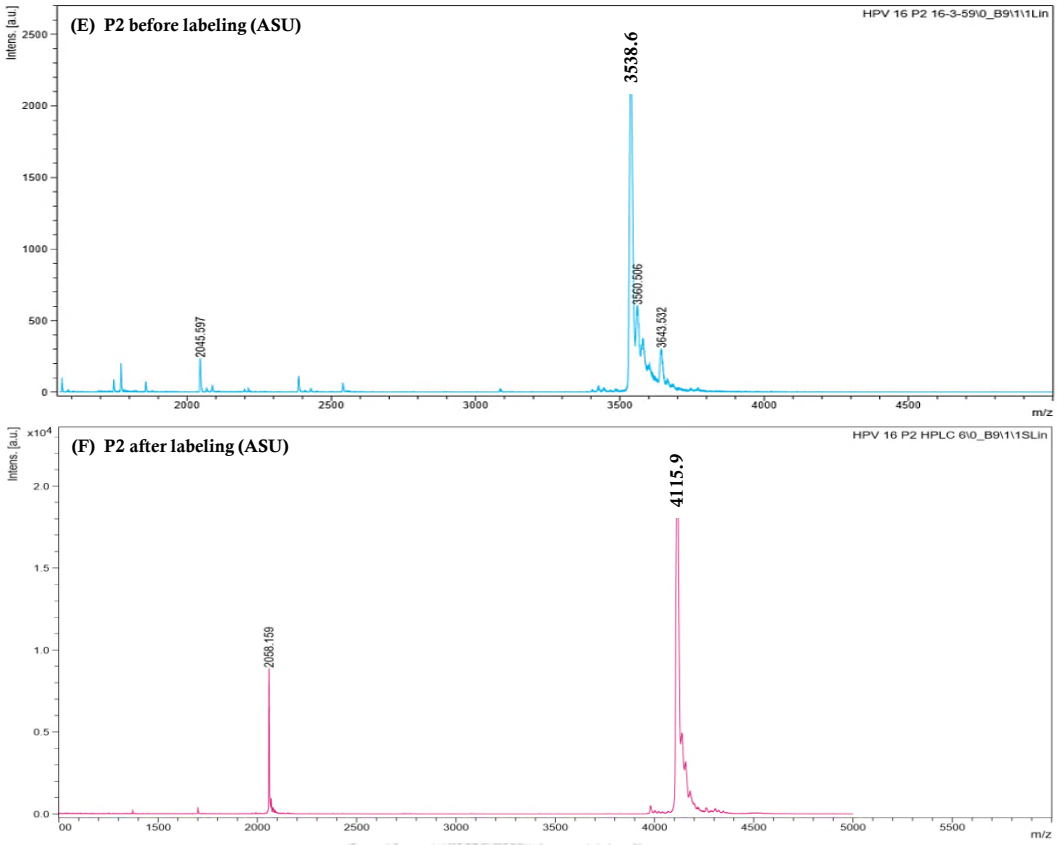


**Figure 3.8** MALDI-TOF mass spectra of P1 probe (A and C) and before and after P2 probe labeling with AQ (B, D, E and F).

In this work, ASU and ASD represent the hybridization regions of the reporter probe at the upstream and downstream sites relative to the P1 probe hybridization region, respectively. To investigate the sensor behaviors, DPV was first implemented. As shown in Figure 3.9(A), the oxidation peak of the AQ labeling agent appeared at approximately −0.75 V in the presence of the target DNA using the ASD arrangement. In contrast, in the absence of the target DNA, the signaling probe P2 was removed from the electrode during the washing step, and consequently, the AQ peak was not observed. Indeed, after the sandwich hybridization, it was found that the AQ peak current was increased for both the ASU and ASD sensors (Figure 3.9(B)). However, a much smaller current was observed for the ASU sensor, thus indicating less efficient

electron transfer in comparison to the ASD sensor. The change in the position of the recognition site of the signaling probes therefore significantly affects the electron-transfer capability.

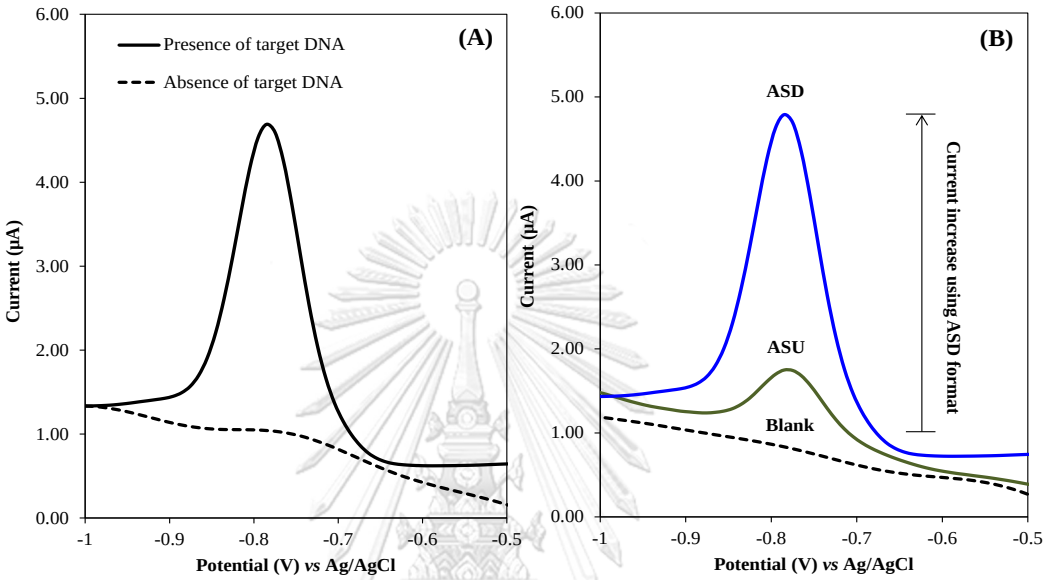


**Figure 3.9** DPV responses of ASD (A) and comparison of different sensor designs between ASD and ASU sensor (B) in the presence and absence of 100 nM target DNA in PBS pH 7.4.



### 3.3.3 Influence of scan rates on the kinetic of sensors

To calculate the electron-transfer rate constant ($k_{et}$), a series of CV scan rates were collected (from 200 to 280 mV $s^{-1}$). With an increase of the scan rate, the reduction peak moved negatively, and the oxidation peak moved positively. The increasing value of the CV peak separation ($\Delta E_p = E_{p,a} - E_{p,c}$) as a function of the increasing scan rate (v) suggests that the rate of heterogeneous electron transfer changed. As shown in Figures 3.10(A) and (B), a plot of $E_p$ versus log (v) yields a straight line that is in accordance with the Laviron equation (Equations 3.2, 3.3 and 3.4) [72, 81].

$E_{p,a} = E° + 2.3RT\log(v)/(1-\alpha)nF$ (Equation 3.2)

$E_{p,c} = E° - 2.3RT\log(v)/\alpha nF$ (Equation 3.3)

$\log k_{et} = \alpha\log(1-\alpha) + (1-\alpha)\log\alpha - \log(RT/nFv) - \alpha(1-\alpha)nF\Delta E_p/2.3RT$ (Equation 3.4)

where $k_{et}$ is the electron transfer rate constant ($s^{-1}$), $\alpha$ is the electron transfer coefficient, v is the CV potential scan rate ($V\ s^{-1}$), and $\Delta E_p$ is the difference between the anodic potential ($E_{p,a}$) and cathodic potential ($E_{p,c}$) (V). The value of $\alpha$ can be determined from the slope of a linear fit, and $k_{et}$ can be calculated from the y-intercept. Two linear regression equations for $E_{p,a}$ and $E_{p,c}$ versus log(v) were obtained and are expressed as:

$E_{p,a}$ (V) = 0.1043 log(v) - 0.6412 ($R^2$ = 0.997) for the ASD sensor (Figure 3.10(A))

$E_{p,c}$ (V) = -0.128 log(v) - 0.8064 ($R^2$ = 0.991) for the ASD sensor (Figure 3.10(A))

$E_{p,a}$ (V) = 0.1895 log(v) - 0.5887 ($R^2$ = 0.992) for the ASU sensor (Figure 3.10(B))

$E_{p,c}$ (V) = -0.0611 log(v) - 0.7688 ($R^2$ = 0.997) for the ASU sensor (Figure 3.10(B))

The $k_{et}$ values were calculated to be $31.35 \times 10^6\ s^{-1}$ and $15.80 \times 10^3\ s^{-1}$ for the ASD and ASU sensors, respectively. The $k_{et}$ value of the ASD sensor was found to be considerably greater than that for the ASU sensor ($k_{et}$ ASD = $31.35 \times 10^6 \pm 0.23\ s^{-1}$ vs $k_{et}$ ASU = $15.80 \times 10^3 \pm 0.17\ s^{-1}$). The effect of the distance between the redox-active label and the electrode surface on the signaling behavior is consistent with the designs proposed. The evidence here indicates that the design affects the sensor performance [67, 68, 70-72].

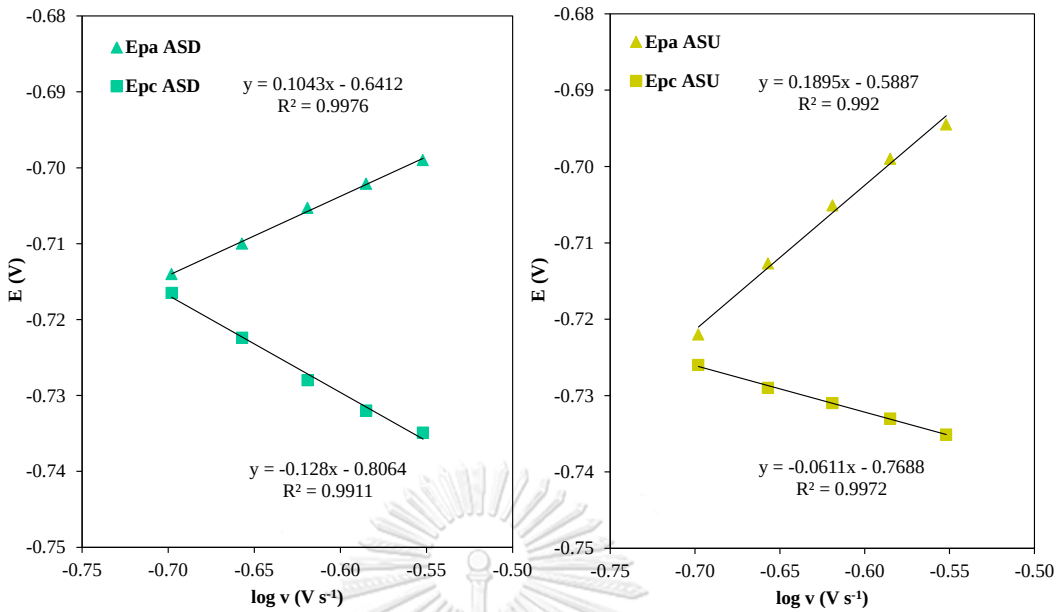


**Figure 3.10** A graph of $E_{p,a}$ and $E_{p,c}$ versus log v for ASD (A) and ASU (B) sensors at 100 nM target DNA in PBS pH 7.4.

### 3.3.4 Application of the developed sensor for the detection of HPV DNA

From the obtained results, the ASD sensor was applied to detect HPV type 16 and 18 DNA. The specific P1 probes of each HPV type were individually immobilized onto a dual-working electrode surface for the simultaneous detection of HPV type 16 and 18 DNA (Figure 3.11(A)). From Figure 3.11(B), when the sample solution contained both HPV DNAs, the characteristic AQ peak currents appeared at both WE1 and WE2 carrying the immobilized P1 probes specific for each HPV type. A cross-interference assay was also conducted as illustrated in Figure 3.11(C). With the sample solution containing only HPV type 16 DNA, a large peak current appeared only at WE1 containing the P1 probe specific for HPV type 16. Virtually no signal was observed at WE2 containing the P1 probe specific for HPV type 18. This demonstrated that WE1 showed a good response and selectivity for HPV type 16 DNA. Similarly, when the fabricated sensor was exposed to a solution containing HPV type 18 DNA, the peak current of AQ was apparent only at WE2 and not at WE1 (Figure 3.11(D)). The

evidence here indicates that the fabricated sensors have good specificities without cross-interference, which is essential for the simultaneous detection of DNA mixtures.

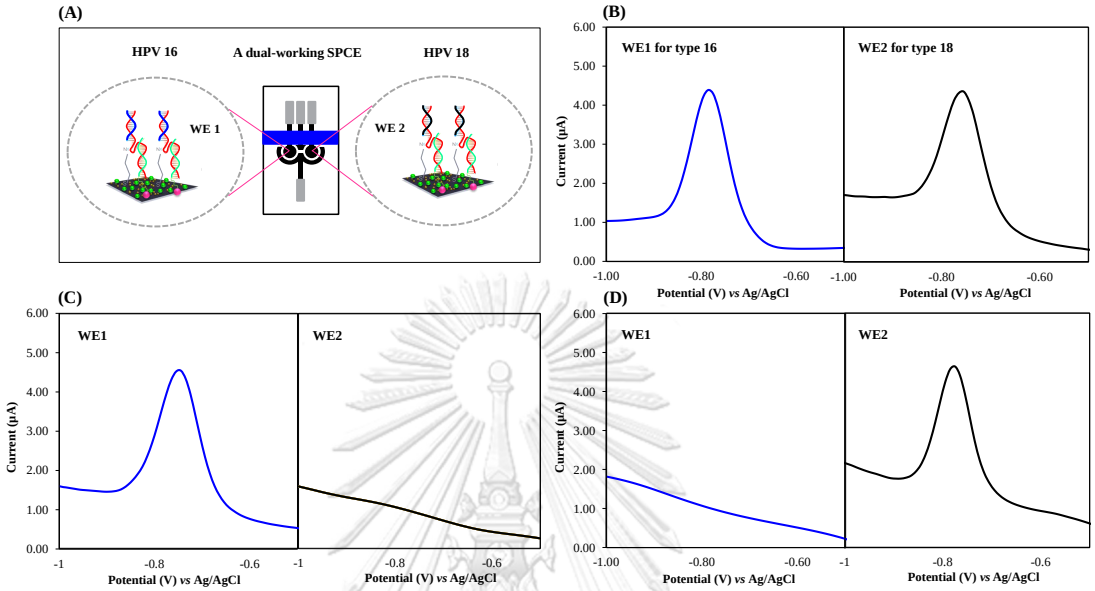


**Figure 3.11** Schematic illustration of a dual-working electrode where a specific probe was immobilized (A), DPVs response for the simultaneous detection of HPV type 16 and 18 DNA (B). Cross-interference assay of the proposed sensor for type 16 (C) and 18 (D) at 100 nM DNA concentration in PBS pH 7.4.



### 3.3.5 Optimization of variable parameters

To achieve an appropriate system, relevant parameters that could possibly affect the performance of the sensor, such as the probe concentration, hybridization time and BSA blocking agent, were individually optimized. All parameters were optimized using HPV type 16 as a representation of both HPVs. The concentration of the target DNA of 100 nM was employed in all the parameter optimizations. These optimized parameters were eventually applied to fabricate the sensor to detect both HPV types. A P1 probe concentration range from 1 to 20 μM was investigated. The result revealed that the electrochemical signal gradually increased with an increasing

P1 probe concentration and reached a maximum current at 5 μM (Figure 3.12(A)). Upon a further increase of the concentration, the obtained current progressively decreased. This could be due to the overcrowding of the probes assembled onto the electrode surface, which led to a difficulty in hybridizing with the target DNA and consequently decreased the signal. Therefore, 5 μM of the P1 probe was selected as the optimal probe concentration. For the optimization of the P2 signaling probe, the results exhibited that the signal amplified upon an increase of the P2 concentration from 10 to 30 μM and then reached a plateau (Figure 3.12(B)). This indicated that 30 μM was the optimal concentration. These results suggest that the electrode surface could be oversaturated, and therefore, there are a limited number of hybridized P1-DNA duplexes that could be formed on the electrode surface [52].

The effect of the hybridization time was studied in the time range of 5-80 min. The current signal increased gradually within 20 min for the first (Figure 3.12(C)) and 30 min for the second hybridization steps (Figure 3.12(D)). Lengthening the hybridization time showed a plateau of the signal for both hybridization steps. The signal plateau observed for both hybridization steps could be explained by the limited number of P1 probe molecules or P1-DNA duplexes that could be formed on the surface. Considering the hybridization efficiency, 20 min was used as the appropriate time for the first hybridization, and 30 min was used for the second hybridization.



The surface conditions of the fabricated sensor are especially important for the performance of the DNA sensor, and hence, the effect of a BSA blocking content was studied. The electrode surface was blocked after the P1 probe immobilization step. In this section, we only focused on the elimination of the background signal produced from non-specific adsorption of the signaling probe on the electrode surface by adding BSA. The amount of BSA was varied from 0 to 1% (w/v). This valuable parameter was investigated in the absence of the target DNA (negative

control). The results showed that the amount of BSA blocking agent obviously influenced the obtained background signal. The sensor fabricated without the blocking agent showed an increase in the background current due to non-specific adsorption of the signaling probe onto the electrode surface (Figure 3.12(E)). However, this background current was eliminated after a BSA concentration of 0.2% (w/v) or higher was applied. This result suggests that the bare region of the electrode could be successfully blocked. We also expected that not only the signaling probe but also the non-specific adsorption of the DNA target on the bare region were blocked. Hence, 0.2% BSA (w/v) was selected.

In all cases, the DPV was performed with the optimized parameter of a 50 mV amplitude and 15 mV step potential, where the optimization range were from 10 to 90 mV and 5 to 25 mV for the amplitude and step potential, respectively.

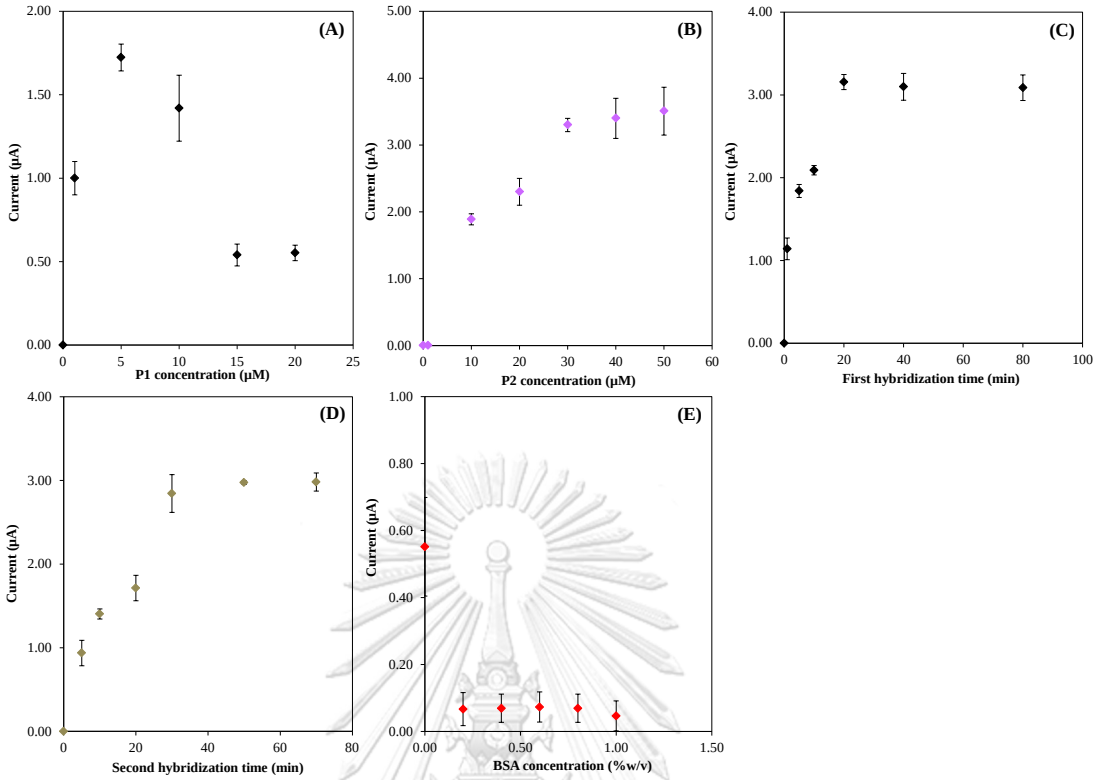


**Figure 3.12** Optimization of the variable parameters: P1 concentration (A), AQ-P2 concentration (B), first (C) and second (D) hybridization time at 100 nM of DNA target, and BSA content (E), using DPV technique in PBS of pH 7.4.



### 3.3.6 Analytical performance

Under the optimized conditions, fixed concentrations of the target DNA type 16 and 18 solutions in the range of 0.1 to 1000 nM were examined (Figures 3.13(B) and (D)). The results showed that the current responses were linear over the range from 0.1 to 100 nM for both HPV DNA strains (Figures 3.13(A) and (C)). The limits of detection (LODs) were experimentally obtained (S/N = 3) and found to be 40 and 60 pM for HPV types 16 and 18, respectively. The linear regression equations were $I$ (μA) = 0.0355$C$ (nM) + 0.1779 ($R^2$ = 0.9938) for HPV type 16 (Figure 3.13(B) (inset)) and $I$ (μA) = 0.0289$C$ (nM) + 0.1877 ($R^2$ = 0.9901) for HPV type 18 (Figure 3.13(D) (inset)). The

limits of quantitation (LOQs) (3SD/slope = 10) were estimated to be 0.1 nM for both HPV DNA strains.

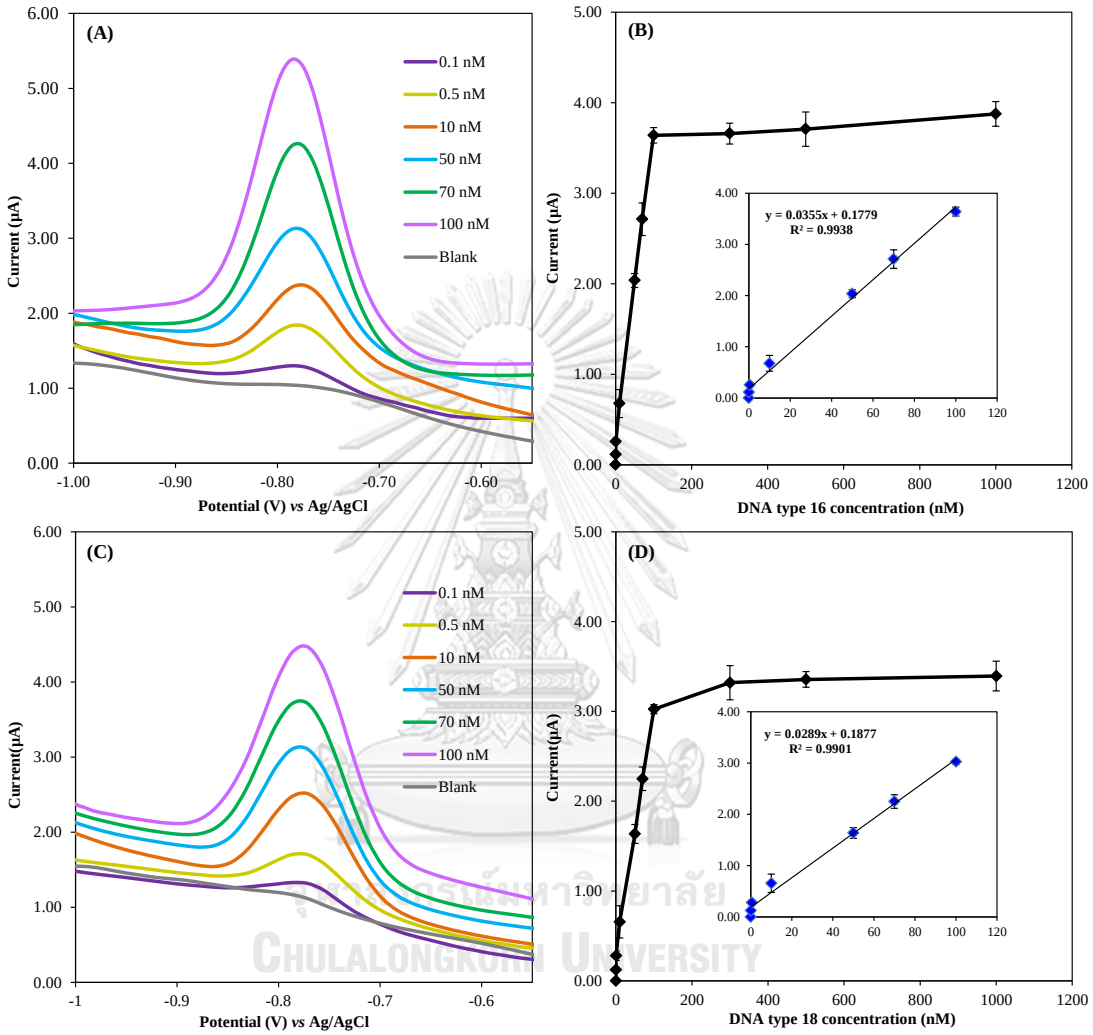


**Figure 3.13** Representative electrochemical signal responses of HPV type 16 (A) and 18 (C) DNA detection from 0.1 to 100 nM DNA concentration. (B) Plot of peak current vs. the concentration of HPV DNA from 0.1 to 1000 nM and from 0.1 to 100 nM (inset) for type 16. (D) Plot of peak current vs. the concentration of HPV DNA from 0.1 to 1000 nM and from 0.1 to 100 nM (inset) for type 18.

The analytical performance of this proposed DNA sensor was compared to other previously reported sensors, as presented in Table 3.2. Note that this DNA sensor platform showed better performance than the other methods in terms of both the analytical range and detection limit. All data shown are representative of three replicates (n = 3).

**Table 3.2** Comparison of different DNA biosensors for determination of HPV type 16 and 18 DNA

| DNA biosensor | Limit of detection (nM) | | Linear range (nM) | | Reference |
|---|---|---|---|---|---|
| | HPV 16 | HPV 18 | HPV 16 | HPV 18 | |
| AQ[a]/CHT[b]/SPCE[c] | 4.00 | - | 20-12000 | - | [73] |
| MB[d]/CYSFILM[e]/AuE[f]/ | 18.13 | - | 18.75-250 | - | [82] |
| MB/PG[g] | 1.49 | - | 2-10 | - | [83] |
| AQ/G-PANI[h]/SPCE | 2.30 | - | 10-200 | - | [84] |
| TMB[i]/HRP[j]/AuE | 490 | - | 0.10-10 | - | [85] |
| TMB/HRP/AuE | 0.22 | 0.17 | 0.10-10 | 0.10-12 | [86] |
| AQ/AuNPs[k]/SPCE | 0.04 | 0.06 | 0.10-100 | 0.10-100 | This work |



[a] Anthraquinone
[b] Chitosan
[c] Screen-printed carbon electrode
[d] Methylene blue
[e] L-cysteine film
[f] Gold electrode
[g] Pencil graphite electrode
[h] Graphene polyaniline
[i] 3,3´,5,5´-Tetramethylbenzidine
[j] Enzyme horseradish peroxidase
[k] Gold nanoparticles

To estimate the selectivity of the fabricated DNA sensor, four kinds of target sequences, including a complementary DNA and three non-complementary DNA strains, were tested with the developed sensor under the same experimental conditions. The signal was observed only in the presence of the complementary DNA and was negligible for the other three non-complementary DNA sequences (Figure 3.14). The %RSDs were found to be in the range from 1.37% to 5.21%, which were acceptable. These signal responses indicated that the proposed electrochemical DNA sensor displayed a high selectivity and specificity to discriminate complementary DNA as the detection target.

Reproducibility of the electrochemical sensor was verified at concentrations of 10, 50 and 70 nM for each DNA target (n = 7). For HPV type 16 DNA, %RSDs of 1.21%, 4.52% and 2.23% were obtained. Good reproducibility was also obtained for the detection of HPV type 18, where the %RSDs were found to be 4.11%, 3.82% and 1.15%, respectively. The results indicate that the constructed DNA sensor possesses excellent reproducibility by showing minimal sensor-to-sensor deviation.



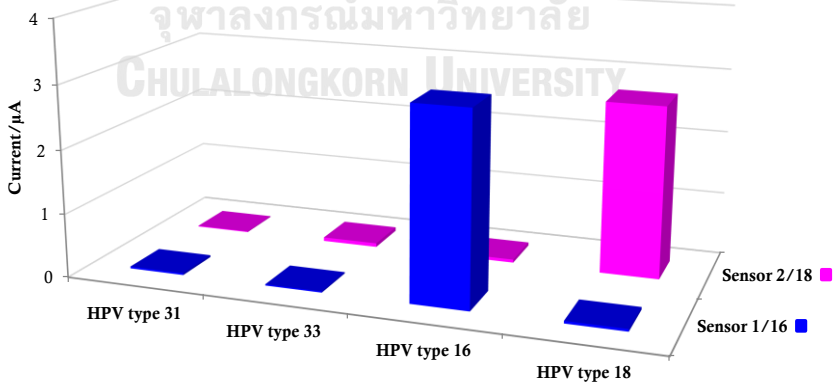


**Figure 3.14** Effect of various 28-base oligonucleotides (sequence from different HPV types) at specific sensor for type 16 (blue) and 18 (pink) at 70 nM DNA concentration.

### 3.3.7 Detection of real DNA samples obtained from PCR

To demonstrate the practical use of the developed E-DNA sensor with real samples, DNAs from three cell lines including SiHa (type 16), HeLa (type 18) and C33a (negative) were isolated and amplified by PCR. The success of the PCR amplification was confirmed by agarose gel electrophoresis (Figure 3.15), which showed the presence of bands at 240 bp, 195 bp and no bands for SiHa, HeLa and C33a samples, respectively.

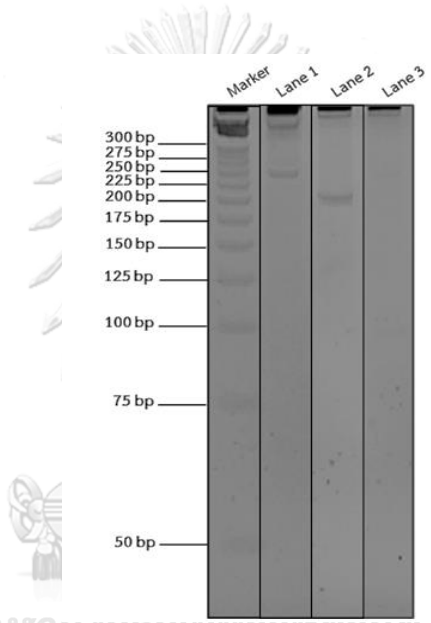




**Figure 3.15** Illustration of the agarose gel electrophoresis of the obtained PCR products, DNA marker, C33a as negative (lane 3), SiHa (lane 1) and HeLa (lane 2) as positive cell-lines.

The DNA concentrations of the SiHa, HeLa and C33a samples were spectroscopically determined to be 198.4 ng/μL, 203.5 ng/μL and 179.1 ng/μL, respectively. As expected, after the sandwich hybridizations were conducted, no signal change was detected with the PCR reaction from the HPV-negative cell line (Figure 3.16(A)), but the DPV signal increased after exposure to the PCR reaction

products from the HPV type 16 (Figure 3.16(B)) and 18 (Figure 3.16(C)) positive cell lines in a concentration-dependent manner. Thus, this developed electrochemical sensor displayed good selectivity and has the potential to be successfully applied to distinguish HPV type 16 and 18 DNA in PCR samples.

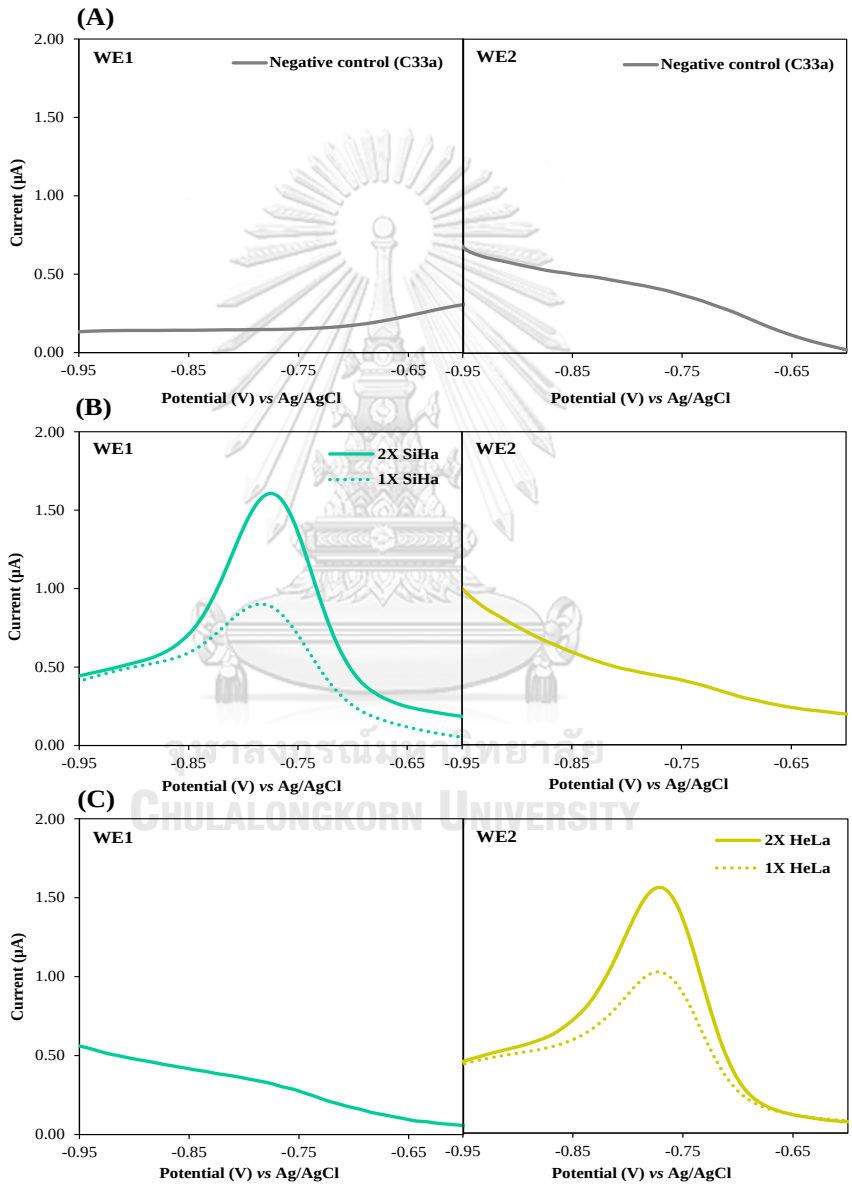


**Figure 3.16** Comparison of DPV signals of specific sensors in the presence of PCR reaction from a HPV negative (A), HPV type 16 (B) and 18 (C) positive cell-lines.

### 3.4 Conclusions

In this study, two new “signal-on” E-DNA sensors with different designs based on a sandwich-hybridization with PNA probe and electrochemical sensing were designed and evaluated. The capture PNA probe was first immobilized on a gold-deposited SPCE via glutaraldehyde cross-linking. The ASD sensor design having the second signaling AQ-labeled PNA probe hybridized to the target DNA at the position downstream to the capture probe binding site presented a higher signal response than the alternative ASU design in terms of the electron-transfer rate constant ($k_{et}$). The results revealed that the signaling performance was dependent on the distance between the signaling probe and the electrode surface after hybridization with the target DNA. The sensor with dual electrodes with two different immobilized PNA probes was successfully applied to simultaneously detect HPV type 16 and 18 DNA. The target DNA was detected in the range of 0.1 to 100 nM, and the limits of detection (LODs) of 40 and 60 pM (S/N = 3) were obtained for HPV types 16 and 18, respectively. In addition, the limits of quantitation (LOQs) (3SD/slope = 10) were estimated to be 0.1 nM for both HPV DNA strains. This proposed sensor was also employed to specifically detect PCR-amplified samples derived from HPV type 16 (SiHa) and 18 (HeLa) positive human cancer cell lines. Excellent selectivity was observed since the sensor specifically detect HPV types 16 and 18 without showing cross reactivities, and the sensor was insensitive to the HPV-negative C33a cell line. This work demonstrates that the sensor design tremendously affects the sensor performance. These findings are relevant for designing effective sensors, and the developed sensor can be readily applied to detect a wide range of DNA targets.

# Part II

## Electrochemical detection of C-reactive protein based on anthraquinone-labeled antibody using a screen-printed graphene electrode

Sakda Jampasa [a], Weena Siangproh [b], Rawiwan Laocharoensuk [c], Tirayut Vilaivan [d], Orawon Chailapakul [e, f,*]

[a] Program in Petrochemistry, Faculty of Science, Chulalongkorn University, Pathumwan, Bangkok 10330, Thailand

[b] Department of Chemistry, Faculty of Science, Srinakharinwirot University, Bangkok 10110, Thailand

[c] National Nanotechnology Center (NANOTEC), National Science and Technology Development Agency (NSTDA), Pathumthani 12120, Thailand

[d] Organic Synthesis Research Unit, Department of Chemistry, Faculty of Science, Chulalongkorn University, Pathumwan, Bangkok 10330, Thailand

[e] Electrochemistry and Optical Spectroscopy Center of Excellence , Department of Chemistry, Faculty of Science, Chulalongkorn University, Pathumwan, Bangkok 10330, Thailand

[f] National Center of Excellence for Petroleum, Petrochemicals, and Advanced Materials, Chulalongkorn University, Pathumwan, Bangkok 10330, Thailand

[*] Author for correspondence

Manuscript submitted to: Talanta

## ABSTRACT

The nature of the redox-active label tags and labeling methods, greatly contribute to the performance of electrochemical sensors. In this present work, a novel electrochemical immunosensor employing a screen-printed graphene electrode (SPGE) for a simple and highly sensitive determination of C-reactive protein (CRP) in a sandwich-type format was proposed. The sensors comprised of two CRP-specific antibodies: an unlabeled capture primary antibody (anti-CRP 1°Ab) and a redox-labeled signaling secondary (AQ-2°Ab) antibody. The signaling antibody was covalently modified with anthraquinone (AQ) tag to make it electrochemically detectable. The capture anti-CRP 1°Ab was covalently anchored onto an L-cysteine/gold-modified disposable SPGE (L-Cys/Au/SPGE) to create the anti-CRP surface, followed by adsorption of the CRP and AQ-2°Ab signaling antibody, respectively. Both anti-CRP 1°Ab immobilizing and 2°Ab labeling steps were performed using EDC/sulfo-NHS chemistry. The determination of CRP was conducted by measuring the electrochemical signal response of the AQ labeled molecules using differential pulse voltammetry (DPV). In the presence of CRP, the sensor exhibited a significant increase in the AQ current compared to the negative control, where the redox peak appeared at approximately -0.75 V. The CRP concentration was detected in the range of 0.01 to 150 µg/mL, and the limit of detection (LOD) and limit of quantitation (LOQ) were 1.5 ng/mL (S/N = 3) and 10 ng/mL (S/N = 10), respectively. This sensor exhibited very high sensitivity in determining CRP and was successfully applied to detect CRP in certified human serum with satisfactory results. We do hope that the developed sensor may be used as an alternative method for determination of CRP and further apply to monitor other clinically important target molecules.

### 3.5 Introduction

The rapid growth of technologies makes changes in human lifestyles, causing a considerable problem in health. Various non-communicable diseases have been discovered and are affecting millions of people each year worldwide**.** According to clinical diagnosis, most symptoms appear in the late stages of the diseases. For many diseases, early diagnosis is essential for the success of the treatment and improving patient survival rate [2]. In general, measuring the level of one or more biomarkers associated with the disease is a better indicator of the presence and/or severity of the disease than physical examination.

C-reactive protein (CRP) is an acute-phase protein produced in the liver and is considered as a valuable biomarker of inflammation or cardiovascular diseases for clinical diagnosis. Currently, the level of CRP has been used to identify specific diseases such as diabetes and cancers [12]. According to the American Heart Association and the United States Centers for Disease Control and Prevention (AHA/CDC), the cardiovascular disease risk levels are assessed by CRP concentrations in human blood serum: CRP concentration less than 1 μg/mL represents a low-risk state, concentration between 1 and 3 μg/mL is considered as moderate risk and any concentration above 3 μg/mL represents high risk [13-15]. In clinical laboratories, CRP is usually determined by immunonephelometric or immunoturbidimetric assays [16]. These approaches are expensive, time-consuming, require expertise and advanced instrumentation. Moreover, its poor sensitivity also limits its robustness to detect low levels of CRP. Therefore, a rapid, highly sensitive, selective and operationally convenient approach is still in great demand for determination of trace CRP levels with rapid turn-around time.



In the past few decades, several immunobiosensors using electrochemical, surface plasmon resonance, piezoelectric and fluorescent techniques have been established as portable and convenient tools for determination of CRP in complex

matrices [87-91]. Among them, electrochemical immunoassays have attracted more and more attention for biomolecular applications, since it allows a rapid, sensitive, selective determination, and requires only low sample volume.

Recently, ultrasensitive electrochemical determinations of CRP through detection of magnetic bead nanoparticles and metallic cations released from QDs labels have been reported [92, 93]. The enhanced sensitivity of these immunoassays increases by selecting appropriate combinations of various transducers and nanoparticle materials (such as Hg, Bi, and Graphene) and compositions of QDs (such as PbS and CdS). Nevertheless, the uses of magnetic or QDs-based immunoassays do not fulfil the analytical criteria due to multiple preparation steps and potential toxicity from the heavy metals. It is, therefore, necessary to develop a simple, non-toxic and highly sensitive redox-active label for electrochemical determination of CRP.

Anthraquinone (AQ) is an attractive alternative redox label for electrochemical immunosensing assay since it is a stable redox-active molecule that is simple to introduce to any biomolecules. Its small size minimizes the interference with the biomolecular interaction to be investigated. In our recent publication, AQ was employed as a redox label in an electrochemical DNA biosensor (E-DNA). This labeling molecule was covalently attached to the distal end of polyamide nucleic acid (PNA) capture probe. The developed E-DNA sensor was highly selective and sensitive to detect target DNA with a limit of detection in pM range [73]. Due to the high sensitivity obtained, AQ was chosen for this work as a redox label for a simple and highly sensitive electrochemical determination of CRP via CRP-specific antibodies in a sandwich-type assay format. In the presence of CRP, this detection mode offers a stronger signal, which increases proportionally to the CRP concentration present.

To fabricate a portable, low-cost and sensitive electrochemical immunosensor, screen-printed graphene electrode (SPGE) was employed. This type

of electrode can be easily and inexpensively prepared by in-house screen printing technique which enables the mass-production of disposable sensors on flexible substrates. In addition, a dual-working electrode was custom-designed to simultaneously compare the presence and absence of CRP to reduce analysis time. Analytical performances, such as the sensitivity, specificity, and reproducibility of the proposed sensors were evaluated. This developed immunosensor was eventually applied to determine CRP in human serum samples to evaluate the applicability of this sensor in determining CRP level.

## 3.6 Experimental

### 3.6.1 Chemicals and reagents

All chemicals and reagents employed in this work are of analytical grade. Graphene ink and silver/silver chloride pads were purchased from The Gwent Group, United Kingdom for the fabrication of SPGE. The pattern of dual-working SPGE was designed using Adobe Illustrator. The screen-printed block was made by Chaiyaboon Co. Ltd. (Bangkok, Thailand). Polyvinyl chloride (PVC) was used as a substrate for the fabrication of SPGE, which was obtained from a local market. 1-Ethyl-3-(3-dimethylaminopropyl) carbodiimide (EDC), *N*-Hydroxysulfosuccinimide (sulfo-NHS) and L-Cysteine (L-Cys) were purchased from sigma-Aldrich. Potassium tetrachloroaurate(III) was purchased from Wako Company, Japan. C-reactive protein (CRP) (Lot: 081M1600V) was purchased from Sigma-Aldrich. CRP-specific primary (Anti-CRP 6402 SPTN-5, Lot: 0036770) and secondary monoclonal antibodies (Anti-CRP 6403 SP TN-5, Lot: 0034926), (capture and signaling anti-CRP) were obtained from MedixBiochemica, Finland. The redox reporter, 4-(anthraquinone-2-oxy) butyric acid, was synthesized as previously reported [49]. Phosphate buffer saline (PBS) of pH 7.4 consisted of 140 mMNaCl, 2 mM $KH_2PO_4$, 10 mM $Na_2HPO_4$, and 2 mMKCl. Chemicals

employed in this step were purchased from Merck and were of analytical grade. Millipore Milli-Q purified water (18.2 MΩ) was used throughout the experiments.

### 3.6.2 Apparatus and measurements

All electrochemical measurements and electrochemical impedance spectroscopy (EIS) were performed on a PGSTAT 30 Potentiostat (Metrohm Siam Company Ltd.) and controlled with the General Purpose Electrochemical System (GPES) software. A disposable SPGE was employed and fabricated using an in-house screen-printing method. A conductive silver/silver chloride (Ag/AgCl) ink was utilized as a pseudo-reference electrode (RE). Graphene ink was employed to prepare the working electrode (3 mm i.d.) (WE) and counter electrode (CE) (see details of the preparation in section 3.6.4). Electrochemical measurements of CRP were accomplished using differential pulse voltammetry (DPV) under optimized conditions: 60 mV amplitude and 15 mV step potential. Calibration curves were constructed by sequential additions of CRP standard solution from 0.02 to 250 µg/mL.

### 3.6.3 Sample preparation



Standard stock solutions of the capture and signaling anti-CRPs (1 mg/mL) were prepared in purified water and kept frozen in the refrigerator until use. The working solution with the designated concentrations of both capture and signaling anti-CRP and CRP were diluted from stock solutions using phosphate buffer pH 7.4. Milli-Q purified water was used throughout the experiments.

### 3.6.4 Fabrication of dual-working screen-printed graphene electrode (SPGE)

Electrode employed in this work was a disposable SPGE as it can be easily and inexpensively prepared. The design and construction of the SPGE were

previously described [76]. The pattern consisted of a dual-working electrode was designed to facilitate simultaneous comparison between the presence (WE1) and absence (WE2) of CRP. Silver/silver chloride ink was first printed onto a polyvinyl chloride (PVC) substrate to be used as both the RE and the conductive pads. Commercial graphene ink was then printed onto the same PVC substrate to form both the WE and CE. Finally, the insulator (nail polish) was screened as the top layer. The finished electrode was dried at 55 °C for 1 h to remove residual solvent.

**3.6.5 Conjugation of the AQ-carboxyl containing molecule on secondary antibody**

In the present work, conjugation of AQ on the antibody was simply achieved using standard EDC/sulfo-NHS chemistry [94]. This can be simple and rapidly performed in aqueous solution. The redox active label 4-(anthraquinone-2-oxy)butyric acid (3.2 µmol) was activated using EDC/sulfo-NHS (9.6 µmol) in PBS at pH 7.4 (500 µL) for 1 h, followed by coupling with the antibody (1 mg/mL, 50 µL) overnight. The AQ-conjugated antibody was subsequently purified in a dialysis bag (MWCO 12,000-14,000) for 2 days at 4 °C to remove excess unreacted residual small molecules. This method provides direct conjugation of the AQ with a carboxylic group (–COOH) to free primary amines ($–NH_2$) on the antibody. The AQ-labeled anti-CRP was freshly prepared before use. The procedure of the labeled method is summarized in Figure 3.17.

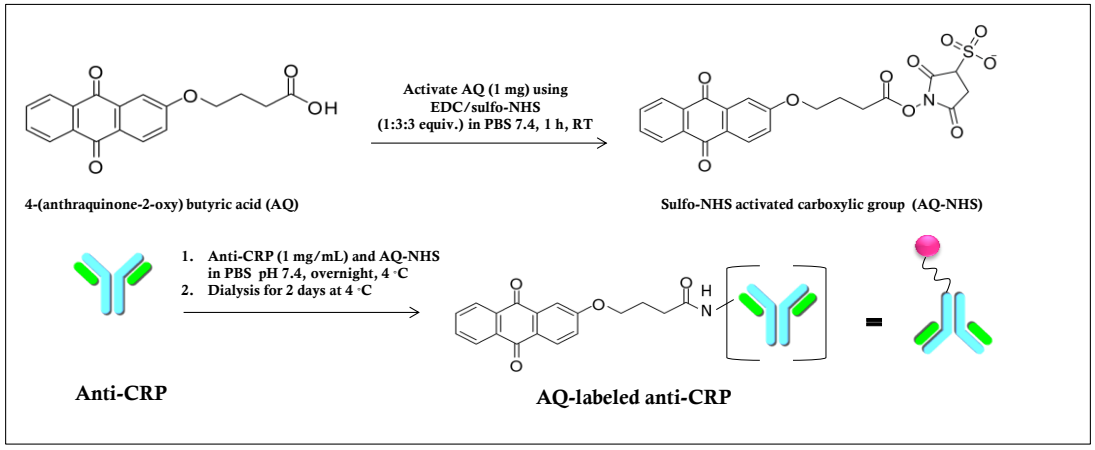


**Figure 3.17** Schematic illustration of conjugation of the AQ-carboxyl containing compound onto antibody in PBS of pH 7.4.

### 3.6.6 Preparation of CRP immunosensor and electrochemical measurement

In this work, a sandwich-type format was employed since it is robust and selective. The sensor is comprised of unlabeled and labeled monoclonal antibodies. The unlabeled anti-CRP was covalently immobilized onto the electrode via EDC/sulfo-NHS chemistry. Prior to the preparation, the electrode surface was cleaned with MQ water. The preparation of the sensor was previously described [77]. Briefly, 20 µL of 5 mM potassium tetrachloroaurate(III) solution containing 0.5 M $H_2SO_4$ was dropped onto the electrode and gold nanoparticles (AuNPs) was subsequently electrodeposited onto the electrode surface with a constant potential of -0.5 V for 100 s. The Au-modified electrode (Au/SPGE) was then rinsed with MQ water and dried at ambient temperature. These electrodes were subsequently treated with 3 µL of 5 mM L-Cys in PBS (pH 7.4) and left overnight at room temperature in a sealed box under a humid environment (minimum 90% RT) to prevent evaporation of the solution. The prepared electrodes consisting of a self-assembled monolayer (SAM) of L-Cys were rinsed twice with PBS and MQ water, respectively. Activation of L-

Cys/Au/SPGE surface was then completed by dropping the solution containing 20 mM EDC and 20mM sulfo-NHS (3 µL) and incubated at RT for 1 h. The modified electrode was then rinsed twice with PBS. After this step, the carboxyl group was converted to amine-reactive sulfo-NHS esters. The first capture anti-CRP (Anti-1°Ab) was then immobilized onto the sulfo-NHS-activated surface via its free amino group by dropping a 2.5 µL of anti-CRP solution (100 µg/mL) and left at RT for 1 h. The electrodes were then thoroughly washed twice with PBS (pH 7.4) to remove the excess and non-specifically adsorbed antibody on the electrode surface. The blocking step was subsequently introduced by dropping 2.5 µL of 0.3% (w/v) bovine serum albumin (BSA) solution onto the anti-CRP-modified electrodes, followed by curing at RT for 1h and washing twice with PBS. These electrodes were denoted as Anti-1°Ab/BSA/L-Cys/Au/SPGE. For the conjugation step, a designated concentration of CRP or human serum CRP (2.5 µL) was dropped onto the working electrode region and left for 40 min, followed by extensive washing with PBS. After the formation of anti-CRP and CRP, the AQ-2°Ab solution obtained from the dialysis step, without further dilution (90 µg/mL, 2.5 µL), was dropped onto the electrode surface and left for 40 min. The modified electrode was then rinsed with PBS to remove the excess signaling antibody. PBS buffer (20 µL) was lastly dropped onto the electrode surface again prior to electrochemical measurement. Preparations of the sensor are summarized in Figure 3.18.



In all cases, DPV was carried out at room temperature (25 ± 1 °C) with 80 mV amplitude and 10 mV step potential. These employed experimental parameters were the optimized parameters. For the optimization of each parameter, the amplitude interval was investigated from 50 to 100 mV and the step potential was from 5 to 30 mV (data not shown). The electrochemical measurement was performed after the conjugation of the signaling anti-CRP. Limits of detection (LOD) and quantification (LOQ) were calculated from the S/N = 3 and $10SD_b/S$, respectively,

where $SD_b$ is the standard deviation of blank (n = 10), and S is the slope of the linear fit.

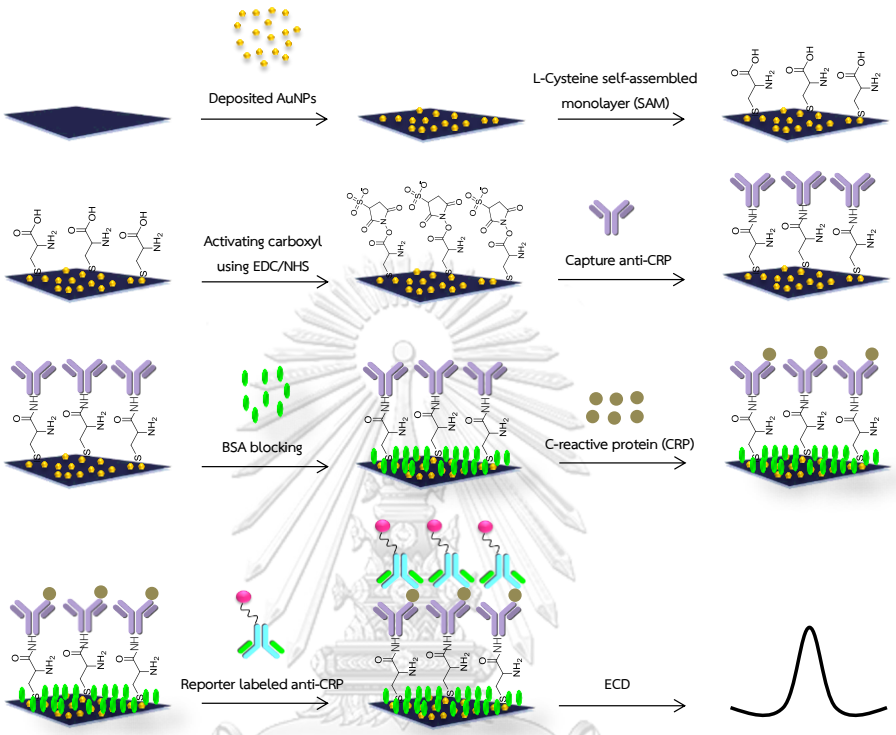


**Figure 3.18** Schematic illustration of preparation of the developed electrochemical immunosensor for CRP determination and electrochemical measurement.



## 3.7 Results and Discussion

### 3.7.1 Characterization of the modified electrode

To illustrate that the graphene ink used could improve the sensitivity of the developed sensor, the current obtained from using graphene and graphite electrodes was compared. As can be seen in Figure 3.19, graphene (G) electrode exhibited the higher current in comparison to graphite electrode for $Fe(CN)_6^{4-/3-}$ detection (Figure 3.19(C)). However, the highest current was obtained at Au modified graphene electrode, where both materials possess conductive properties (data not shown). The

electro-active surface areas (A) of these electrodes were determined by employing CV in 5.0 mM $Fe(CN)_6^{4-/3-}$ solution containing 0.1 M KCl at various scan rates (v) according to the Randles-Sevcik equation, as follows: $i_p = 2.69 \times 10^5 A D^{1/2} n^{3/2} v^{1/2} C$, where D is the diffusion coefficient of $Fe(CN)_6^{4-/3-}$, C is the concentration of $Fe(CN)_6^{4-/3-}$, n is the number of involved electrons. As exhibited in Figure 3.19, the peak currents ($i_p$) of the graphite (Figures 3.19(A) and (B)) and graphene (Figures 3.19(C) and (D)) electrodes proportionally increased with increase in the square root of the scan rate. According to the Randles-Sevcik equation, the electroactive surface areas were calculated to be 0.035 ± 0.0343 $cm^2$ and 0.056 ± 0.0551 $cm^2$ for the graphite and G electrodes, respectively. It was evidenced that the electroactive surface area of the electrode increased by 1.52-fold by employing graphene ink in place of graphite ink. These results support the superior conductive property of G ink as expected. Therefore, the use of G ink could improve the sensitivity of detection [52, 76].

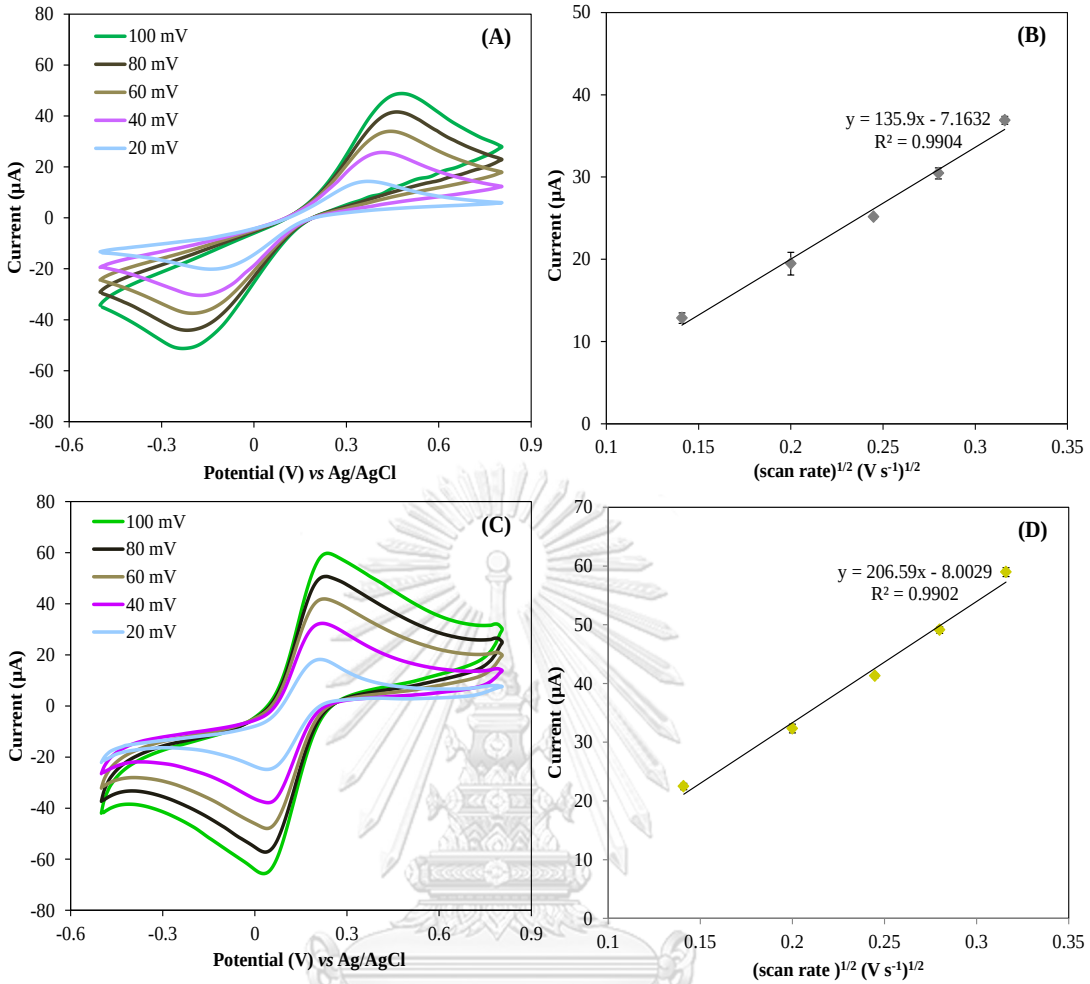


**Figure 3.19** CV comparison of the graphite (A and B) and graphene electrodes (C and D) in 10.0 mM $Fe(CN)_6^{4-/3-}$ at different scan rates from 20 to 100 mV $s^{-1}$.



AuNPs were electro-deposited onto the electrode surface for immobilization of the capture antibody. SEM technique was employed to confirm the presence of AuNPs on the electrode surface after the electrodeposition step. As can be seen in Figure 3.20, after the AuNPs, were electro-deposited onto the electrode surface, a homogenous distribution and size were observed (Figure 3.20(B)), while the unmodified electrode showed no presence of AuNPs (Figure 3.20(A)). The results confirmed that AuNPs were successfully deposited onto the electrode surface. The

uniform distribution of granular AuNPs could largely increase the effective surface area and the antibody loading amount on the electrode [52].

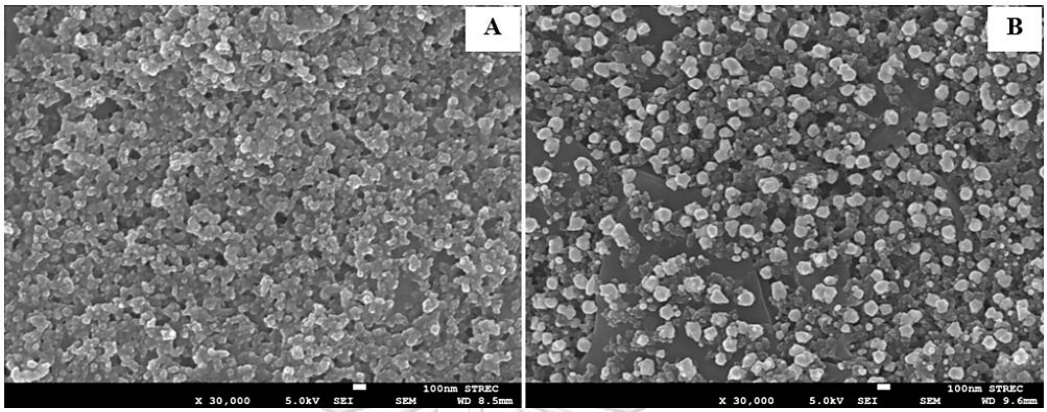


**Figure 3.20** SEM images of the SPGE (A) and Au-modified SPGE (B).

### 3.7.2 Electrochemical detection of CRP using the developed immunosensor

According to the electrode design, simultaneous detection of the presence and absence of CRP can be accomplished (Figure 3.21(A)). After preparation of the sensor, it was then exposed to a solution containing CRP. As can be seen in Figure 3.21(B), when the sample solution containing CRP (positive control) was applied onto WE1, the characteristic AQ peak appeared at approximately -0.76 V but no signal was observed for WE2 (negative control). This demonstrated that the developed sensor responded selectively to CRP. This sensor design facilitates the simultaneous comparison of positive and negative results, which may allow and reduce analysis time for CRP determination in complicated interferences.

Moreover, to verify the successful modification of the proposed sensor step by step, EIS technique was implemented. This characterization technique examines the impedance changes of the modified electrodes. Semicircle diameters in the high-

frequency region reflected the electron-transfer resistance ($R_{et}$), which controls the electron-transfer kinetics of the redox probe employed $Fe(CN)_6^{4-/3-}$ at the electrode interface. As shown in Figure 3.21(C), the Au/SPGE showed a small curve of 0.12 kΩ (%RSD = 0.91) (curve A) at high frequencies. This clearly demonstrates the excellent electron-transfer kinetics of the Au-modified electrode. When L-Cys was self-assembled on the AuNP-modified SPGE, a 0.31 kΩ (%RSD = 2.13) increase in $R_{et}$ (curve B) was observed. This increment of the resistance can be explained by the blocking of the electrode surface by L-Cys, making it less accessible for the $Fe(CN)_6^{4-/3-}$ redox couple. Additionally, after the immobilization of the capture anti-CRP and the blocking step, the $R_{et}$ further increased to 0.41 kΩ (curve C) (%RSD = 2.13) and 0.68 kΩ (curve D) (%RSD = 1.99), respectively. This indicates that the immobilization of the capture anti-CRP was successful. When the CRP protein was added, $R_{et}$ greatly increased to 1.39 kΩ (%RSD = 2.31) (curve E). This is likely attributed to the conjugation of antibody-antigen complexes formed on the electrode surface, which resulted in a further increase in the negative charge of the electrode surface. Therefore, the electrostatic barrier to the negatively charged $Fe(CN)_6^{4-/3-}$ redox couple increased, causing an increase in the charge-transfer resistance [95, 96]. This result suggests that all the electrode modification were successful and that the immobilized anti-CRP can capture the CRP protein as proposed. The evidence here can also indicate that the EIS method can be applied to identify CRP.

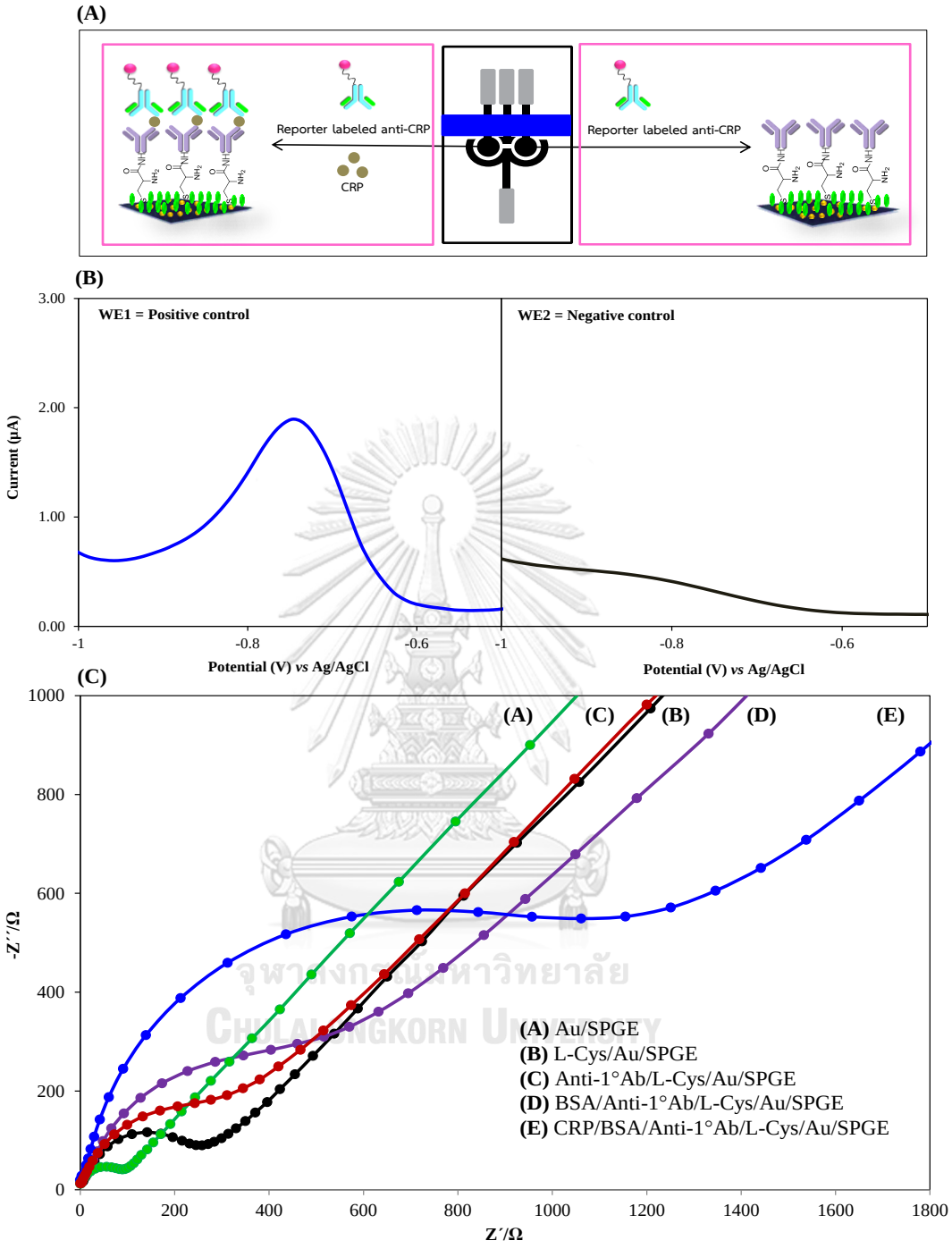


**Figure 3.21** Schematic illustration of a dual-working electrode where negative and positive controls were performed (A). DPV responses for the simultaneous comparison in the presence and absence of CRP (B). Nyquist impedance comparison of the modified electrode (C) in 5 mM $Fe(CN)_6^{4-/3-}$.

### 3.7.3 Optimization of variable parameters

To achieve the optimal CRP sensing system, relevant parameters that could possibly affect the performance of the sensor, such as the capture and signaling anti-CRP concentrations, Au concentration, BSA blocking loading amount and incubation time were collectively optimized, respectively. The first optimized parameter was the anti-CRP antibody concentration. A CRP concentration of 20 µg/mL was employed in all parameter optimizations. The capture anti-CRP concentrations ranging from 10 to 150 µg/mL were investigated using the condition of 90 µg/mL signaling antibodies, 5 mM Au and 0.3% (w/v) BSA concentrations, and 50 min for the first and second incubation time. Similarly, the signaling antibodies concentrations were observed in the range from 10 to 90 µg/mL with the conditions as follow: 100 µg/mL anti-CRP, 5 mM Au, 0.3% (w/v) BSA concentration, and 50 min for the first and second incubation time. The results revealed that the electrochemical signal gradually increased with increasing capture anti-CRP (Figure 3.22(A)) and signaling antibody concentrations (Figure 3.33(B)), and reached the maximum value at 100 and 90 µg/mL for the capture and signaling anti-CRP concentrations, respectively. This indicated that 100 and 90 µg/mL were the optimal concentrations. At conditions above these limits, the electrode surface could be oversaturated, and therefore, there are a limited number of conjugated anti-CRP/CRP complexes that could be formed on the electrode surface under these excess antibodies conditions.



For the optimization of the Au concentration, the parameters of 100 µg/mL anti-CRP, 90 µg/mL signaling antibody, 0.3% (w/v) BSA concentrations and 50 min for the first and second incubation time were employed. The results showed that the signal amplified upon an increase of the Au concentration from 1 to 5 mM and then slightly decreased when the Au concentration was further increased (Figure 3.22(C)). This could be due to the formation of larger Au nanoparticle agglomerates at high concentrations, which led to the decrease of electrode surface area and

consequently decreased the signal [80]. Therefore, 5 mM of Au concentration was used.

The surface conditions of the fabricated sensor are especially important for the performance of the developed immunosensor. To reduce the non-specific adsorption of CRP and signaling antibody on the bare region of the electrode surface, the electrode surface was blocked after the first anti-CRP immobilization step. The effect of concentration of BSA as a blocking agent was therefore determined. In this section, we only emphasized on the elimination of the background signal produced from non-specific adsorption of the signaling antibody on the electrode surface by varying BSA contents in the blocking step since the non-specific adsorption can cause the high background current which would lead to false-positive results. The amount of BSA was varied from 0 to 1% (w/v). The employed conditions were 100 µg/mL anti-CRP, 90 µg/mL signaling antibody, 5 mM Au concentrations and 50 min for the first and second incubation time. This parameter was investigated in the absence of CRP, whereby the signal should theoretically be close to zero if there is no non-specific adsorption of the signaling antibody. The results showed that the background signal was significantly influenced by the concentration of the BSA blocking agent. The sensor fabricated without BSA showed a rather high background current due to non-specific adsorption of the signaling antibody onto the electrode surface (Figure 3.22(D)). However, this observed background current was reduced after blocking with BSA at concentrations of 0.3% (w/v) or higher. This indicates that the bare region of the electrode could be successfully blocked. We also suspected that the blocking also minimizes non-specific adsorption of the CRP on the bare region of the electrodes as well. Consequently, 0.3% BSA (w/v) was selected.



According to the sandwich assay format, the effect of incubation time was next studied. The incubation time was examined over the time range of 20-100 min using the optimal conditions of each optimized parameters. The current signal

increased gradually within 40 min for both the first (Figure 3.22(E)) and second incubation steps (Figure 3.22(F)). After that, the observed signals for both incubation steps reached a plateau, which could be explained by the limited number of conjugated anti CRP/CRP complexes that could be formed on the surface [97]. Considering the incubation time efficiency, 40 min was chosen as the appropriate time for the first and second incubation time.

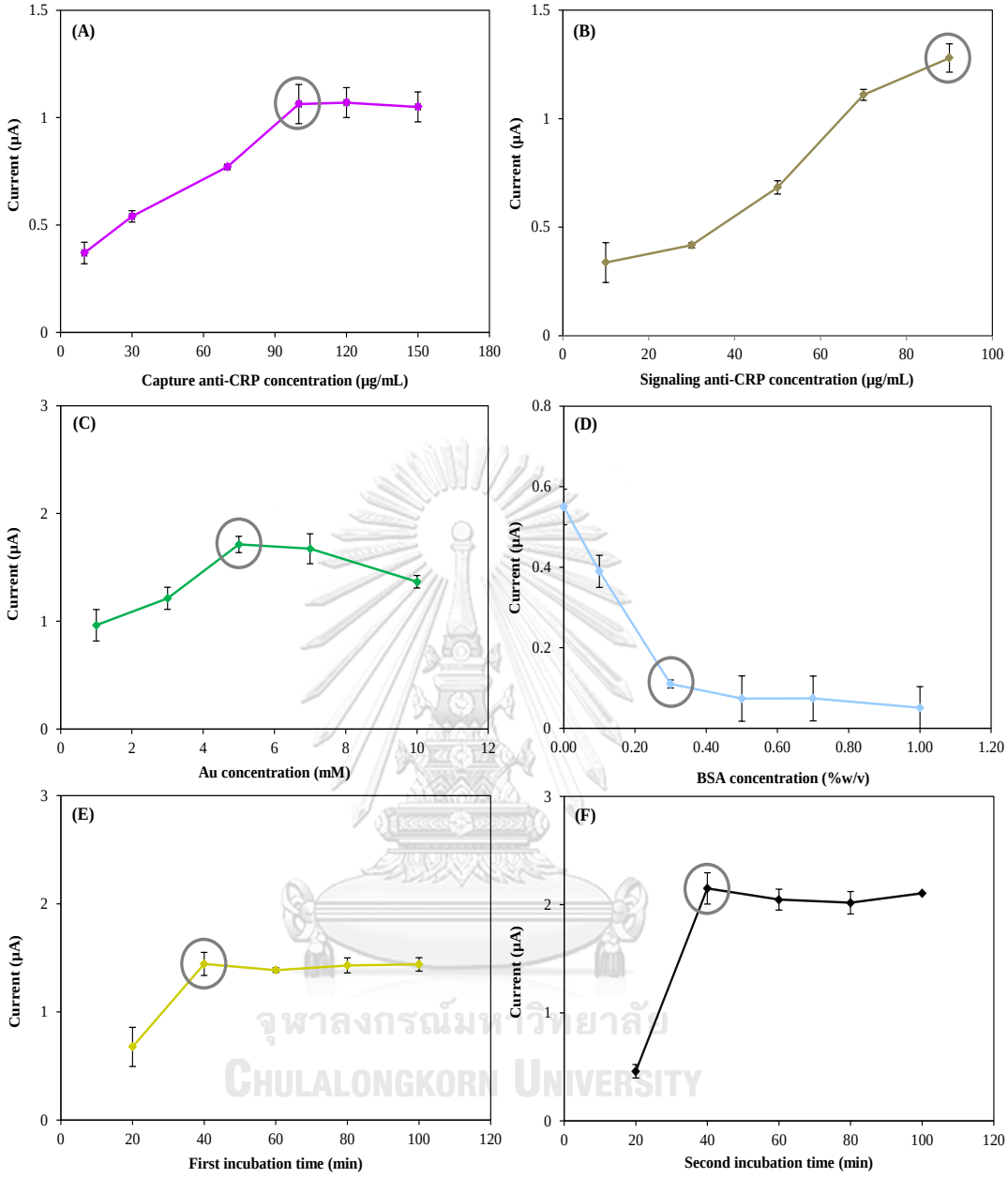




**Figure 3.22** Optimization of variable parameters: capture anti-CRP concentration (from 10 to 150 μg/mL) (A), signaling antibodies (from 10 to 90 μg/mL) (B), Au concentration (from 1 to 10 mM) (C), BSA loading amount (from 0 to 1 (%w/v)) (D), the first incubation time (from 20 to 100 min) (E), the second incubation time (from 20 to 100 min) (F), at 20 μg/mL of CRP, using DPV in PBS (pH 7.4).

### 3.7.4 Analytical performance

After the construction of CRP immunosensor and obtaining the optimized conditions, fixed concentrations of CRP solutions in the range of 0.01 to 200 µg/mL were examined. Calibration plot between the current signals and various tested CRP concentrations were obtained from the DPV analysis. The current responses were linear over the range from 0.01 to 150 µg/mL of the CRP concentrations (Figures 3.23(A) and (B)). The limit of detection (LOD) was experimentally obtained and found to be 1.50ng/mL (S/N = 3). The linear regression equations were $I$ (µA) = 0.0165$C$ (µg/mL) + 0.3214 ($R^2$ = 0.9928) (Figure 3.23(B) (inset)). The limit of quantitation (LOQ) (at S/N = 10) were estimated to be 10 ng/mL. The analytical performance of this proposed sensor was compared to other previously reported CRP immunosensors, as presented in Table 3.3. Note that this developed sensor showed a wider dynamic range than existing methods. The LOD and LOQ were comparable to immunonephelometric and immunoturbidimetric standard methods, and is well below the 1 µg/mL low-risk limit of AHA/CDC. In addition, this developed method was simple, inexpensive and disposable in nature, which makes it attractive for rapid point-of-care applications.

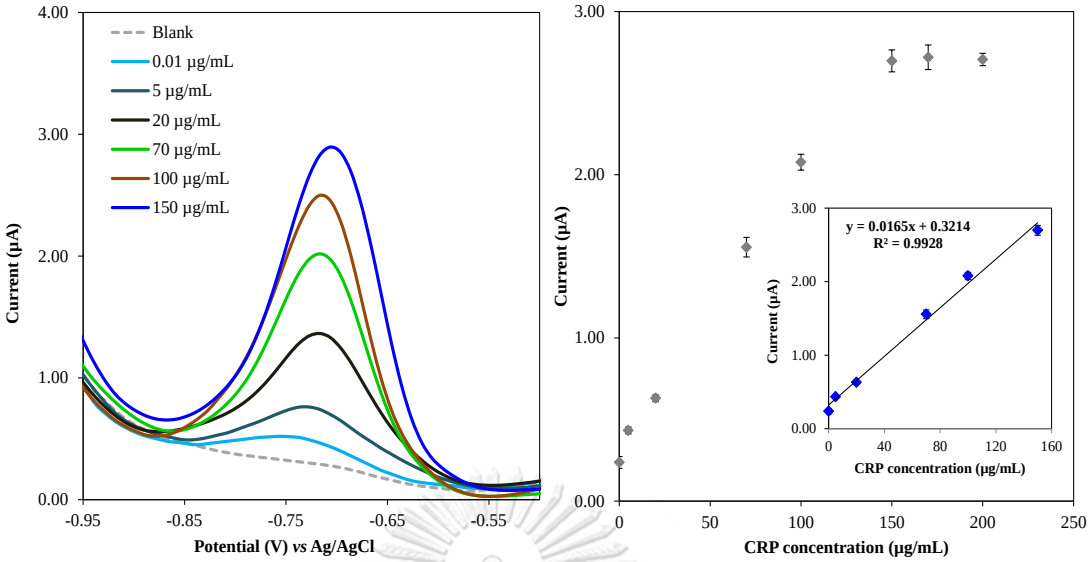


**Figure 3.23** Electrochemical signal responses of CRP detection from 0.01 to 150 µg/mL (A). (B) Plot of peak current vs. the concentration of CRP from 0.01 to 200 µg/mL and from 0.01 to 150 µg/mL (inset).

In addition, reproducibility (expressed as the % relative standard deviation (%RSD) of repetitive measurements (n = 7)) of the developed CRP immunosensor was examined. Seven sensors were constructed using the same process. An exceptional reproducibility was obtained for the detection of CRP, where %RSD was found to be lower than 5%. This value reflects that the constructed immunosensor has remarkably low sensor-to-sensor deviation, and excellent fabrication reproducibility was obtained.

**Table 3.3** Comparison of the obtained results between the proposed immunosensor and the certified CRP amount on the label.

| Electrode | Label | Limit of detection (ng/mL) | Linear range (ng/mL) | Reference |
|---|---|---|---|---|
| Bis[a]/SPEs[b] | QDs | 0.05 | 0.2 – 100 | [93] |
| HOOC-MBs[g]/SPCE | HRP | 0.47 | 2-200 | [92] |
| ssDNA[c]/Au[d] | - | 200 | $3.125\times10^{6}$ – $25\times10^{6}$ | [98] |
| Aptamer-MBs[e]/SPCE[f] | Strept/AP | 54 | $0.1\times10^{3}$ – $50\times10^{3}$ | [99] |
| AuNPs[h]/SPGE[i] | AQ | 1.5 | $0.01\times10^{3}$ – 150 $10^{3}$ | This work |

[a] Bismuth

[b] Graphite screen-printed electrode

[c] Single-strand DNA

[d] Gold electrode

[e] Aptamer-modified magnetic beads

[f] Carbone-based screen-printed electrode

[g] Carboxylic acid-modified magnetic beads

[h] Gold nanoparticles

[i] Screen-printed graphene electrode

### 3.7.5 Application in analysis of CRP in human serum samples

To demonstrate whether the fabricated sensor could examine practical samples sensitively and specifically, certified CRP in human serum was examined. The certified CRP was first diluted to designated concentration using PBS (pH 7.4). As expected, the oxidation peak currents increased in a concentration-dependent manner at WE1 in the presence of CRP (Figure 3.24(A)) and no response was observed at WE2 in all cases (Figure 3.24(B)). The contents of CRP in the sample can then be achieved using the external standard calibration. The results obtained using this platform was compared to the certified amounts on the label. The values obtained from the developed method were in agreement with the certified amounts shown in Table 3.4. Each reported value is the mean replicates (n = 5), and the relative standard deviation (RSD ≤ 2%) obtained from the measurement by this method was acceptable. A paired t-test at a 95% confidential interval was achieved on the results obtained from certified samples analysis. The experimental t-values (t calculated) obtained by this proposed method are 1.31 and 0.29 at CRP concentrations of at 40.2 μg/mL and 20.6 CRP μg/mL, respectively, and are lower than the critical t-value (2.44). This suggests that there is no significant difference between the proposed and standard methods. Therefore, our proposed strategy can be used as a new and reliable alternative assay for the sensitive and rapid determination of CRP.

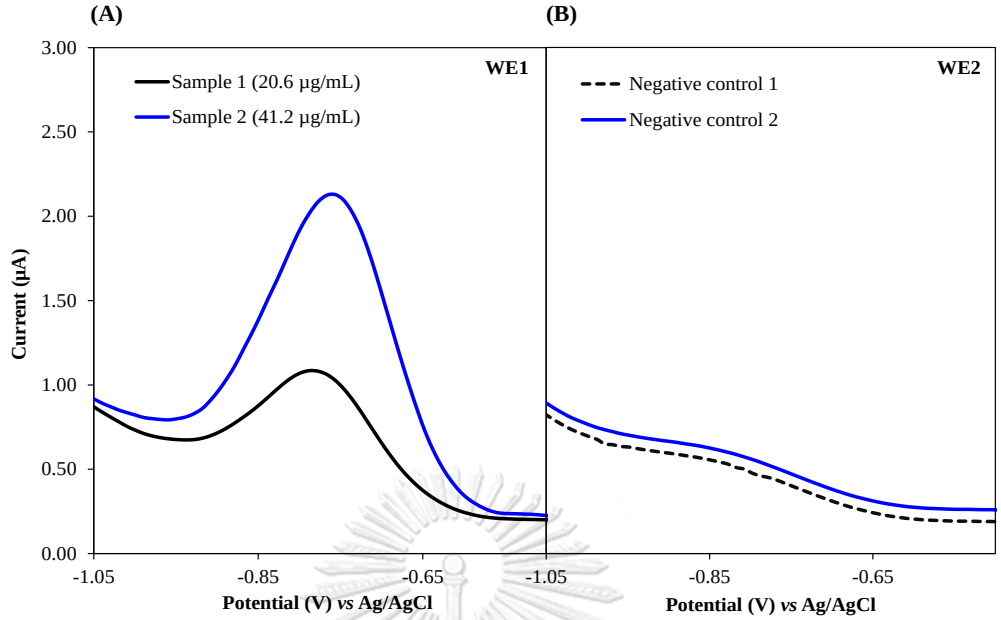


**Figure 3.24** Comparison of DPV signals for determination of the certified CRP using the proposed sensor.

**Table 3.4** Comparison of the obtained results between the proposed immunosensor and the certified CRP amount on the label

| Sample No. | By developed sensor (µg/mL) | Certified CRP in human serum (µg/mL) | Relative error (%) |
|---|---|---|---|
| 1 | 41.03 ± 1.26 | 41.20 | -0.41 |
| 2 | 20.69 ± 1.20 | 20.60 | +0.29 |

Note: values reported are mean of three replicates (n = 3).

### 3.8 Conclusions

In this present work, a novel electrochemical immunosensor of CRP employing a screen-printed graphene electrode was proposed. The electrochemical detection principle is based on a sandwich-conjugation format comprising of two CRP-specific monoclonal antibodies: a primary capture antibody (anti-CRP 1°Ab) and anthraquinone-labeled secondary (AQ-2°Ab) antibody. In the presence of CRP, the obtained current obviously increased in a CRP concentration-dependent manner. The dual-electrode design allows simultaneous inclusion of a negative control. This may allow and reduce analysis time for CRP determination in complicated interferences. Moreover, we systematically evaluated the performance of the sensor including the limit of detection, selectivity, and reproducibility. The CRP concentration was detected in the range of 0.01 to 150 µg/mL, and the limit of detection (LOD) and limit of quantitation (LOQ) were 1.5 ng/mL (S/N = 3) and 10 ng/mL (S/N = 10), respectively. The proposed sensor was highly sensitive with a limit of detection in the ng/mL range and was successfully applied to selectively and specifically detect certified CRP samples. Using the proposed method, the obtained results agreed well with those obtained from the conventional method. The advantages of this sensor include the ease of sensor fabrication and measurement and reduced analysis time without the use of toxic heavy metals. The electrode is easily and inexpensively prepared, and it requires only a small sample volume (2.5 µL). The instrument set-up is also simple. This sensing platform may provide a promising alternative choice for practical application in biological and environmental analyses.

# CHAPTER IV

# DEVELOPMENT OF ELECTROCHEMICAL SENSOR FOR DETERMINATION OF SYNTHETIC FOOD COLORANTS

## Electrochemically reduced graphene oxide-modified screen-printed carbon electrodes for a simple and highly sensitive electrochemical detection of synthetic colorants in beverages

Sakda Jampasa [a], Weena Siangproh [b], Kiattisak Duangmal [c], Orawon Chailapakul [d,*]

[a] Program in Petrochemistry, Faculty of Science, Chulalongkorn University, Pathumwan, Bangkok 10330, Thailand

[b] Department of Chemistry, Faculty of Science, Srinakharinwirot University, Bangkok 10110, Thailand

[c] Department of Food Technology, Faculty of Science, Chulalongkorn University, Pathumwan, Bangkok 10330, Thailand

[d] Electrochemistry and Optical Spectroscopy Research Unit, Department of Chemistry, Faculty of Science, Chulalongkorn University, Pathumwan, Bangkok 10330, Thailand

* Corresponding author

Talanta 160 (2016): 113-124

**ABSTRACT**

A simple and highly sensitive electrochemical sensor based on an electrochemically reduced graphene oxide-modified screen-printed carbon electrode (ERGO-SPCE) for the simultaneous determination of sunset yellow (SY) and tartrazine (TZ) was proposed. An ERGO film was coated onto the electrode surface using a cyclic voltammetric method and then characterized by scanning electron microscopy (SEM). In 0.1 M phosphate buffer at a pH of 6, the two oxidation peaks of SY and TZ appeared separately at 0.41 and 0.70 V, respectively. Surprisingly, the electrochemical response remarkably increased approximately 90- and 20-fold for SY and TZ, respectively, using the modified electrode in comparison to the unmodified electrode. The calibration curves exhibited linear ranges from 0.01 to 20.0 μM for SY and from 0.02 to 20.0 μM for TZ. The limits of detection were found to be 0.50 and 4.50 nM (at S/N = 3) for SY and TZ, respectively. Furthermore, this detection platform provided very high selectivity for the measurement of both colorants. This electrochemical sensor was successfully applied to determine the amount of SY and TZ in commercial beverages. Comparison of the results obtained from this proposed method to those obtained by an in-house standard technique proved that this developed method has good agreement in terms of accuracy for practical applications. This sensor offers an inexpensive, rapid and sensitive determination. The proposed system is therefore suitable for routine analysis and should be an alternative method for the analysis of food colorants.

## 4.1 Introduction

With the beginning of a new era in the food industry, more food additives have been introduced to aid in food preservation and processing. The use of food additives has also been proven to extend the shelf-life and/or enhance the food quality and texture [100, 101]. However, these food additives can only be incorporated in certain food products, and they must fall within a specified dosage as well as have a justified purpose. A food additive overdose is considered as food adulteration, as these foods possess toxicity or lack any technical-functional purpose. Therefore, the use of food additives in the food industry requires ethical consideration [102].

Food colorants, either synthetic or in a natural form, are normally used as food additives to enhance consumer acceptance. Sunset yellow (SY, E110) and tartrazine (TZ, E102), classified as azo dyes, are common synthetic colorants that are extensively employed in the food industry due to their low production cost, charming color uniformity and excellent water solubility as well as their high stability to light, oxygen and pH [17-19]. However, they can cause detrimental effects to health when they are excessively consumed. In recent studies, extensive consumption of SY and TZ was found to significantly decrease the thymus weight and alter the monocyte counts as well as induce allergic responses including contact urticaria, angioneurotic edema, asthma, contact anaphylaxis and immunosuppression in humans [101-103]. Because they are harmful to human health, the use of colorants as food additives is strictly controlled by laws and regulations. The maximum acceptable content by the international and national legislation is 100 μg/mL when they are employed individually or in combination [30]. The European University Association and some European countries such as Finland and Norway have already excluded these colorants and consider them to be carcinogenic agents [104]. According to Thai Food Act B.E. 2547, notification 281, colorants are not

permitted to be incorporated into many food categories such as pickled/osmosed fruit, fresh-cut fruit, processed meat, smoked meat and dried meat. Yet, some manufacturers illegally incorporate these substances into their products. The presence of colorants in food samples indicates that some food producers lack responsibility and ethics, and it also indicates that these colorants are still widely used in foods beyond the use permitted by rules and regulations [102].

Various techniques have been developed and applied over the last few decades for the examination of SY and TZ. Currently, the most widely used techniques for the determination of colorants are spectrophotometry, high performance liquid chromatography (HPLC), column chromatography, and capillary electrophoresis [20-23]. Nevertheless, the first two aforementioned techniques have some disadvantages. In particular, these two techniques exhibit low sensitivity and specificity, require expertise, are time-consuming, and require instrumentation that is complicated as well as expensive. Therefore, a detection method that offers a short analysis time, a simple and low cost process, high sensitivity and high selectivity is still in demand and important for food safety and human health.

Different electrochemical methods for the simultaneous determination of SY and TZ in commercial beverages have been reported. The high sensitivity, small sample volume requirement, low cost, simplicity, short analysis time and portability are the key requirements of a detection method. Various types of electrodes have been employed to successfully fabricate a sensor that allowed simultaneous measurement of SY and TZ. Examples of such electrodes include a pretreated boron-doped diamond electrode (BDDE), a graphene phosphotungstic-modified glassy carbon electrode (GN-PTA/GCE), a graphene $TiO_2$-modified GCE (GN-$TiO_2$/GCE), a gold nanoparticle-modified carbon paste electrode (Au NPs/CPE), a multi-walled carbon nanotubes-modified GCE (MWCNT/GCE) and a platinum wire-coated electrode [28-30, 105-107]. Unfortunately, these electrodes are non-disposable and rather

expensive to use for the routine analysis of food colorants. Therefore, a critical step towards routine analysis is the development of a disposable sensor that simultaneously detects SY and TZ without compromising the electrochemical sensitivity and selectivity.

Graphene, a single sheet of carbon atoms settled in a honeycomb lattice, has recently received research interest due to its potential in improving the conductivity of the modified sensor. It has been applied in many applications, especially in the electrochemical field. Graphene-modified electrochemical sensors have been reported in the detection of phytohormones, biomolecules, pharmaceuticals, food additives and environmental pollutants [108-112]. However, it was found that graphene tends to form irreversible agglomerates through strong ¶-¶ stacking and Van der Waals interactions, which restricts its application and storage [113].

Chemically synthesized graphene has been considered to be a new substitute for graphene because of its similar characteristics and ease of synthesis. Synthetic graphene is usually obtained from reduced graphite oxide prepared via Hummers's method, followed by reducing the ultrasonically exfoliated graphene oxide (GO) with hydrazine [114]. An alternative method reported for the preparation of graphene involves reacting sodium metal and ethanol, followed by thermal exfoliation and reduction of the GO intermediate [115]. Although a simpler method for graphene synthesis has been reported, preparation of a graphene solution for further electrode modification is troublesome. Recently, the GO intermediate has received intense research interest due to its convenience in storage and fast dissolution in water without any dispersing agents. However, among these reduction methods, both chemical and physical reduction of an intermediate still possess some disadvantages because of the toxicity of reducing agents, expense and several steps in the reduction process.

Recently, an environmentally friendly electrochemical reduction of GO with controllable size and thickness has been reported. This technique is an attractive alternative method for the reduction of GO to obtain a graphene sheet due to its simple instrumental setup. Moreover, it also offers easy preparation, cost-effectiveness and non-toxicity. The electrochemical reduction of GO film (ERGO) obtained by employing this technique can enhance the large specific surface area and electrochemical conductance of the electrochemical sensor, thus improving the analytical performance [116].

An electrochemical sensor for the simultaneous determination of SY and TZ using an electrochemically reduced graphene oxide-modified screen-printed carbon electrode (ERGO-SPCE) has not yet been reported. Therefore, the main objective of this work is to propose a simple and highly sensitive electrochemical sensor based on an ERGO-SPCE to use as a novel method for the determination of SY and TZ. A green and facile routine electrochemical reduction method was employed to produce an ERGO film onto the electrode surface in one step. This disposable SPCE employed was inexpensively and easily prepared. Analytical parameters, such as the sensitivity, selectivity and reproducibility, were also investigated. This developed electrochemical sensor was also applied to quantify the amounts of SY and TZ in practical samples to validate the performance of the developed sensor.



## 4.2 Experimental

### 4.2.1 Chemicals and apparatus

Graphite powder (mesh size < 100 micron) was purchased from Sigma Aldrich (CA, USA). Carbon ink and silver/silver chloride were purchased from Acheson (CA, USA). The screen-printed block was made by Chaiyaboon Co. Ltd. (Bangkok, Thailand). Analytical grade diethylene glycol monobutyl ether and ethylene glycol monobutyl ether acetate, as binder solution in the ink preparation step, and other

analytical grade reagents were purchased from Merck (CA, USA). Food grade, sunset yellow (batch: 21023) and tartrazine (batch: 20633) standard samples were obtained from BRENNTAG Co. Ltd. (Bangkok, Thailand). Graphene oxide (GO) was purchased from XF Nano, Inc. (Nanjing, China).

All electrochemical measurements were performed on a PGSTAT 30 potentiostat (Metrohm Siam Co. Ltd.) and controlled with the general purpose electrochemical system (GPES) software (Utrecht, Netherlands). A disposable screen-printed carbon electrode (SPCE) was fabricated using an in-house screen-printing method. All measurements were conducted using a differential pulse voltammetric method at room temperature (25 °C). The surface morphologies of the unmodified and modified electrode were verified using scanning electron microscopy (SEM). The presence of the ERGO film on the electrode surface was monitored employing infrared spectroscopy (IR).

For the analysis employing compendium of method, used in parallel with the proposed approach to confirm the accuracy and acceptability of method, the system consisted of a pump (Model CM 3200), UV-vis detector (absorbance at 235 nM, model SM 3200), C18 column (250 mm x 4.6 mm i.d.; particle size, 5 µm, Phenomenex). The separation was carried out with an isocratic elution consisting of 5 mM tetra-n-buthyl ammonium hydroxide (TBAH), pH 4.5: ACN (52:48 v/v) with an injection volume of 20 µm, flow rate of 1.2 mL $min^{-1}$.

### 4.2.2 Preparation of the screen-printed carbon electrode (SPCE)

A disposable SPCE was used in this present work because of its cost-effectiveness and ease of preparation. The design and praparation of the three-electrode system were previously described [73]. A pattern of electrode, designed using Adobe Illustrator program (Figure 4.1).

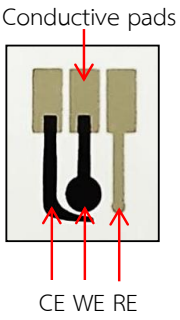


**Figure 4.1** The design of the three-electrode system.

The SPCE was fabricated using an in-house screen-printing method. The ink composition included graphite powder and carbon ink at a ratio of 0.2:1 (w/w). Silver/silver chloride ink was first printed onto a polyvinyl chloride (PVC) substrate to be used as both the pseudo-reference electrode (RE) and the conductive pads. Next, the carbon ink was printed onto the same PVC substrate as the second layer to form both the working electrode (WE, 3 mm i.d.) and counter electrode (CE). The finished electrode was then heated at 55 °C for 1 h to remove the solvent and dry the electrode.

### 4.2.3 Electrochemical reduction of graphene oxide (ERGO)

A protocol of ERGO preparation was previously described [116]. GO sheet (1mg) was first dissolved in 1 mL deionized water with applying sonication for 1 h to achieve homogeneous solution. The GO solution was subsequently diluted with 0.1 M phosphate buffer (0.1 M $Na_2HPO_4$ and 0.1 M $KH_2PO_4$) of pH 6 to give a final concentration of GO in working solution of 70 % (v/v). The working solution (40 µL) was then dropped onto the electrode surface, and followed by the electrochemical reduction of GO using a cyclic voltammatric technique. The reduction potential was scanned from 0.1 to -1.5 V with a scan rate of 100 mV $s^{-1}$ for 16 cycles. The modified

electrode was then rinsed twice with deionized water. The schematic illustration of an ERGO is shown in Figure 4.2.

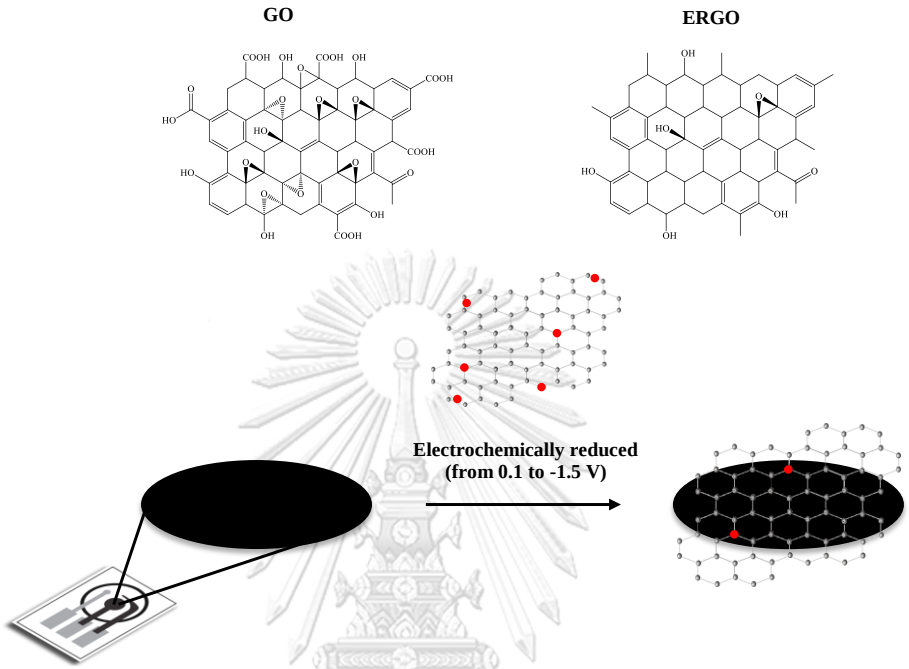


**Figure 4.2** Schematic illustration of ERGO-modified SPCE, Condition: CV was scanned from 0.1 to -1.5 V for sixteen cycles, scan rate of 100 mV $s^{-1}$.



**4.2.4 Preparation of standard solutions and electrochemical measurements**

Food grade synthetic colorants, SY and TZ, were selected as the analytes in this work. A stock standard solution (5 mM) was freshly prepared for each determination in phosphate buffer of pH 6. For the study of pH effect, a solution pH was adjusted using NaOH (1 M) and conc.$H_3PO_4$. The designated concentrations of analytes were diluted from stock solutions. For electrochemical measurement, the analytes solution (40 µL) was dropped onto a freshly prepared electrode and subsequently accumulated at open-circuit for 3 min, and followed by

electrochemical measurement. Limits of detection (LOD) and quantification (LOQ) were calculated from the S/N = 3 and $10SD_b/S$, respectively, where $SD_b$ is the standard deviation of blank (n = 10), and S is the slope of the linearity.

Evaluation of the selectivity, largely reflects the analytical performance, was also examined using the same protocol as mentioned above using 50-fold excess of interfering substances. The selectivity was determined by comparing the signals obtained from the ERGO-SPCE with and without the presence of interferences such as glucose, ascorbic acid, sodium and iron, which are commonly added in drinks.

In all cases, the differential pulse voltammetry (DPV) was performed with 60 mV amplitude, 50 mV $s^{-1}$ scan rate and 10 mV step potential. These employed experimental parameters were the optimized parameters. For the optimization of each parameter, the amplitude interval was investigated from 10 to 80 mV, and the step potential was from 2 to 20 mV.

**4.2.5 Sample preparation**

The seven beverages employed in this work consisted of two soft drinks, two juice concentrate drinks, two energy drinks and one thirst quencher sample, which were purchased from a local supermarket and used directly without further pretreatment. When measuring SY and TZ using a ERGO-SPCE, a designated sample concentration was diluted employing 0.1 M phosphate buffer of pH 6, and then analyzed according to the analytical procedure.

In addition, compendium of methods for food analysis was also used to determine the amount of SY and TZ in these samples in parallel with the results obtained from the proposed approach to confirm the accuracy and acceptability of method. Compendium of method is applicable to the determination of food containing SY and TZ by high performance liquid chromatography method (HPLC). The preparation of sample was performed as previously described [117]. Briefly,

liquid sample of 10 g was weighed accurately (or appropriate amount) and 50 mL of distilled water was subsequently added into the samples with constant stirring. After that, 10 mL of each sample was pipetted into each 50 mL beaker, followed by the addition of 30 mL of distilled water and acidified using glacial acetic acid. Finally, polyamide powder of 0.2 - 5.0 g is added into the adjusted samples, stirred with a stirring rod and left for 10 min or until all colors from the solution are adsorbed onto polyamide. Next, polyamide was subsequently added into the column and followed by a washing step using 5 mL acetone until no color is adsorbed onto polyamide and then combined all eluted fraction. These fractions were evaporated until nearly dry and small amount of distilled water was subsequently added into the samples to dissolve residue as final step. The results obtained from the ERGO-SPCE and compendiums of method were compared.

Furthermore, the recovery was determined by spiking known SY and TZ concentrations into the samples and then analyzed according to the same procedure.

## 4.3 Results and Discussion



### 4.3.1 Characterization of the ERGO-SPCE

#### 4.3.1.1 Scanning electron microscopy (SEM)

The surface morphologies of bare and ERGO-modified SPCEs were verified using SEM to confirm the presence of ERGO sheets on the electrode surface. As shown in Figure 4.3(B) and (C), after the electrochemical reduction of GO, the surface became more rough and non-exquisite compared to the bare electrode (Figure 4.3(A)). SEM images of the electrode surface obviously showed that the surface was dominantly covered by the irregularly crumbled and sheet-like structure of ERGO. Furthermore, it seemingly appears that the density and thickness of the EGRO sheet was gradually increased with increasing the number of scan cycle, as shown in Figure

4.3(A), B (eight cycles) and C (sixteen cycles), respectively. This led to an increase in the effective surface on the electrode and improvement in the conductivity of the modified sensor, which helps determine the detection sensitivity [116]. The obtained results indicated that GO was electrochemically reduced onto the electrode surface during the operation.

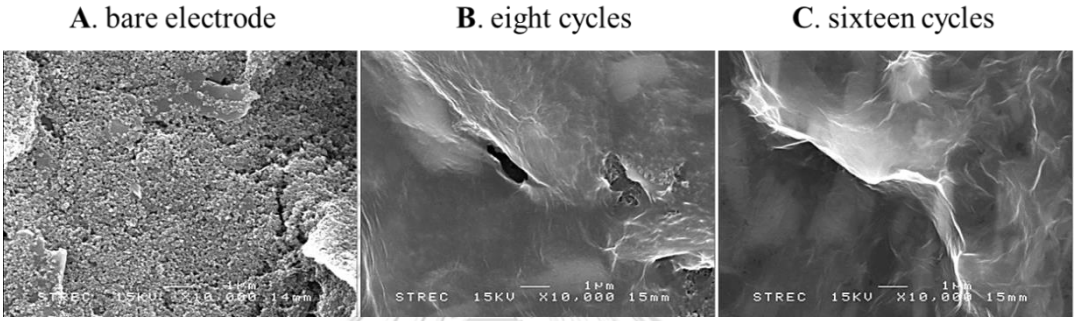


**Figure 4.3** SEM images of the bare (A) and ERGO-modified SPCE at eight (B) and sixteen (C) scan cycles.

#### 4.3.1.2 Electrochemical impedance spectroscopy (EIS)

To confirm the improvement of the conductivity of the modified sensor, an experiment using the EIS technique for measuring the charge transfer resistance ($R_{et}$) of active species on electrode surface was carried out. The obtained results displayed that a semicircle with a large diameter was observed on the unmodified electrode (SPCE), and the semicircle became much smaller on the modified electrode (ERGO-SPCE) (Figure 4.4). In a Nyquist plot, the semicircle diameter represents the $R_{et}$ of the active species, which is $Fe(CN)_6^{4-/3-}$, on the electrode surface. Herein, the $R_{et}$ values of $Fe(CN)_6^{4-/3-}$ on the SPCE, GO-SPCE and ERGO-SPCE were found to be 20.29 kΩ, 8.09 kΩ and 0.43 kΩ, respectively. The greatly depressed $R_{ct}$ values revealed that conductivity of the developed sensor was improved after

the formation of the ERGO-SPCE, consequently resulting in higher signals and sensitivity [118].

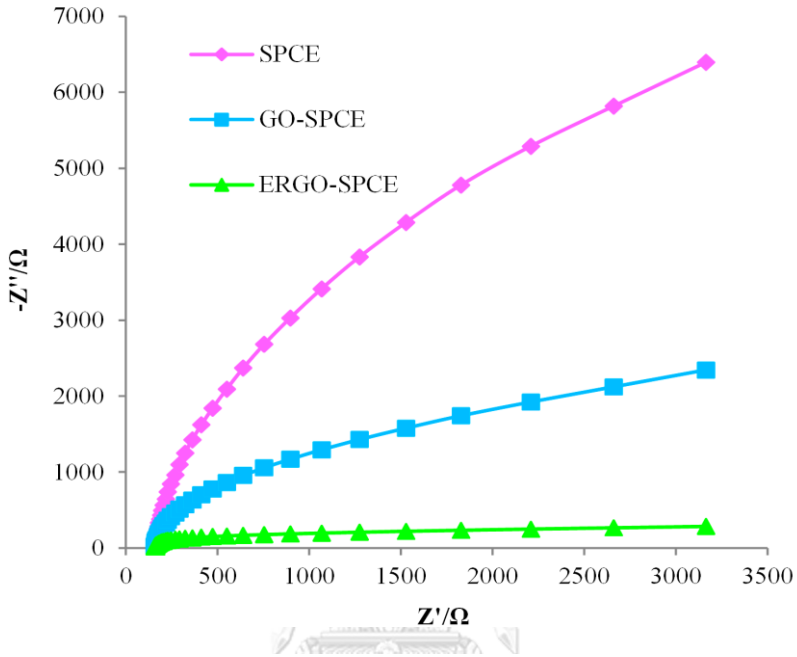


**Figure 4.4** Nyquist impedance comparison of 5 mM $Fe(CN)_6^{4-/3-}$ on SPEC, GO-SPCE and ERGO-SPCE.

From the relationship between $R_{ct}$ and the heterogeneous electron-transfer rate constant ($k_{et}$) according to Equation 4.1, the $k_{et}$ value could be successfully obtained.

$$k_{et} = \frac{RT}{n^2F^2R_{et}AC_{redox}} \quad \text{(Equation 4.1)}$$

In equation (1), A is the geometrical area of the electrode surface, and $C_{redox}$ corresponds to the concentration of the redox couple. According to equation (1), the $k_{et}$ values were calculated to be $3.74 \times 10^{-5}$ cm $s^{-1}$, $9.39 \times 10^{-5}$ cm $s^{-1}$ and $176.9 \times 10^{-5}$ cm $s^{-1}$ for the SPCE, GO-SPCE and ERGO-SPCE, respectively. The ERGO-SPCE exhibited a noticeable increase in the $k_{et}$ value in comparison to the SPCE. Based on this evidence, it can be concluded that the electron transfer process on the ERGO-SPCE is easier and faster than that on the SPCE [119].

Furthermore, to illustrate that the ERGO could improve the surface area of the SPCE, the electroactive surface areas (A) of ordinary SPCE and ERGO-modified electrodes were determined employing CV in a 5.0 mM $Fe(CN)_6^{4-/3-}$ solution containing 0.1 M KCl at various scan rates (v) according to the Randles-Sevcik equation, as follows: $i_p = 2.69 \times 10^5$ A $D^{1/2}$ $n^{3/2}$ $v^{1/2}$ C, where D is the diffusion coefficient of $Fe(CN)_6^{4-/3-}$, C is the concentration of $Fe(CN)_6^{4-/3-}$, and n is the number of involved electrons. As shown in Figure 4.5, both the peak currents ($i_p$) of ERGO-modified (Figure 4.5(A)) and unmodified electrodes (Figure 4.5(B)) were proportional to the square root of the scan rate. With the constant parameters of D ($7.6 \times 10^{-6}$ $cm^2$ $s^{-1}$), C (5 mM) and n (1 electron), an approximate value of A according to the Randles-Sevcik equation could be successfully achieved. The electroactive surface areas were calculated to be 0.335 $cm^2$ and 0.186 $cm^2$ for the modified and unmodified electrodes, respectively, where the electroactive surface area of the

electrode increased 1.86-fold. This result provided effective evidence for the superior conductivity of ERGO as expected [120].

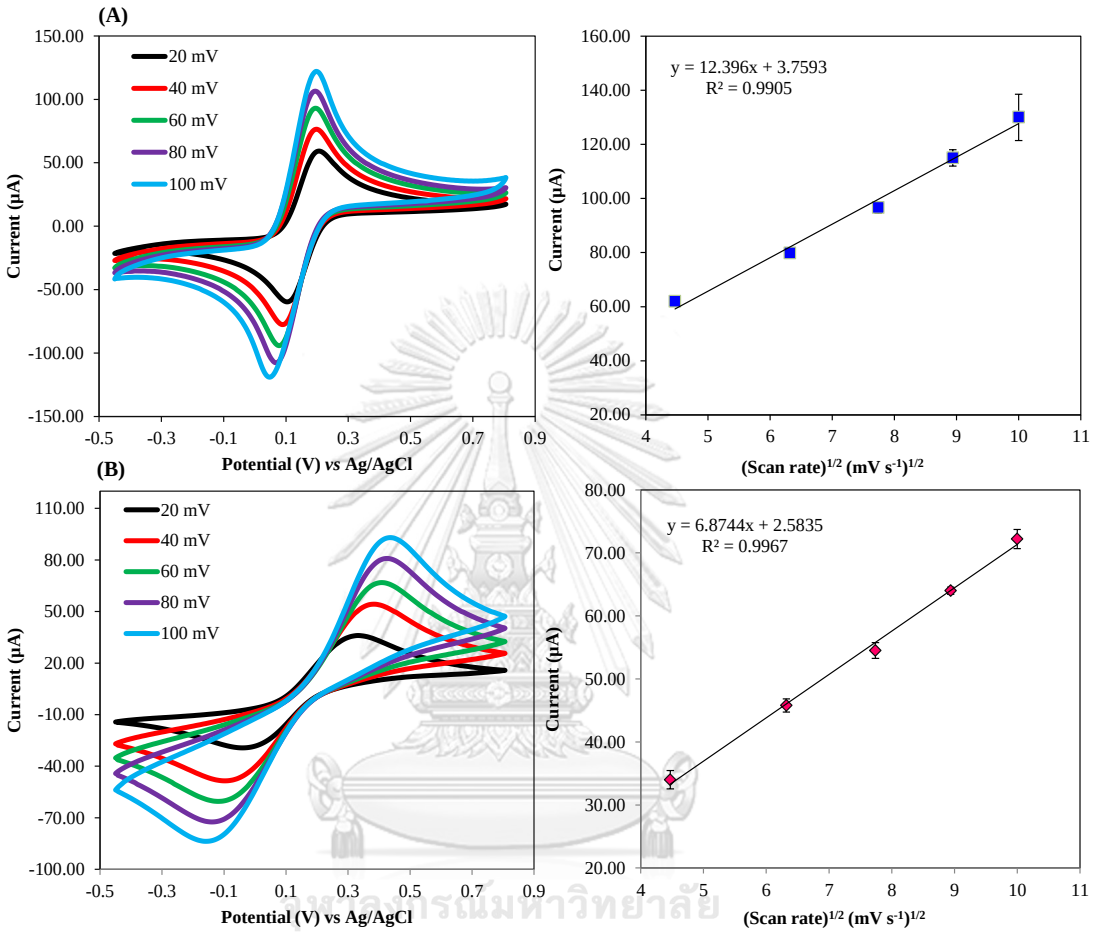




**Figure 4.5** CVs of the modified (A) and unmodified SPCE (B) in 5.0 mM $Fe(CN)_6^{4-/3-}$ at different scan rates from 20 to 100 mV $s^{-1}$.

#### 4.3.1.3 Infrared spectroscopy (IR)

According to sensor preparation, to prove that GO was electrochemically reduced by voltammetric cycling, an IR technique was carried out. The IR spectrum of the GO-SPCE showed all of the characteristic bands for GO including the following: C=O stretching at 1,574 $cm^{-1}$, C-O stretching at 1,051 $cm^{-1}$, and finally the OH stretching at 3,350 $cm^{-1}$. The IR of the ERGO-SPCE preserved all of the characteristic

bands of GO, except that the peak due to C=O stretching at 1,574 $cm^{-1}$ completely disappeared. This result indicates that the C=O functional group in GO was reduced during the voltammetric cycling (Figure 4.6). Moreover, the IR of ERGO-SPCE also exhibited the appearance of the new peak at 2,949 $cm^{-1}$, which is due to the $CH_2$ vibrations. This suggests that GO was converted to ERGO by voltammetric cycling [121].

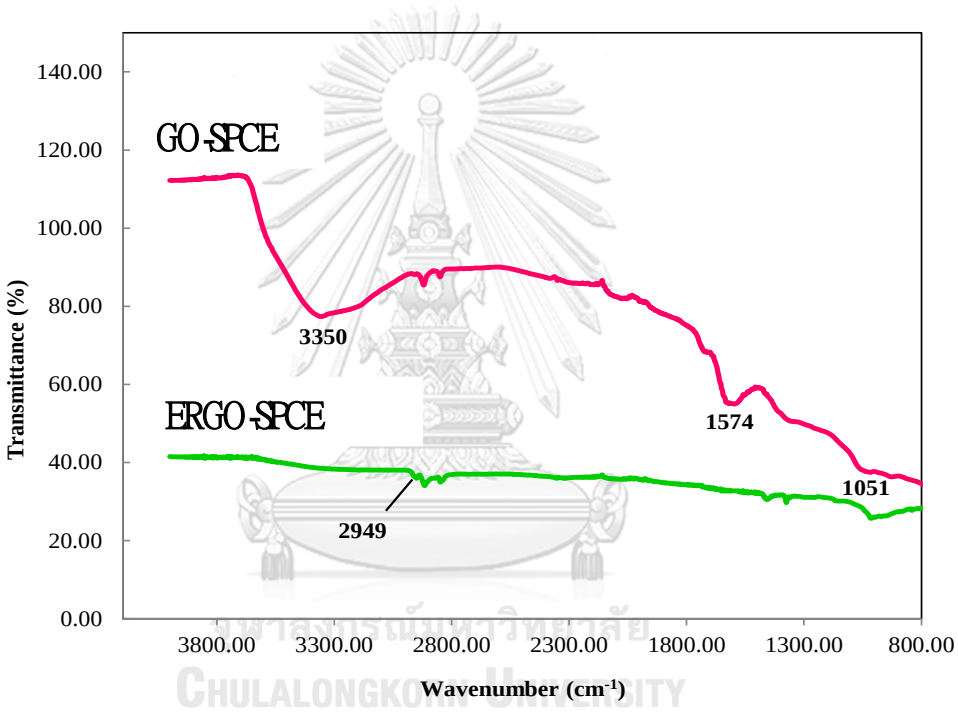


**Figure 4.6** IR spectra of GO and ERGO-SPCE.

### 4.3.2 Electrochemical behaviors of food colorants on the developed sensor

The electrochemical behaviors of SY and TZ on the SPCE, GO-SPCE and ERGO-SPCE were first investigated by a cyclic voltammetric (CV) technique to differentiate the oxidation peak potential of each colorant. As shown in Figure 4.7(A), the SPCE and GO-SPCE showed almost no anodic peaks of SY and TZ. This was due

to that GO is electrochemically insulating by nature [113]. In contrast, the comparison exhibited that the peak currents of SY and TZ were significantly improved and well-defined peaks were observed on the ERGO-SPCE. Using a DPV technique, the results displayed that the peak separation between SY and TZ was increased at the ERGO-SPCE. The potential difference of the modified electrode was higher than that of the bare electrode by approximately 0.3 mV. The oxidation peaks appeared separately at approximately 0.41 and 0.70 V for SY and TZ, respectively, on the modified electrode (Figure 4.7(B)). Surprisingly, the oxidation current was remarkably increased by approximately 90- and 20-fold for SY and TZ, respectively, in comparison to the unmodified electrode. These results suggested that the ERGO-modified electrode could improve the sensitivity of detection, which is consistent with the previously reported results [122].

To enhance the sensitivity of detection, the effect of accumulation time with and without applying potential on the current response of these colorants was examined. With applying potential, (at +0.4 V with various times from 0 to 120 s), the current signal was almost unchanged or negligible for the oxidation current of both SY and TZ (data not show). More interestingly, as shown in Figure 4.7(C), the current signals of both colorants with different accumulation times at the open-circuit were enhanced and reached maximums at 3 min. The current signal then reached a plateau after further increasing the accumulation time, and an accumulation time of 3 min was therefore selected. As a result, it can be concluded that the accumulation time affects the increase of the current signal. In other words, it can be assumed that the accumulation potential has no effect on the current responses of SY and TZ, which is consistent with the previous report [123].

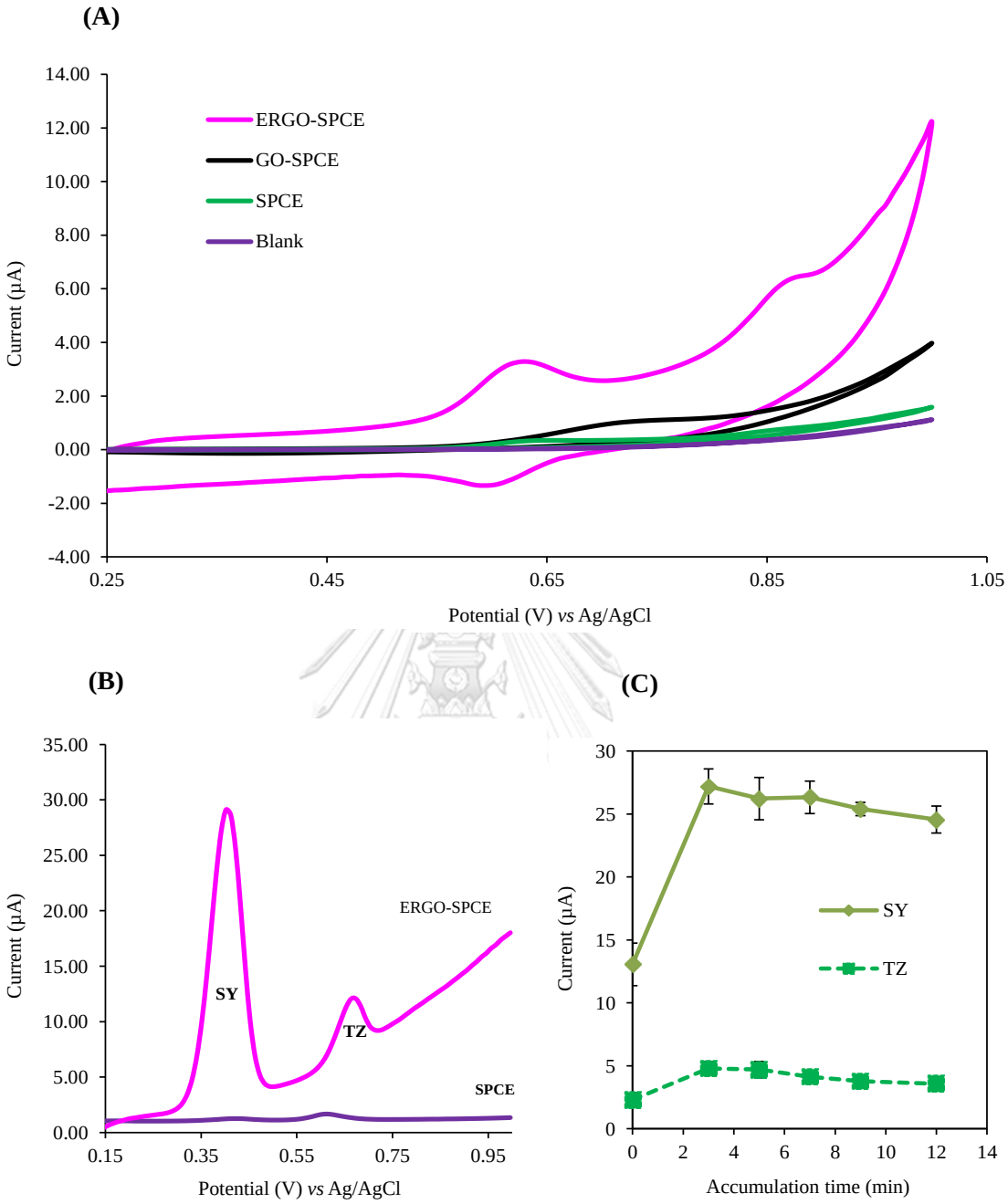


**Figure 4.7** CV (A) and DPV voltammograms (B) of the modified and unmodified SPCE, (C) accumulation time effect on the oxidation current of SY and TZ (10 µM) in 0.1 M phosphate buffer solution of pH 6.0.

**4.3.3 Influence of the GO concentrations on the current responses of SY and TZ**

As the electrochemical reduction of GO can control the thickness and size of the produced ERGO film by varying either the electrochemical parameters or GO concentration [116], to achieve proper conditions for detection, the effects of the GO concentration and number of reduction cycles on the current responses of SY and TZ were examined. For the optimization of the GO loading, a gradual increase in the concentrations of GO in the working solution from 0 to 0.7 mg/mL results in remarkable increases in the oxidation peak currents of both colorants (Figure 4.8(A)). During this period, the surface concentration of GO greatly increases, showing a higher accumulation efficiency and current responses to SY and TZ. The maximum currents of both colorants were obtained at 0.7 mg/mL of GO, and the oxidation peak currents gradually decrease as the GO concentration was further raised from 0.7 to 1.1 mg/mL. As for the decreases in the analytical signals of both analytes, a possible explanation could be that multiple layers of graphene (more than 10 layers) are generated on the electrode surface when a high concentration of GO is employed, which makes it characteristically similar to graphite material. The GO concentration of 0.7 mg/mL was therefore selected to modify the sensors.

Additionally, to achieve the optimal conditions, the effect of the number of scan cycles was examined. The obtained results exhibited that the current responses of both colorants gradually increase with increasing the number of scan cycles (Figure 4.8(B)) and reach a maximum current at sixteen scan cycles. After more cycles, the decreased signal might be caused by the same reason aforementioned, which is that multiple layers of the ERGO film are generated on the electrode surface affecting the electron transfer between the analytes and the electrode surface.

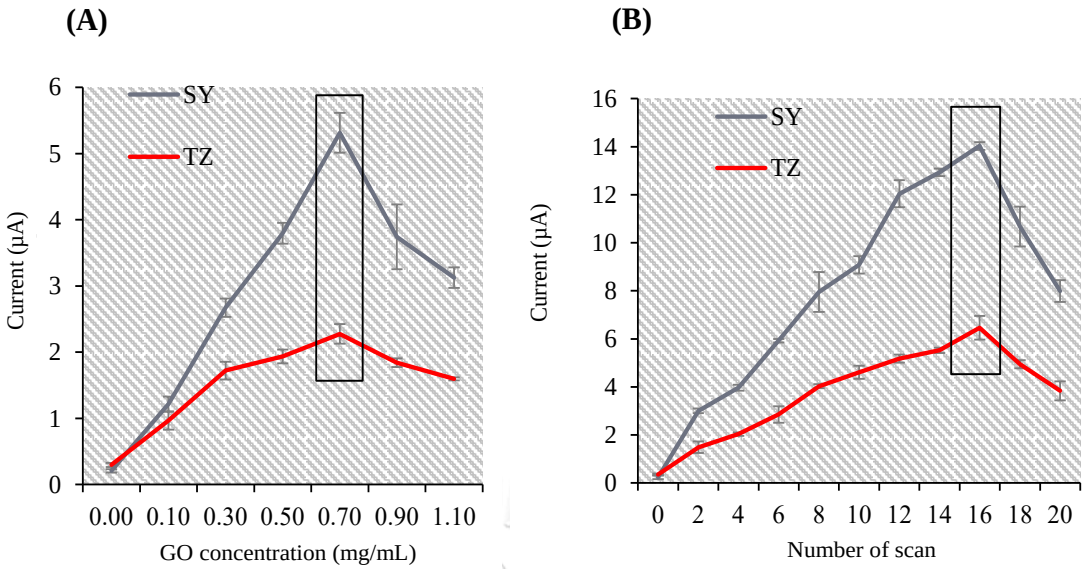


**Figure 4.8** Influence of GO concentrations and number of scan cycles on the oxidation current of SY and TZ (10 μM) in 0.1 M phosphate buffer of pH 6.

### 4.3.4 Effect of the scan rate

In this section, to fit a diffusion-controlled redox process, the influence of the scan rate on the peak currents of SY and TZ was examined by cyclic voltammetry. From this study, the results revealed that the peak potentials ($E_p$) of both colorants shifted positively with faster scan rates. As shown in Figures 4.9(A) and (B), linear relationships between the square root of the scan rate and current response were obtained from 20 to 100 mV $s^{-1}$ and 25 to 125 mV $s^{-1}$ for SY and TZ, respectively, which are typical of diffusion controlled currents, and the equations can be expressed as follows:

$I_p$ (SY) = 0.6369 $v^{1/2}$ - 2.6707, $R^2$ = 0.9955

$I_p$ (TZ) = 0.0307 $v^{1/2}$ - 0.0460, $R^2$ = 0.9988

In addition, to confirm a diffusion-controlled redox process, plots of the log $I_p$ verses the log v were established corresponding to the following equation:

$\log I_p$ (SY) = 0.5688log v - 0.7804, $R^2$ = 0.9918

$\log I_p$ (TZ) = 0.6102log v - 1.7952, $R^2$ = 0.9994

The slopes of 0.56 (Figure 4.9(C)) and 0.61 (Figure 4.9(D)) for SY and TZ, respectively, were close to the theoretically expected value of 0.5 for a purely diffusion controlled current [124]. This result further confirms that the electro-oxidation of SY and TZ was a diffusion controlled process.

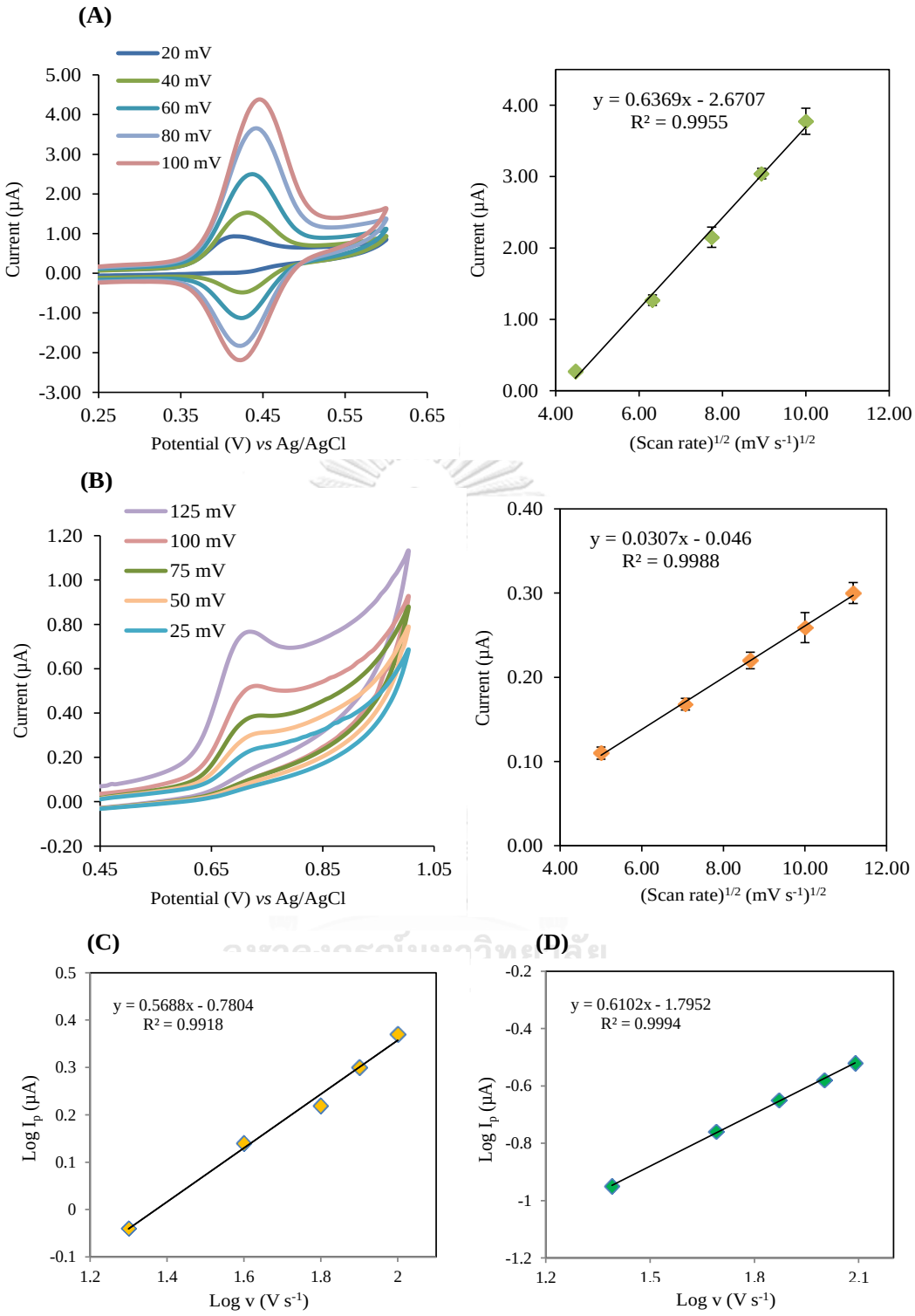


**Figure 4.9** CV curves of 10 µM SY (A) and TZ (B) in phosphate buffer solution of pH 6 under different scan rates and linear relation between logarithm of peak current and logarithm of scan rate for SY (C) and TZ (D).

### 4.3.5 Study of the electrochemical mechanism at the ERGO-SPCE

To determine the number of electrons and protons in the reaction of each analyte at the ERGO-SPCE, the influence of pH on the $E_p$ of SY and TZ was examined using a DPV technique. A plot of $E_p$ vs pH values was first constructed to obtain the ratio between protons and electrons in the reaction. As exhibited in Figure 4.10, the anodic potentials of SY (Figure 4.10(A)) and TZ (Figure 4.10(B)) were found to be dependent on pH values and shifted to more negative values when the pH of the medium was increased. This suggested that a proton participates in the oxidation of both SY and TZ. The equations of pH dependency can be expressed as follows: $E_{p,a}$ (SY) = -0.0520pH + 0.904, $R^2$ = 0.9912 and $E_{p,a}$ (TZ) = -0.0658pH + 1.215, $R^2$ = 0.9965. Slopes of -0.052 mV and -0.065 mV for SY and TZ, respectively, were obtained and are near the theoretical value of -0.059 mV per unit. This result confirms that an equal number of electrons and protons are involved in the reaction [29]. The highest peak current was obtained at a pH of 6. This pH was then employed in this study. It is noted that the oxidation signals of both SY and TZ gradually increased with increasing pH values from 4 to 6 and then slightly decreased with further pH increases. Thus, pH values higher than 6 were unsuitable for electrochemical determination of these colorants. The decreases of oxidation signals at pH higher than 6 could be attributed to the oxidation of phenolic hydroxyl group with one proton transferred in the electrochemical reaction [125]. The $pK_a$ values of these synthetic colorants are 9.4 and 10.4 for TZ and SY, respectively. As the obtained results, it can be concluded that pH value is the most important parameter for electrochemical detection of these colorants.



To propose a possible mechanism, the electrochemical behaviors of SY and TZ on the ERGO-SPCE were studied using a CV technique at the different scan rates. The oxidation currents of SY (Figure 4.9(A), section 4.3.4) and TZ (Figure 4.9(B)), section 4.3.4) increased linearly with the square root of the scan rate, which is typical

of diffusion controlled currents. The oxidation peaks of both SY and TZ shifted positively with ascending scan rates. Additionally, the oxidation peak of SY exhibited a reversible process, while TZ displayed an irreversible electrode process. This relationship is in accordance with Equation (4.2).

$$\begin{aligned} Ep &= E^{\circ} + \frac{RT}{\alpha nF}\left[0.780 + \ln\left(D_R{}^{\frac{1}{2}} \div k^{\circ}\right) + \ln\left(\frac{\alpha nFv}{RT}\right)^{1/2}\right] \\ &= K + \frac{RT}{2\alpha nF}\ln v \end{aligned} \qquad \text{(Equation 4.2)}$$

In Equation (4.2), **α** is the transfer coefficient, k° is the standard heterogeneous rate constant of the reaction, n is the number of electrons transferred, v is the scan rate, and E° is the formal redox potential. Other symbols have their usual meanings. Based on this result, to obtain the number of electrons participating in the reaction, plots of Ep vs ln v for SY (Figure 4.10(C)) and TZ (Figure 4.10(D)) were constructed.

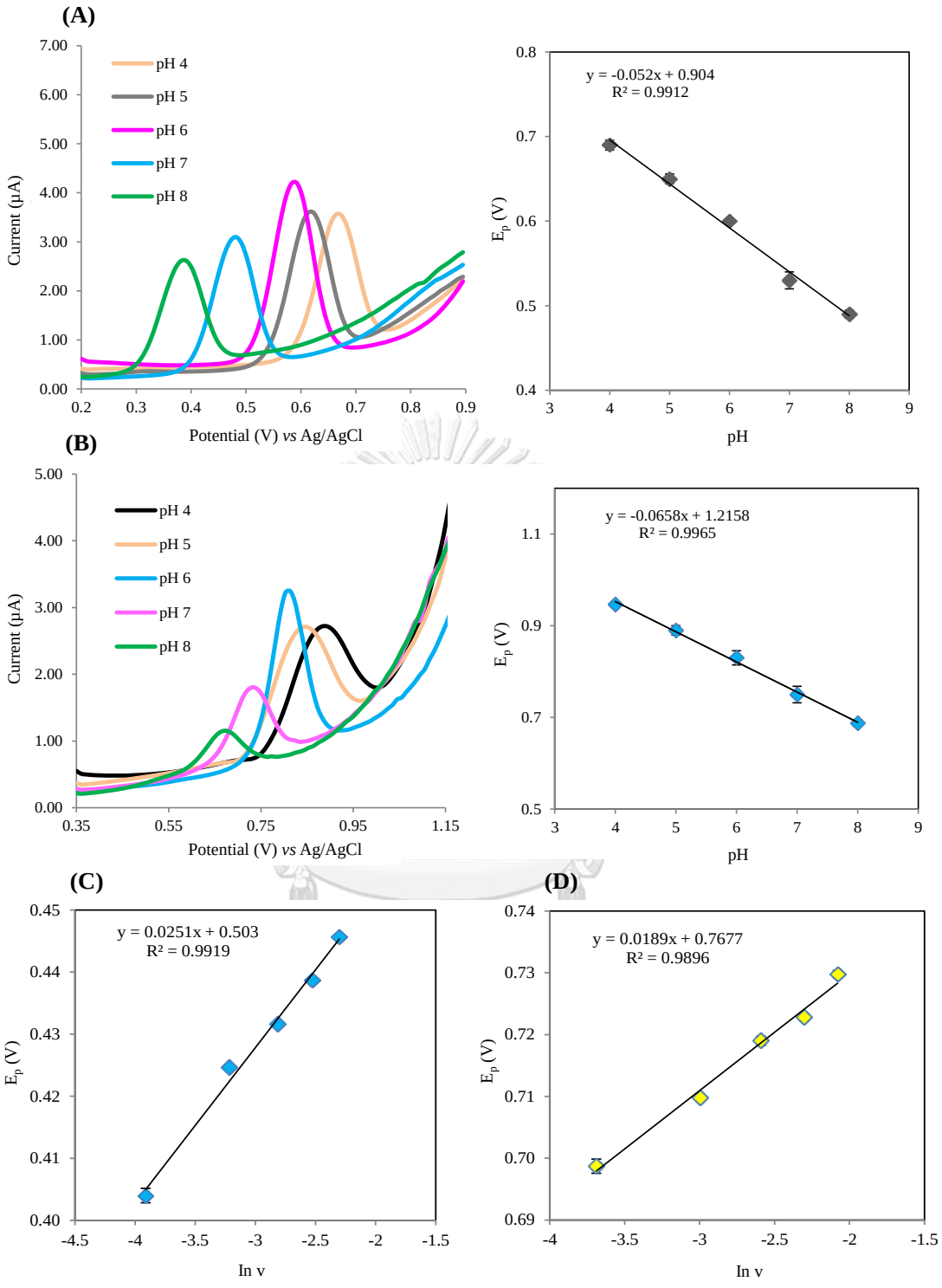


**Figure 4.10** DPV voltammgrams represent the influence of pH values on the $E_p$ of 7 µM SY (A) and 10 µM TZ (B) and dependence of $E_p$ on the natural logarithms of scan rate of SY (C) and TZ (D) at ERGO-SPCE under the optimized condition.

According to equation (4.2), the plots of $E_p$ vs ln v have good correlation, and the values of **α**n can be calculated to be 0.51 and 0.67 for SY and TZ, respectively, from the slope of each (0.0251 and 0.0189). Commonly, **α** is assumed to be 0.5. Consequently, the involvement of one electron was concluded for the reactions of both SY and TZ.

According to the relationship of $E_p$ and pH, we know that an equal number of electrons and protons participated in the oxidation reaction of both SY and TZ. Based on this result, it can be concluded that the oxidation mechanisms of SY and TZ involve one electron and one proton being transferred, which is consistent with the previously reported results [29, 126]. The proposed mechanisms are illustrated in Figure 4.11(A) and (B) for SY and TZ, respectively.

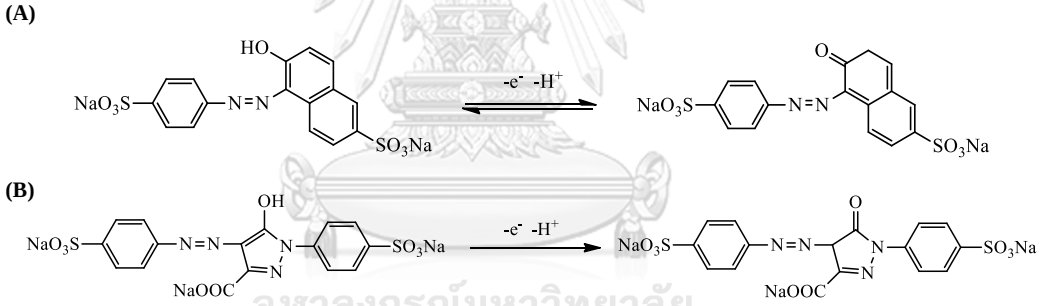




**Figure 4.11** The mechanisms for electrochemical process of SY (A) and TZ (B).

### 4.3.6 Calibration curve

After the formation of the ERGO-SPCE and obtaining the optimized conditions, calibration plots of the current signals obtained from the DPV analysis and various tested colorant concentrations were constructed. Figures 4.12(A) and (B) illustrate the DPV responses of SY and TZ under different concentrations, respectively. To observe the synergistic interference of them, the concentrations were fixed at 0.2 μM and 5 μM for SY and TZ, respectively. As shown in Figure 4.12(A), it was found that the

oxidation signal of 5 μM TZ was almost unchanged as the concentration of SY increased from 0.01 to 20 μM. A similar experiment was also carried out for TZ, as shown in Figure 4.12(B). When the concentration of TZ was increased from 0.02 to 20 μM, the oxidation current of 0.2 μM SY appeared to be stable. Therefore, the oxidation signals of SY and TZ on ERGO-SCPE were independent, and their synergistic interference was negligible. The calibration curve of SY exhibited a linear range from 0.01 to 20.0 μM with a $R^2$ value of 0.9958. For TZ determination, it was found that the oxidation peak current plotted against various tested concentrations of TZ exhibited linear correlation in the range from 0.02 to 20.0 μM with a $R^2$ value of 0.9949. The LODs were experimentally obtained (S/N = 3) and found to be 0.50 nM for SY and 4.50 nM for TZ. The LOQs were calculated to be 0.029 and 0.190 μM (at S/N = 10) for SY and TZ, respectively. The percent relative standard deviations (%RSD) for each set of SY and TZ determinations (n = 3) including the slope, intercept, LOD and LOQ were found to be in the range from 2.07 to 11.51. These %RSD values indicated that excellent reproducibility was achieved.

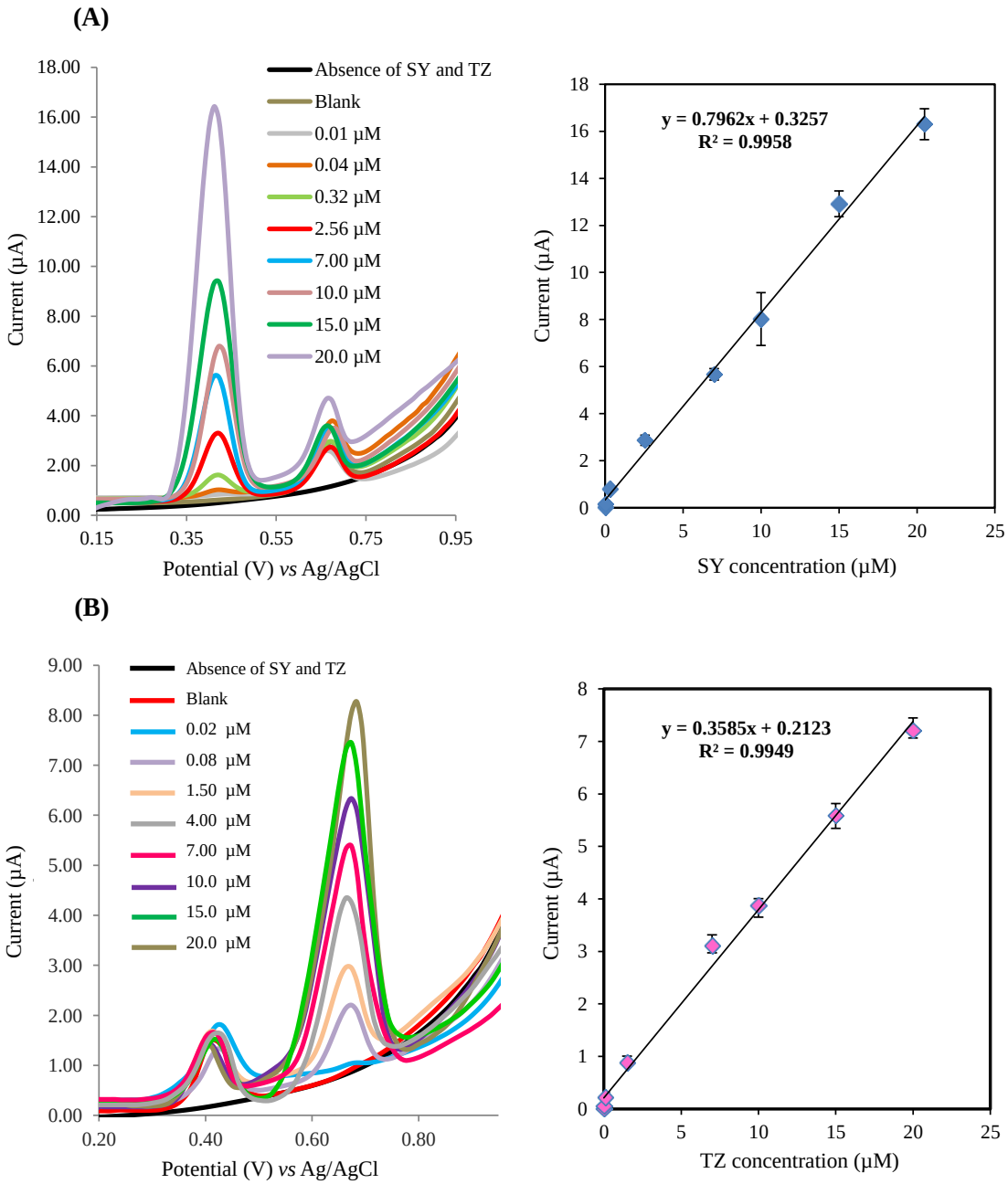


**Figure 4.12** Representative DPV of ERGO-SPCE with various SY (A) and TZ (B) concentrations, under the optimized parameters.

Compared with the previously reported electrochemical methods for the simultaneous determination of SY and TZ, this new sensing platform exhibited a

wider dynamic range and higher sensitivity. Additionally, the detection limits were as low as 0.50 and 4.50 nM for SY and TZ, respectively, as confirmed in Table 4.1.

**Table 4.1** Comparison of the analytical performance between the developed and previously reported electrochemical sensor for the simultaneous determination of both colorants

| Working electrode | pH | Linear range (μM) | | Limit of detection (μM) | | Reference |
|---|---|---|---|---|---|---|
| | | SY | TZ | SY | TZ | |
| β-CD-PDDA-GR[a]/GC-RDE[b] | 5 | 0.05-20 | 0.05-20 | 0.0120 | 0.0140 | [104] |
| Pretreated-BDD[c] | $H_2SO_4$ | 0.02-4.76 | 0.0999-5.660 | 0.0131 | 0.0627 | [106] |
| GN-PTA[d]/GCE[e] | 4.4 | 0.0332-0.464 | 0.112-2.810 | 0.0011 | 0.0561 | [29] |
| GN-$TO_2$/CPE[f] | $H_2SO_4$ | 0.02-2.050 | 0.02-1.180 | 0.0060 | 0.0080 | [107] |
| AuNPs/CPE | 4 | 0.1-2.0 | 0.05-1.6 | 0.0300 | 0.0020 | [30] |
| MWCNT[g]/GCE | 8 | 0.0553-11.053 | 0.374-74.86 | 0.0200 | 0.1880 | [18] |
| ERGO/SPCE | 6 | 0.01-20 | 0.02-20 | 0.0005 | 0.0045 | This work |



[a] β-cyclodextrin-coated poly (diallyldimethylammonium chloride)-functionalized graphene

[b] Glassy carbon-rotating disk electrode

[c] Boron-doped diamond electrode

[d] Graphene layer-wrapped phosphotungstic acid hybrid

[e] Glassy carbon electrode

[f] Carbon paste electrode

[g] Multi-walled carbon nanotubes

### 4.3.7 Selectivity and reproducibility of the detection

The selectivity of a method is a crucial factor for a practical measurement due to various interfering substances present in the system, such as glucose, ascorbic acid, sodium and iron. The results displayed that when interfering substances are present, the peak current changed insignificantly, indicating that the developed ERGO-SPCE sensor had good selectivity for the determinations of SY and TZ (Figures 4.13(A) and (B)).

To evaluate the reproducibility of the proposed method, seven sensors were prepared by the same process. The electrochemical sensor was tested at concentrations of 2, 5 and 10 μM for each colorant. For SY determination, %RSDs of 7.8%, 4.5% and 1.6% were obtained, respectively. An excellent reproducibility was also obtained for TZ detection, and the %RSDs of reproducibility were found to be 7.11%, 6.82% and 2.15%, respectively. The obtained results suggested that the proposed method remarkably minimized the sensor-to-sensor deviation, and excellent fabrication reproducibility was achieved.



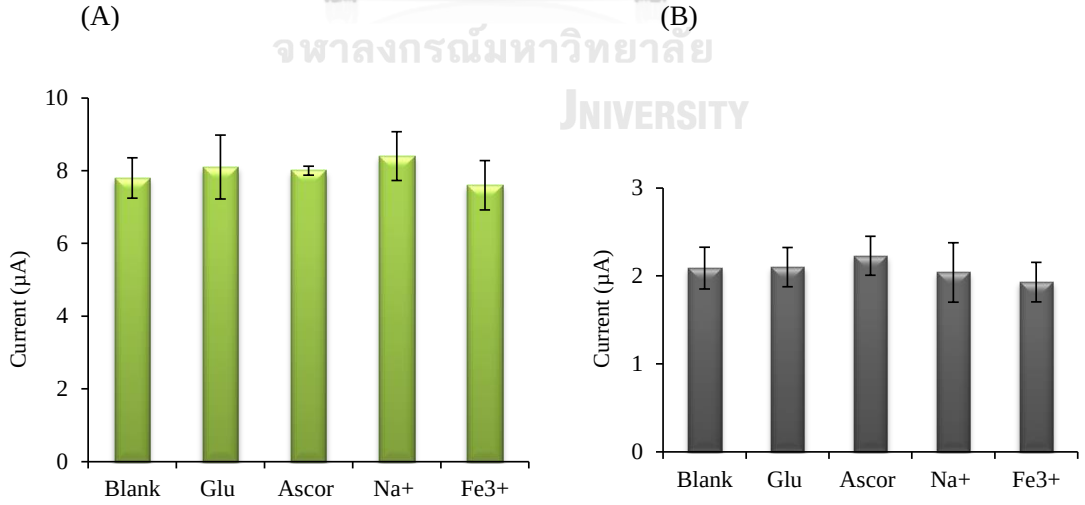


**Figure 4.13** Effect of various interfering substances at 50-fold excess on the electrochemical signal responses of SY (A) and TZ (B) obtained from the ERGO-SPCE.

**4.3.8 Application of a ERGO-SPCE for the determination of SY and TZ in practical samples**

To demonstrate its suitability and potential application for practical sample analysis, the proposed method was applied to determine SY and TZ in seven selected beverages, which were purchased from a local supermarket. The seven beverages employed in this work consisted of two soft drinks, two juice concentrate drinks, two energy drinks and one thirst quencher sample. In one type of soft drink, in 0.1 M phosphate buffer at a pH of 6 after 3 min of accumulation time, two oxidation peaks appeared at approximately 0.4 V and 0.7 V with the ERGO-SPCE, which imply that both SY and TZ were present. After standard solutions of both colorants were added, it was found that the oxidation peak currents increased (Figure 4.14). Otherwise, the contents of SY and TZ in the sample can be achieved according to the oxidation peak current ratio.

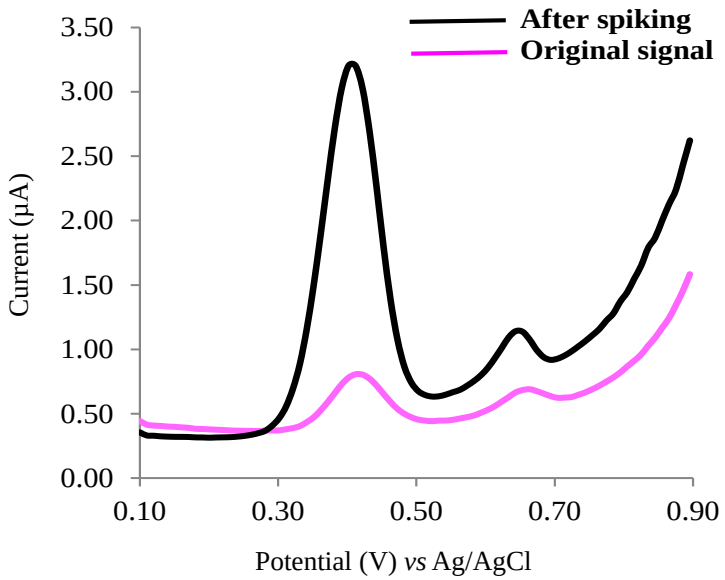


**Figure 4.14** Differential pulse voltammograms of SY and TZ at ERGO-SPCE in original soft drink sample, and after SY (4 µM) and TZ (7 µM) standard solution were added.

The contents of both colorants were also validated employing the compendium of methods to confirm the accuracy of this method. The comparison of the results between the proposed system and compendium method agreed as displayed in Table 4.2. Each reported value is a mean of three replicates (n = 3), and the relative standard deviation (RSD ≤ 5) using this method was acceptable, indicating good repeatability. A paired t-test at a 95% confidential interval was achieved on the results obtained from real samples analysis. The experimental t-value (t-calculated) obtained by this novel method is in the range from 1.2318 to 2.0334 and is lower than the critical t-value (2.920). It can be concluded that there is no significant difference between proposed method and the compendium of methods. Therefore, our proposed strategy is reliable and can be used as a new alternative assay for the determination of SY and TZ with highly sensitive and rapid analysis.

In addition, the accuracy of the proposed method was evaluated by performing a recovery test after introducing known amounts of SY and TZ into the samples and then analyzing them according to the same procedure. The amounts of SY and TZ were determined using the standard addition method. The %recovery values are in the range from 80.74 to 117.59, suggesting that the determination of SY and TZ using an ERGO-SPCE is precise and feasible (Table 4.3).

**Table 4.2** Comparison of the obtained results between the proposed method and HPLC for detection of SY and TZ in seven beverages, accumulation time was 3 min at open-circuit

| Sample No. | Analyte | By developed sensor (mg/L) | Compendium of method (HPLC) (mg/L) | Relative error (%) |
|---|---|---|---|---|
| 1 | SY | 4.10 ± 0.04 | 3.95 ± 0.02 | 3.79 |
| | TZ | 19.04 ± 0.91 | 18.55 ± 0.07 | 2.64 |
| 2 | SY | 5.70 ± 0.05 | 5.56 ± 0.24 | 2.51 |
| | TZ | 5.04 ± 0.09 | 4.83 ± 0.01 | 4.34 |
| 3 | SY | 4.54 ± 0.53 | 4.75 ± 0.03 | -4.42 |
| | TZ | 16.56 ± 0.16 | 15.80 ± 0.01 | 4.81 |
| 4 | SY | 28.95 ± 0.75 | 30.43 ± 0.01 | -4.86 |
| | TZ | 31.49 ± 1.21 | 32.45 ± 0.03 | -2.95 |
| 5 | SY | 43.33 ± 1.70 | 43.14 ± 0.03 | 0.44 |
| | TZ | - | - | - |
| 6 | SY | 10.17 ± 0.41 | 9.93 ± 0.05 | 2.41 |
| | TZ | - | - | - |
| 7 | SY | - | - | - |
| | TZ | 1.49 ± 0.07 | 1.55 ± 0.02 | -3.87 |

Note: values reported are mean of three replicates (n = 3).

**Table 4.3** Determination of SY and TZ in soft drink samples

| Samples | Spiked (μM) | Spiked (μM) | Expected (μM) | | Found (μM) | | Recovery (%) | |
|---|---|---|---|---|---|---|---|---|
| No. | SY | TZ | SY | TZ | SY | TZ | SY | TZ |
| 1 | 0 | 0 | - | - | 0.04 | 0.35 | - | - |
| | 1.0 | 1.0 | 1.04 | 1.35 | 1.06 | 1.09 | 102 | 80.74 |
| | 7.0 | 8.0 | 7.04 | 8.35 | 6.86 | 7.48 | 97 | 89.58 |
| | 10.0 | 12.0 | 10.04 | 12.35 | 10.22 | 12.48 | 101.73 | 101.05 |
| 3 | 0 | 0 | - | - | 0.12 | 0.10 | - | - |
| | 0.1 | 0.3 | 0.22 | 0.40 | 0.25 | 0.39 | 117.59 | 97.50 |
| | 5.0 | 4.0 | 5.12 | 4.10 | 4.87 | 3.94 | 95.19 | 96.17 |
| | 14.0 | 12.0 | 14.12 | 12.10 | 14.31 | 12.48 | 101.31 | 103.19 |
| 3 | 0 | 0 | - | - | 0.19 | 0.03 | - | - |
| | 0.1 | 1.0 | 0.29 | 1.03 | 0.28 | 1.20 | 96.55 | 116.80 |
| | 5.0 | 8.0 | 5.19 | 8.03 | 4.66 | 7.40 | 89.78 | 92.14 |
| | 15.0 | 14.0 | 15.19 | 14.03 | 15.36 | 14.55 | 101.11 | 103.69 |
| 4 | 0 | 0 | - | - | 0.32 | 0.59 | - | - |
| | 0.5 | 0.3 | 0.82 | 0.89 | 0.72 | 0.83 | 87.8 | 92.83 |
| | 4.0 | 6.0 | 4.32 | 6.59 | 4.76 | 6.03 | 110.18 | 91.53 |
| | 12.0 | 12.0 | 12.32 | 12.59 | 12.20 | 12.54 | 99.02 | 99.63 |
| 5 | 0 | - | - | - | 0.38 | - | - | - |
| | 2.0 | - | 2.38 | - | 2.24 | - | 93.99 | - |
| | 7.0 | - | 7.38 | - | 6.46 | - | 87.62 | - |
| | 12.0 | - | 12.38 | - | 12.42 | - | 100.33 | - |
| 6 | 0 | - | - | - | 0.22 | - | - | - |
| | 1.0 | - | 1.22 | - | 1.24 | - | 101.63 | - |
| | 7.0 | - | 7.22 | - | 6.59 | - | 91.27 | - |
| | 12.0 | - | 12.22 | - | 12.29 | - | 99.75 | - |
| 7 | - | 0 | - | - | - | 0.66 | - | - |
| | - | 0.1 | - | 0.76 | - | 0.65 | - | 85.52 |
| | - | 6.0 | - | 6.66 | - | 6.0 | - | 90.09 |
| | - | 15.0 | - | 15.66 | - | 15.62 | - | 99.74 |

Note: values reported are mean of three replicates (n = 3).

## 4.4 Conclusions

A novel electrochemical sensor for the simultaneous determination of SY and TZ based on an ERGO-modified disposable SPCE was successfully developed and applied to detect the SY and TZ contents in some commercial beverages. The ERGO-modified SPCE can greatly enhance the electrochemical signals of both colorants, suggesting remarkable surface enhancement effects. The calibration curves of SY and TZ exhibited linear correlation from 0.01 to 20.0 μM, and 0.02 to 20.0 μM, respectively, and the corresponding LODs were as low as 0.50 and 4.50 nM, respectively. Furthermore, the peak current was changed insignificantly in the presence of interfering substances, suggesting that the selectivity of the developed sensor was excellent. For practical analysis, the obtained results from this proposed method agreed well with those obtained from the compendium of methods, in-house standard technique. The advantages of this sensor include the ease of preparation, reduced time comsumption and non-toxicity. The electrode is easily and inexpensively prepared, and it requires only a small sample volume (40 μL). The instrument set-up is also simple. Therefore, the present technique should be suitable as a novel method for the rapid determination of these food colorants. Additionally, this sensing platform may provide a promising alternative choice for practical application in biological and environmental analysis.

# CHAPTER V

# CONCLUSIONS AND FUTURE WORKS

## 5.1 Conclusions

This dissertation can be concluded into three parts as follows:

**Part I**: Influence of the DNA sensor design on the performance of the multiplex detection of HPV type 16 and 18 DNA

The part describes significance of sensor architecture and signaling mechanism which are greatly contributed to the detection sensitivity. Two new "signal-on" E-DNA sensors were designed and fabricated for DNA diagnosis purpose. The sensor format is dependent upon a recognition site of signaling probe (AQ-P2) on the ssDNA. AQ-P2 can selectively bind to the target DNA at upstream (5′ on ssDNA) (ASU) or downstream (3′ on ssDNA) (ASD) positions on the DNA sequence hybridized by the P1 capture probe. In the presence of target DNA, sensors exhibited large increases in the AQ signal where the peak potential appeared at approximately -0.75 V. The ASD format exhibited a higher signal response in DNA detection compared to the ASU format. This designed format was further applied to simultaneously detect HPV type 16 and 18 DNA. The proposed sensor can detect HPV DNA specifically and sensitively. LODs were obtained in the pM range for both HPV type 16 and 18. Besides, this fabricated DNA biosensor was successfully applied to simultaneously detect a PCR-amplified sample derived from HPV type 16 (SiHa) and 18 (HeLa) positive human cancer cell lines. Evidence here indicated that the designing of effective DNA biosensors was successfully developed and can be readily applied to detect a wide range of DNA targets.

**Part II**: Electrochemical detection of C-reactive protein based on antraquinone-labeled antibody using a screen-printed graphene electrode

This work develops a novel electrochemical immunosensor based on anthraquinone-labeled signaling antibody using a screen-printed graphene electrode (SPGE) for a simple and highly sensitive determination of C-reactive protein (CRP). In this present work, a sandwich-type format with "signal-on" electrochemical sensing was employed. The sensors comprised of an unlabeled primary capture (anti-CRP 1°Ab) and anthraquinone-labeled secondary (AQ-2°Ab) antibodies. Conjugation of the signaling anti-CRP with AQ redox label can be simply performed in an aqueous solution. In the presence of CRP, the sensor exhibited a considerable increase in the AQ current compared to the absence of CRP, where the redox peak appeared at approximately -0.75 V. The CRP concentration was linear in the range from 0.01 to 150 µg/mL, and the limit of detection (LOD) was found to be 1.5 ng/mL (S/N = 3). This sensor exhibited very high sensitivity and selectivity in determining CRP and was successfully applied to determine CRP in the certified human serum with satisfied results.

**Part III**: Electrochemically-reduced graphene oxide modified screen-printed carbon electrodes for a simple and highly sensitive electrochemical detection of synthetic colorants in beverages



A novel electrochemical sensor for a highly sensitive and selective determination of SY and TZ employing electrochemically-reduced graphene oxide modified screen-printed carbon electrodes (ERGO-SPCE) was developed in this work. A green and facile routine electrochemical reduction method was employed to produce ERGO film onto the electrode surface within one operation step. The disposable SPCE employed was inexpensively and easily prepared. The electrochemical signal response on ERGO-SPCE enhanced greatly about 90 and 20 folds for SY and TZ, respectively. Excellent selectivity and specificity of the

developed sensor were also achieved. A detection limit of this method was as low as 0.5 and 4.5 nM for SY and TZ respectively. Furthermore, this electrochemical sensor was successfully applied to determine the amount of SY and TZ in commercial beverages.

**5.2 Future works**

The developed electrochemical sensor is very attractive platform to be employed as an alternative tool for various applicational purposes in our life sciences especial point-of-care diagnosis. The three-developed sensors demonstrate a simple, highly sensitive and selective determination of the interested analytes, and require uncomplicated and inexpensive instrumentation. These make them have an opportunity to apply for simultaneous determination of multi-analytes in complicated samples in order to reduce analysis time and cost. In addition, different electroactive species and material can be employed as a new modifier or labeled molecule to achieve higher sensitivity for chemical or biochemical analysis. These developed sensors are relevant for designing and fabricating effective sensors which can be readily applied for practical application to detect a wide range of analytes.

# REFERENCES


[1] McMichael, A.J., Woodruff, R.E., and Hales, S. Climate change and human health: present and future risks. The Lancet 367(9513) (2006): 859-869.

[2] Gupta, R.K., Periyakaruppan, A., Meyyappan, M., and Koehne, J.E. Label-free detection of C-reactive protein using a carbon nanofiber based biosensor. Biosensors and Bioelectronics 59 (2014): 112-9.

[3] DiNunzio, J.E. Determination of caffeine in beverages by high performance liquid chromatography. Journal of Chemical Education 62(5) (1985): 446.

[4] Ramesh, A. and Ravi, P.E. Electron ionization gas chromatography-mass spectrometric determination of residues of thirteen pyrethroid insecticides in whole blood. Journal of Chromatography. B Analytical Technologies in Biomedical and Life Science 802(2) (2004): 371-6.

[5] Valverde, J., This, H., and Vignolle, M. Quantitative Determination of Photosynthetic Pigments in Green Beans Using Thin-Layer Chromatography and a Flatbed Scanner as Densitometer. Journal of Chemical Education 84(9) (2007): 1505.

[6] Hird, S.J., Lau, B.P.Y., Schuhmacher, R., and Krska, R. Liquid chromatography-mass spectrometry for the determination of chemical contaminants in food. TrAC Trends in Analytical Chemistry 59 (2014): 59-72.

[7] Bosch, F.X., Lorincz, A., Muñoz, N., Meijer, C.J.L.M., and Shah, K.V. The causal relation between human papillomavirus and cervical cancer. Journal of Clinical Pathology 55(4) (2002): 244.

[8] Parkin, D.M., Bray, F., Ferlay, J., and Pisani, P. Estimating the world cancer burden: Globocan 2000. International Journal of Cancer 94(2) (2001): 153-156.

[9] Castle, P.E., et al. Restricted Cross-Reactivity of Hybrid Capture 2 with Nononcogenic Human Papillomavirus Types. Cancer Epidemiology Biomarkers & Prevention 11(11) (2002): 1394.

[10] Zandnia, F., Doosti, A., Mokhtari-Farsani, A., Kardi, M.T., and Movafagh, A. Application of multiplex PCR for Rapid and sensitive detection of human

papillomaviruses in cervical cancer. Pakistan Journal of Medical Sciences 32(2) (2016): 444-447.

[11] Villa, L.L. and Denny, L. CHAPTER 7 Methods for detection of HPV infection and its clinical utility. International Journal of Gynecology & Obstetrics 94 (2006): S71-S80.

[12] Pradhan, A.D., Manson, J.E., Rifai, N., Buring, J.E., and Ridker, P.M. C-reactive protein, interleukin 6, and risk of developing type 2 diabetes mellitus. JAMA 286(3) (2001): 327-334.

[13] Wilson, P.W. CDC/AHA Workshop on Markers of Inflammation and Cardiovascular Disease: Application to Clinical and Public Health Practice: ability of inflammatory markers to predict disease in asymptomatic patients: a background paper. Circulation 110(25) (2004): e568-71.

[14] Casas, J.P., Shah, T., Hingorani, A.D., Danesh, J., and Pepys, M.B. C-reactive protein and coronary heart disease: a critical review. Journal of Internal Medicine 264(4) (2008): 295-314.

[15] Buckley, D.I., Fu, R., Freeman, M., Rogers, K., and Helfand, M. C-reactive protein as a risk factor for coronary heart disease: A systematic review and meta-analyses for the u.s. preventive services task force. Annals of Internal Medicine 151(7) (2009): 483-495.

[16] Sisman, A.R., Kume, T., Tas, G., Akan, P., and Tuncel, P. Comparison and evaluation of two C-reactive protein assays based on particle-enhanced immunoturbidimetry. Journal of Clinical Laboratory Analysis 21(2) (2007): 71-6.

[17] Wang, P., Hu, X., Cheng, Q., Zhao, X., Fu, X., and Wu, K. Electrochemical Detection of Amaranth in Food Based on the Enhancement Effect of Carbon Nanotube Film. Journal of Agricultural and Food Chemistry 58(23) (2010): 12112-12116.

[18] Zhang, Y., Zhang, X., Lu, X., Yang, J., and Wu, K. Multi-wall carbon nanotube film-based electrochemical sensor for rapid detection of Ponceau 4R and Allura Red. Food Chemistry 122(3) (2010): 909-913.

[19] Zhang, Y., Gan, T., Wan, C., and Wu, K. Morphology-controlled electrochemical sensing amaranth at nanomolar levels using alumina. Analytica Chimica Acta 764 (2013): 53-8.

[20] Jager, A.V., Tonin, F.G., and Tavares, M.F.M. Optimizing the separation of food dyes by capillary electrophoresis. Journal of Separation Science 28(9-10) (2005): 957-965.

[21] Ma, M., Luo, X., Chen, B., Su, S., and Yao, S. Simultaneous determination of water-soluble and fat-soluble synthetic colorants in foodstuff by high-performance liquid chromatography–diode array detection–electrospray mass spectrometry. Journal of Chromatography A 1103(1) (2006): 170-176.

[22] Alves, S.P., Brum, D.M., Branco de Andrade, É.C., and Pereira Netto, A.D. Determination of synthetic dyes in selected foodstuffs by high performance liquid chromatography with UV-DAD detection. Food Chemistry 107(1) (2008): 489-496.

[23] Oakley, L.H., Fabian, D.M., Mayhew, H.E., Svoboda, S.A., and Wustholz, K.L. Pretreatment Strategies for SERS Analysis of Indigo and Prussian Blue in Aged Painted Surfaces. Analytical Chemistry 84(18) (2012): 8006-8012.

[24] Aikens, D.A. Electrochemical methods, fundamentals and applications. Journal of Chemical Education 60(1) (1983): A25.

[25] Dr, M.R.d.R. Electrochemical Methods: Fundamentals and Applications. Anti-Corrosion Methods and Materials 50(5) (2003).

[26] Arning, M.D. and Minteer, S.D. Electrode Potentials. in Handbook of Electrochemistry, pp. 813-827, 2007.

[27] Kissinger, P.T. and Heineman, W.R. Cyclic voltammetry. Journal of Chemical Education 60(9) (1983): 702.

[28] Rouhani, S. Novel Electrochemical Sensor for Sunset Yellow Based on a Platinum Wire–Coated Electrode. Analytical Letters 42(1) (2009): 141-153.

[29] Gan, T., Sun, J., Cao, S., Gao, F., Zhang, Y., and Yang, Y. One-step electrochemical approach for the preparation of graphene wrapped-phosphotungstic acid hybrid and its application for simultaneous

determination of sunset yellow and tartrazine. Electrochimica Acta 74 (2012): 151-157.

[30] Ghoreishi, S.M., Behpour, M., and Golestaneh, M. Simultaneous determination of Sunset yellow and Tartrazine in soft drinks using gold nanoparticles carbon paste electrode. Food Chemistry 132(1) (2012): 637-641.

[31] Krause, M.S. and Ramaley, L. Analytical application of square wave voltammetry. Analytical Chemistry 41(11) (1969): 1365-1369.

[32] Zhu, L., Xu, L., Huang, B., Jia, N., Tan, L., and Yao, S. Simultaneous determination of Cd(II) and Pb(II) using square wave anodic stripping voltammetry at a gold nanoparticle-graphene-cysteine composite modified bismuth film electrode. Electrochimica Acta 115 (2014): 471-477.

[33] Lovrić, M. and Komorsky-Lovric, Š. Square-wave voltammetry of an adsorbed reactant. Journal of Electroanalytical Chemistry and Interfacial Electrochemistry 248(2) (1988): 239-253.

[34] Aoki, K., Tokuda, K., and Matsuda, H. Theory of differential pulse voltammetry at stationary planar electrodes. Journal of Electroanalytical Chemistry and Interfacial Electrochemistry 175(1) (1984): 1-13.

[35] Mehrvar, M. and Abdi, M. Recent Developments, Characteristics, and Potential Applications of Electrochemical Biosensors. Analytical Sciences 20(8) (2004): 1113-1126.

[36] Pethig, R. Dielectric and Electrical Properties of Biological Materials. Journal of Bioelectricity 4(2) (1985): vii-ix.

[37] Chen, T.L., Chang, J.W., Hsieh, J.J., Cheng, H.Y., and Chiou, C.C. A Sensitive Peptide Nucleic Acid Probe Assay for Detection of BRAF V600 Mutations in Melanoma. Cancer Genomics Proteomics 13(5) (2016): 381-6.

[38] Staiano, M., et al. Enzymes as Sensors. Methods Enzymol 589 (2017): 115-131.

[39] Zhang, S., Wright, G., and Yang, Y. Materials and techniques for electrochemical biosensor design and construction. Biosensors and Bioelectronics 15(5) (2000): 273-282.

[40] Nielsen, P.E., Egholm, M., Berg, R.H., and Buchardt, O. Sequence-selective recognition of DNA by strand displacement with a thymine-substituted polyamide. Science 254(5037) (1991): 1497-500.

[41] Egholm, M. Recognition of guanine and adenine in DNA by cytosine and thymine containing peptide nucleic acids. Journal of the American Chemical Society 114 (1992): 9677-9678.

[42] Egholm, M., et al. PNA hybridizes to complementary oligonucleotides obeying the Watson–Crick hydrogen-bonding rules. Nature 365 (1993): 566.

[43] Wang, J., et al. Peptide Nucleic Acid Probes for Sequence-Specific DNA Biosensors. Journal of the American Chemical Society 118(33) (1996): 7667-7670.

[44] Vilaivan, T. and Lowe, G. A Novel Pyrrolidinyl PNA Showing High Sequence Specificity and Preferential Binding to DNA over RNA. Journal of the American Chemical Society 124(32) (2002): 9326-9327.

[45] Vilaivan, T. and Srisuwannaket, C. Hybridization of Pyrrolidinyl Peptide Nucleic Acids and DNA: Selectivity, Base-Pairing Specificity, and Direction of Binding. Organic Letters 8(9) (2006): 1897-1900.

[46] Boontha, B., Nakkuntod, J., Hirankarn, N., Chaumpluk, P., and Vilaivan, T. Multiplex Mass Spectrometric Genotyping of Single Nucleotide Polymorphisms Employing Pyrrolidinyl Peptide Nucleic Acid in Combination with Ion-Exchange Capture. Analytical Chemistry 80(21) (2008): 8178-8186.

[47] Ananthanawat, C., Vilaivan, T., Hoven, V.P., and Su, X. Comparison of DNA, aminoethylglycyl PNA and pyrrolidinyl PNA as probes for detection of DNA hybridization using surface plasmon resonance technique. Biosensors and Bioelectronics 25(5) (2010): 1064-1069.

[48] Vilaivan, T. Pyrrolidinyl PNA with α/β-Dipeptide Backbone: From Development to Applications. Accounts of Chemical Research 48(6) (2015): 1645-1656.

[49] Kongpeth, J., Jampasa, S., Chaumpluk, P., Chailapakul, O., and Vilaivan, T. Immobilization-free electrochemical DNA detection with anthraquinone-labeled pyrrolidinyl peptide nucleic acid probe. Talanta 146 (2016): 318-325.

[50] Zhao, J., Ji, S., Chen, Y., Guo, H., and Yang, P. Excited state intramolecular proton transfer (ESIPT): from principal photophysics to the development of new chromophores and applications in fluorescent molecular probes and luminescent materials. Physical Chemistry Chemical Physics 14(25) (2012): 8803-17.

[51] Luo, C., et al. A sensitive electrochemical DNA biosensor for specific detection of Enterobacteriaceae bacteria by Exonuclease III-assisted signal amplification. Biosensors and Bioelectronics 48 (2013): 132-7.

[52] Wang, L., et al. Graphene sheets, polyaniline and AuNPs based DNA sensor for electrochemical determination of BCR/ABL fusion gene with functional hairpin probe. Biosensors and Bioelectronics 51 (2014): 201-7.

[53] Gao, L., He, X., Ju, L., Liu, X., Li, F., and Cui, H. A label-free method for the detection of specific DNA sequences using gold nanoparticles bifunctionalized with a chemiluminescent reagent and a catalyst as signal reporters. Analytical and Bioanalytical Chemistry 408(30) (2016): 8747-8754.

[54] Fan, C., Plaxco, K.W., and Heeger, A.J. Electrochemical interrogation of conformational changes as a reagentless method for the sequence-specific detection of DNA. Proceeding of the National Academy of Science United States of America 100(16) (2003): 9134-7.

[55] Cui, H.F., Cheng, L., Zhang, J., Liu, R., Zhang, C., and Fan, H. An electrochemical DNA sensor for sequence-specific DNA recognization in a homogeneous solution. Biosensors and Bioelectronics 56 (2014): 124-8.

[56] Aoki, H. and Tao, H. Label- and marker-free gene detection based on hybridization-induced conformational flexibility changes in a ferrocene-PNA conjugate probe. Analyst 132(8) (2007): 784-791.

[57] Luo, X., Lee, T.M.-H., and Hsing, I.M. Immobilization-Free Sequence-Specific Electrochemical Detection of DNA Using Ferrocene-Labeled Peptide Nucleic Acid. Analytical Chemistry 80(19) (2008): 7341-7346.

[58] Singh, A., et al. Graphene oxide-chitosan nanocomposite based electrochemical DNA biosensor for detection of typhoid. Sensors and Actuators B: Chemical 185 (2013): 675-684.

[59] Kuang, H., et al. Fabricated aptamer-based electrochemical "signal-off" sensor of ochratoxin A. Biosensors and Bioelectronics 26(2) (2010): 710-6.

[60] Wu, Y. and Lai, R.Y. Development of a "signal-on" electrochemical DNA sensor with an oligo-thymine spacer for point mutation detection. Chemical Communications 49(33) (2013): 3422-3424.

[61] Lubin, A.A. and Plaxco, K.W. Folding-Based Electrochemical Biosensors: The Case for Responsive Nucleic Acid Architectures. Accounts of Chemical Research 43(4) (2010): 496-505.

[62] Wang, Q., et al. An electrochemical DNA biosensor based on the "Y" junction structure and restriction endonuclease-aided target recycling strategy. Chemical Communications 48(24) (2012): 2982-4.

[63] Anne, A., Bouchardon, A., and Moiroux, J. 3‘-Ferrocene-Labeled Oligonucleotide Chains End-Tethered to Gold Electrode Surfaces: Novel Model Systems for Exploring Flexibility of Short DNA Using Cyclic Voltammetry. Journal of the American Chemical Society 125(5) (2003): 1112-1113.

[64] Mao, Y., Luo, C., and Ouyang, Q. Studies of temperature-dependent electronic transduction on DNA hairpin loop sensor. Nucleic Acids Research 31(18) (2003): e108-e108.

[65] Wu, Y. and Lai, R.Y. Electrochemical Detection of Platinum(IV) Prodrug Satraplatin in Serum. Analytical Chemistry 87(21) (2015): 11092-11097.

[66] Immoos, C.E., Lee, S.J., and Grinstaff, M.W. DNA-PEG-DNA Triblock Macromolecules for Reagentless DNA Detection. Journal of the American Chemical Society 126(35) (2004): 10814-10815.

[67] Xiao, Y., Lubin, A.A., Baker, B.R., Plaxco, K.W., and Heeger, A.J. Single-step electronic detection of femtomolar DNA by target-induced strand displacement in an electrode-bound duplex. Proceedings of the National Academy of Sciences of the United States of America 103(45) (2006): 16677-16680.

[68] Cash, K.J., Heeger, A.J., Plaxco, K.W., and Xiao, Y. Optimization of a Reusable, DNA Pseudoknot-Based Electrochemical Sensor for Sequence-Specific DNA Detection in Blood Serum. Analytical Chemistry 81(2) (2009): 656-661.

[69] White, R.J. and Plaxco, K.W. Exploiting Binding-Induced Changes in Probe Flexibility for the Optimization of Electrochemical Biosensors. Analytical Chemistry 82(1) (2010): 73-76.

[70] Rowe, A.A., et al. Electrochemical Biosensors Employing an Internal Electrode Attachment Site and Achieving Reversible, High Gain Detection of Specific Nucleic Acid Sequences. Analytical Chemistry 83(24) (2011): 9462-9466.

[71] Idili, A., Amodio, A., Vidonis, M., Feinberg-Somerson, J., Castronovo, M., and Ricci, F. Folding-Upon-Binding and Signal-On Electrochemical DNA Sensor with High Affinity and Specificity. Analytical Chemistry 86(18) (2014): 9013-9019.

[72] Yu, Z.-g. and Lai, R.Y. Effect of Signaling Probe Conformation on Sensor Performance of a Displacement-Based Electrochemical DNA Sensor. Analytical Chemistry 85(6) (2013): 3340-3346.

[73] Jampasa, S., et al. Electrochemical detection of human papillomavirus DNA type 16 using a pyrrolidinyl peptide nucleic acid probe immobilized on screen-printed carbon electrodes. Biosensors and Bioelectronics 54 (2014): 428-434.

[74] Egholm, M., Buchardt, O., Nielsen, P.E., and Berg, R.H. Peptide nucleic acids (PNA). Oligonucleotide analogs with an achiral peptide backbone. Journal of the American Chemical Society 114(5) (1992): 1895-1897.

[75] Vilaivan, C., et al. Pyrrolidinyl peptide nucleic acid with alpha/beta-peptide backbone: A conformationally constrained PNA with unusual hybridization properties. Artif DNA PNA XNA 2(2) (2011): 50-59.

[76] Jampasa, S., Siangproh, W., Duangmal, K., and Chailapakul, O. Electrochemically reduced graphene oxide-modified screen-printed carbon electrodes for a simple and highly sensitive electrochemical detection of synthetic colorants in beverages. Talanta 160 (2016): 113-124.

[77] Ge, C., Miao, W., Ji, M., and Gu, N. Glutaraldehyde-modified electrode for nonlabeling voltammetric detection of p16 INK4A gene. Analytical and Bioanalytical Chemistry 383(4) (2005): 651-659.

[78] Yang, Y., et al. Selective detection of silver ions using mushroom-like polyaniline and gold nanoparticle nanocomposite-based electrochemical DNA sensor. Analytical Biochemistry 490 (2015): 7-13.

[79] Yin, H., Zhou, Y., Zhang, H., Meng, X., and Ai, S. Electrochemical determination of microRNA-21 based on graphene, LNA integrated molecular beacon, AuNPs and biotin multifunctional bio bar codes and enzymatic assay system. Biosensors and Bioelectronics 33(1) (2012): 247-253.

[80] Lin, C.Y., Yu, C.J., Lin, Y.H., and Tseng, W.L. Colorimetric sensing of silver(I) and mercury(II) ions based on an assembly of Tween 20-stabilized gold nanoparticles. Analytical Chemistry 82(16) (2010): 6830-7.

[81] Eckermann, A.L., Feld, D.J., Shaw, J.A., and Meade, T.J. Electrochemistry of redox-active self-assembled monolayers. Coordination Chemistry Reviews 254(15-16) (2010): 1769-1802.

[82] Campos-Ferreira, D.S., et al. Electrochemical DNA biosensor for human papillomavirus 16 detection in real samples. Analytica Chimica Acta 804 (2013): 258-263.

[83] Souza, E., et al. Electrochemical DNA biosensor for sequences related to the human papillomavirus type 16 using methylene blue. Biosensors Journal 3 (2014): 107-111.

[84] Teengam, P., Siangproh, W., Tuantranont, A., Henry, C.S., Vilaivan, T., and Chailapakul, O. Electrochemical paper-based peptide nucleic acid biosensor for detecting human papillomavirus. Analytica Chimica Acta 952 (2017): 32-40.

[85] Civit, L., Fragoso, A., and O'Sullivan, C.K. Electrochemical biosensor for the multiplexed detection of human papillomavirus genes. Biosensors and Bioelectronics 26(4) (2010): 1684-1687.

[86] Civit, L., Fragoso, A., Hölters, S., Dürst, M., and O'Sullivan, C.K. Electrochemical genosensor array for the simultaneous detection of multiple high-risk human

papillomavirus sequences in clinical samples. Analytica Chimica Acta 715 (2012): 93-98.

[87] Yen, Y.-K., Lai, Y.-C., Hong, W.-T., Pheanpanitporn, Y., Chen, C.-S., and Huang, L.-S. Electrical Detection of C-Reactive Protein Using a Single Free-Standing, Thermally Controlled Piezoresistive Microcantilever for Highly Reproducible and Accurate Measurements. Sensors 13(8) (2013).

[88] Zhou, J., et al. Ultratrace detection of C-reactive protein by a piezoelectric immunosensor based on $Fe_3O_4$@$SiO_2$ magnetic capture nanoprobes and HRP-antibody co-immobilized nano gold as signal tags. Sensors and Actuators B: Chemical 178 (2013): 494-500.

[89] Kitayama, Y. and Takeuchi, T. Localized surface plasmon resonance nanosensing of C-reactive protein with poly(2-methacryloyloxyethyl phosphorylcholine)-grafted gold nanoparticles prepared by surface-initiated atom transfer radical polymerization. Analytical Chemistry 86(11) (2014): 5587-94.

[90] Yang, X., et al. DNA aptamer-based surface plasmon resonance sensing of human C-reactive protein. RSC Advances 4(58) (2014): 30934-30937.

[91] Zhang, P., Bao, Y., Draz, M.S., Lu, H., Liu, C., and Han, H. Rapid and quantitative detection of C-reactive protein based on quantum dots and immunofiltration assay. International Journal of Nanomedicine 10 (2015): 6161-73.

[92] de Ávila, B.E.-F., et al. Multiplexed Determination of Amino-Terminal Pro-B-Type Natriuretic Peptide and C-Reactive Protein Cardiac Biomarkers in Human Serum at a Disposable Electrochemical Magnetoimmunosensor. Electroanalysis 26(2) (2014): 254-261.

[93] Kokkinos, C., Prodromidis, M., Economou, A., Petrou, P., and Kakabakos, S. Disposable integrated bismuth citrate-modified screen-printed immunosensor for ultrasensitive quantum dot-based electrochemical assay of C-reactive protein in human serum. Analytica Chimica Acta 886 (2015): 29-36.

[94] Vashist, S.K. Comparison of 1-Ethyl-3-(3-Dimethylaminopropyl) Carbodiimide Based Strategies to Crosslink Antibodies on Amine-Functionalized Platforms for Immunodiagnostic Applications. Diagnostics 2(3) (2012): 23-33.

[95] Zhang, D., Peng, Y., Qi, H., Gao, Q., and Zhang, C. Label-free electrochemical DNA biosensor array for simultaneous detection of the HIV-1 and HIV-2 oligonucleotides incorporating different hairpin-DNA probes and redox indicator. Biosensors and Bioelectronics 25(5) (2010): 1088-94.

[96] Yang, Z.-H., Zhuo, Y., Chai, Y.-Q., and Yuan, R. High throughput immunosenor based on multi-label strategy and a novel array electrode. Scientific Reports 4 (2014): 4747.

[97] Clark, M.F. and Adams, A.N. Characteristics of the microplate method of enzyme-linked immunosorbent assay for the detection of plant viruses. Journal of General Virology 34(3) (1977): 475-83.

[98] Songjaroen, T., Feeny, R.M., Mensack, M.M., Laiwattanapaisal, W., and Henry, C.S. Label-free detection of C-reactive protein using an electrochemical DNA immunoassay. Sensing and Bio-Sensing Research 8 (2016): 14-19.

[99] Centi, S., Bonel Sanmartin, L., Tombelli, S., Palchetti, I., and Mascini, M. Detection of C Reactive Protein (CRP) in Serum by an Electrochemical Aptamer-Based Sandwich Assay. Electroanalysis 21(11) (2009): 1309-1315.

[100] Sorrentino, A., Gorrasi, G., and Vittoria, V. Potential perspectives of bio-nanocomposites for food packaging applications. Trends in Food Science & Technology 18(2) (2007): 84-95.

[101] Damodaran, S., Parkin, K.L., and Fennema, O.R. Fennema's food chemistry. 4th ed. ed. Food science and technology; Food science and technology (Taylor & Francis). Boca Raton :: CRC Press/Taylor & Francis, 2008.

[102] Jackson, L.S. Chemical Food Safety Issues in the United States: Past, Present, and Future. Journal of Agricultural and Food Chemistry 57(18) (2009): 8161-8170.

[103] Yadav, A., Kumar, A., Dwivedi, P.D., Tripathi, A., and Das, M. In vitro studies on immunotoxic potential of Orange II in splenocytes. Toxicology Letters 208(3) (2012): 239-245.

[104] Ye, X., Du, Y., Lu, D., and Wang, C. Fabrication of β-cyclodextrin-coated poly (diallyldimethylammonium chloride)-functionalized graphene composite film modified glassy carbon-rotating disk electrode and its application for

simultaneous electrochemical determination colorants of sunset yellow and tartrazine. Analytica Chimica Acta 779 (2013): 22-34.

[105] Zhang, W., Liu, T., Zheng, X., Huang, W., and Wan, C. Surface-enhanced oxidation and detection of Sunset Yellow and Tartrazine using multi-walled carbon nanotubes film-modified electrode. Colloids and Surfaces B: Biointerfaces 74(1) (2009): 28-31.

[106] Medeiros, R.A., Lourencao, B.C., Rocha-Filho, R.C., and Fatibello-Filho, O. Simultaneous voltammetric determination of synthetic colorants in food using a cathodically pretreated boron-doped diamond electrode. Talanta 97 (2012): 291-297.

[107] Gan, T., Sun, J., Meng, W., Song, L., and Zhang, Y. Electrochemical sensor based on graphene and mesoporous TiO2 for the simultaneous determination of trace colourants in food. Food Chemistry 141(4) (2013): 3731-3737.

[108] Gan, T., Hu, C., Chen, Z., and Hu, S. A disposable electrochemical sensor for the determination of indole-3-acetic acid based on poly(safranine T)-reduced graphene oxide nanocomposite. Talanta 85(1) (2011): 310-316.

[109] Huang, K.-J., Miao, Y.-X., Wang, L., Gan, T., Yu, M., and Wang, L.-L. Direct electrochemistry of hemoglobin based on chitosan–ionic liquid–ferrocene/graphene composite film. Process Biochemistry 47(7) (2012): 1171-1177.

[110] Wei, Q., Zhao, Y., Du, B., Wu, D., Li, H., and Yang, M. Ultrasensitive detection of kanamycin in animal derived foods by label-free electrochemical immunosensor. Food Chemistry 134(3) (2012): 1601-1606.

[111] Wu, C., Sun, D., Li, Q., and Wu, K. Electrochemical sensor for toxic ractopamine and clenbuterol based on the enhancement effect of graphene oxide. Sensors and Actuators B: Chemical 168 (2012): 178-184.

[112] Gan, T., Sun, J., Huang, K., Song, L., and Li, Y. A graphene oxide–mesoporous MnO2 nanocomposite modified glassy carbon electrode as a novel and efficient voltammetric sensor for simultaneous determination of hydroquinone and catechol. Sensors and Actuators B: Chemical 177 (2013): 412-418.

[113] Stankovich, S., et al. Synthesis of graphene-based nanosheets via chemical reduction of exfoliated graphite oxide. Carbon 45(7) (2007): 1558-1565.

[114] Hummers, W.S. and Offeman, R.E. Preparation of Graphitic Oxide. Journal of the American Chemical Society 80(6) (1958): 1339-1339.

[115] Choucair, M., Thordarson, P., and Stride, J.A. Gram-scale production of graphene based on solvothermal synthesis and sonication. Nature Nanotechnology 4(1) (2009): 30-33.

[116] Peng, X.-Y., Liu, X.-X., Diamond, D., and Lau, K.T. Synthesis of electrochemically-reduced graphene oxide film with controllable size and thickness and its use in supercapacitor. Carbon 49(11) (2011): 3488-3496.

[117] Lawrence, J.F., Lancaster, F.E., and Conacher, H.B.S. Separation and detection of synthetic food colors by ion-pair high- performance liquid chromatography. Journal of Chromatography A 210(1) (1981): 168-173.

[118] Ji, L., Cheng, Q., Wu, K., and Yang, X. Cu-BTC frameworks-based electrochemical sensing platform for rapid and simple determination of Sunset yellow and Tartrazine. Sensors and Actuators B: Chemical 231 (2016): 12-17.

[119] Arslan, E. and Çakır, S. Electrochemical fabrication of polyproline modified graphite electrode decorated with Pd–Au bimetallic nanoparticles: Application for determination of carminic acid. Journal of Electroanalytical Chemistry 760 (2016): 32-41.

[120] Bai, L., Yuan, R., Chai, Y., Yuan, Y., Wang, Y., and Xie, S. Direct electrochemistry and electrocatalysis of a glucose oxidase-functionalized bioconjugate as a trace label for ultrasensitive detection of thrombin. Chemical Communications 48(89) (2012): 10972-4.

[121] Basirun, W.J., Sookhakian, M., Baradaran, S., Mahmoudian, M.R., and Ebadi, M. Solid-phase electrochemical reduction of graphene oxide films in alkaline solution. Nanoscale Research Letters 8(1) (2013): 397-397.

[122] Liu, C., Wang, K., Luo, S., Tang, Y., and Chen, L. Direct Electrodeposition of Graphene Enabling the One-Step Synthesis of Graphene–Metal Nanocomposite Films. Small 7(9) (2011): 1203-1206.

[123] Wang, M. and Zhao, J. Facile synthesis of Au supported on ionic liquid functionalized reduced graphene oxide for simultaneous determination of Sunset yellow and Tartrazine in drinks. Sensors and Actuators B: Chemical 216 (2015): 578-585.

[124] Azizi, S.N., Ghasemi, S., and Amiripour, F. Nickel/P nanozeolite modified electrode: A new sensor for the detection of formaldehyde. Sensors and Actuators B: Chemical 227 (2016): 1-10.

[125] Song, X., Shi, Z., Tan, X., Zhang, S., Liu, G., and Wu, K. One-step solvent exfoliation of graphite to produce a highly-sensitive electrochemical sensor for tartrazine. Sensors and Actuators B: Chemical 197 (2014): 104-108.

[126] Qiu, X., et al. An enhanced electrochemical platform based on graphene oxide and multi-walled carbon nanotubes nanocomposite for sensitive determination of Sunset Yellow and Tartrazine. Food Chemistry 190 (2016): 889-895.

# VITA

Mr.Sakda Jampasa was born on January 9th, 1988 in Ubon Ratchathani, Thailand. He graduated with a high school diploma from Warinchamrab School, Ubon Ratchathani in 2005. He received his B.S. in Chemistry with first-class honor from Ubonratchani University in 2009. He did his M.S. in Petrochemistry and Polymer Science at Chulalongkorn University and graduated in 2013. He became a Ph.D. student in Petrochemistry as a member of Electrochemistry and Optical Spectroscopy Center of Excellence under the advisory of Prof. Dr.Orawon Chailapakul at Chulalongkorn University. He received a grant from Human Resource Development in Science Project (Science Achievement Scholarship of Thailand, SAST). He graduated with a Ph.D. in Petrochemistry from Chulalongkorn University.